This is an open access article published under an ACS AuthorChoice License, which permits copying and redistribution of the article or any adaptations for non-commercial purposes.

Journal of Medicinal Chemistry

Featured Article

pubs.acs.org/jmc

Novel 2,4-Disubstituted Pyrimidines as Potent, Selective, and Cell-Permeable Inhibitors of Neuronal Nitric Oxide Synthase

Paramita Mukherjee,[†] Huiying Li,[‡] Irina Sevrioukova,[‡] Georges Chreifi,[‡] Pavel Martásek,[§] Linda J. Roman,[§] Thomas L. Poulos,*[,‡] and Richard B. Silverman*[,†]

[†]Department of Chemistry, Department of Molecular Biosciences, Chemistry of Life Processes Institute, Center for Molecular Innovation and Drug Discovery, Northwestern University, Evanston, Illinois 60208-3113, United States

[‡]Departments of Molecular Biology and Biochemistry, Pharmaceutical Sciences, and Chemistry, University of California, Irvine, California 92697-3900, United States

[§]Department of Biochemistry, University of Texas Health Science Center, San Antonio, Texas 78384-7760, United States

Supporting Information

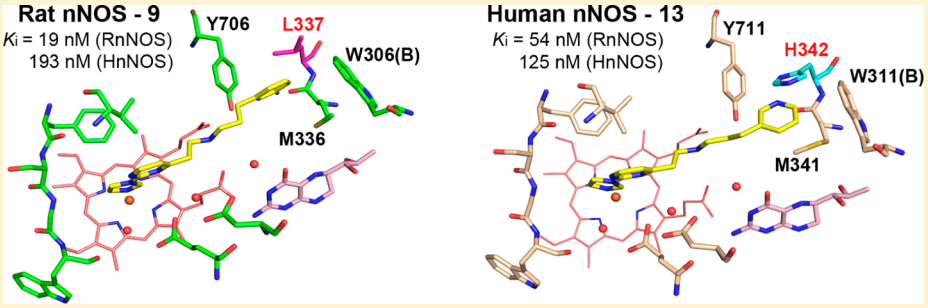

ABSTRACT: Selective inhibition of neuronal nitric oxide synthase (nNOS) is an important therapeutic approach to target neurodegenerative disorders. However, the majority of the nNOS inhibitors developed are arginine mimetics and, therefore, suffer from poor bioavailability. We designed a novel strategy to combine a more pharmacokinetically favorable 2-imidazolylpyrimidine head with promising structural components from previous inhibitors. In conjunction with extensive structure−activity studies, several highly potent and selective inhibitors of nNOS were discovered. X-ray crystallographic analysis reveals that these type II inhibitors utilize the same hydrophobic pocket to gain strong inhibitory potency (**13**), as well as high isoform selectivity. Interestingly, select compounds from this series (**9**) showed good permeability and low efflux in a Caco-2 assay, suggesting potential oral bioavailability, and exhibited minimal off-target binding to 50 central nervous system receptors. Furthermore, even with heme-coordinating groups in the molecule, modifying other pharmacophoric fragments minimized undesirable inhibition of cytochrome P450s from human liver microsomes.

INTRODUCTION

Nitric oxide (NO) is an important biological second messenger in humans, which plays a critical role in cell and neuronal signaling, blood pressure regulation, and the immune response.[1] NO is produced from oxidation of L-arginine (L-Arg) in the presence of NADPH by a class of heme-dependent enzymes, nitric oxide synthases (NOS).[2] Mammals have three dominant isoforms of NOS: constitutively expressed neuronal NOS (nNOS), present throughout the nervous system and skeletal muscles, endothelial NOS (eNOS), also a constitutive enzyme located in the endothelium and functioning in regulation of blood pressure and blood flow, and inducible NOS (iNOS), which is associated with the immune response.

In the brain, low nanomolar concentrations of NO produced by nNOS are neuroprotective, and downstream NO, along with cyclic guanosine 5′-monophosphate (cGMP) in the protein kinase G (PKG) signaling pathway, plays an important role in neurotransmission and other metabolic processes.[3] However, overexpression and overactivation of nNOS following neuronal damage causes NO levels to jump several orders of magnitude,[4] which is neurotoxic. Such NO-mediated neurotoxicity leads to protein degradation, misfolding, and aggregation through tyrosine-nitration,[5] *S*-nitrosylation,[6] and oxidative stress damage through formation of reactive oxygen species (ROS) and reactive nitrogen species (RNS).[7] This neurotoxicity has been implicated in several neurodegenerative disorders that include Alzheimer's, Parkinson's, and Huntington's diseases and amyotrophic lateral sclerosis (ALS).[8] Furthermore, progressive neuronal damage and loss of neural tissue associated with NO overproduction are seen in cerebral palsy, stroke, ischemic brain damage, and migraine headaches.[9] Therefore, with the increasing human and economic costs associated with neurodegenerative diseases, and the lack of existent treatments, there is an urgent need for the development of new therapeutics that would prevent, cure, or attenuate neurodegeneration. With high

Received: November 5, 2014
Published: December 9, 2014

 © 2014 American Chemical Society

DOI: 10.1021/jm501719e
J. Med. Chem. 2015, 58, 1067−1088

levels of NO implicated in these neurodegenerative conditions, and target validation linking nNOS to these pathological conditions,[10] the development of nNOS inhibitors is an important therapeutic approach for neuroprotection.[11]

All NOS isoforms are active only as homodimeric enzymes, where each monomer contains an N-terminal oxygenase domain and a C-terminal reductase domain.[12] The reductase domain contains the FMN, FAD, and NADPH binding-sites,[13] while the oxygenase domain binds the cofactor (6*R*)-5,6,7,8-tetrahydrobiopterin (H_4B) and the substrate L-Arg at the heme catalytic site. Upon dimerization and activation of NOS by Ca^{2+}-mediated calmodulin binding,[14] electrons flow from NADPH to FAD and FMN in the reductase domain to the heme in the oxygenase domain, where conversion of L-Arg to L-citrulline and NO takes place in the presence of oxygen.[15] Therefore, quite predictably, the major approach in the development of NOS inhibitors involves the utilization of arginine mimetics as competitive nNOS inhibitors.[11,16] However, in addition to potent inhibition of nNOS, there are many challenges associated in designing nNOS inhibitors. First, selectivity of nNOS inhibitors over eNOS and iNOS (NOS isoforms share nearly identical active site) is essential to minimize undesired side effects.[17] Second, as arginine isosteres, these inhibitors are highly polar; therefore, they suffer from poor bioavailabilty. Hence, the design of potent nNOS inhibitors with improved pharmacokinetic properties that address high isoform selectivity, blood–brain barrier permeability, and minimal off-target efficacy is crucial.

In this respect, continuing efforts from our laboratories, guided by structure-based drug design and fragment hopping, have resulted in a series of highly potent and selective small molecule nNOS inhibitors based on pyrrolidinomethyl-2-aminopyridine scaffolds (Figure 1, compounds **1** and **2**).[18] Compounds **1** and **2** showed high potency and excellent selectivity over iNOS and eNOS, while **2**, when administered intravenously to a pregnant rabbit dam with induced uterine hypoxia, showed a complete reversal of hypoxia–ischemia induced death in the newborn kits.[19] However, further development of these compounds stalled because of their inability to cross the blood–brain barrier. This was presumably the result of the hydrophilic nature of the molecule (too many basic amines and hydrogen-bond donors, high polar surface area, and a large number of rotatable bonds).[20] Modifications of these pyrrolidinomethyl-2-aminopyridine scaffolds, such as reducing the number of polar charges and basicity by alkylation,[21] fluorination,[22] and intramolecular hydrogen bonding,[23] met with either diminished potency or selectivity or without notable improvement in cellular permeability. Furthermore, synthesis of these pyrrolidinomethyl-2-aminopyridine scaffolds involved more than 12 steps, difficult chiral resolutions, and diastereomer separations. Later modifications of simplified double-headed 2-aminopyridine scaffolds displayed good potency and selectivity;[24] however, they still suffered from poor permeability in a Caco-2 assay, which is used to estimate intestinal cellular permeability and also reflects potential brain permeation.[25]

Therefore, as bioavailability was a major challenge in these nNOS inhibitors, one avenue we explored to improve the cellular permeability of the NOS inhibitors, while maintaining a good potency and selectivity, was replacement of the more basic arginine isosteres with fewer basic groups that engage in heme-coordination in the active site of NOS to arrest L-arginine turnover (for example, the pK_a of conjugate acid of 2-aminopyridine is 7.1). Compared to many inhibitors designed as arginine mimetics, only a few reports exist that explore the heme-coordination of NOS.[11] However, imidazole (pK_a of its conjugate acid is 6.9) is known to weakly bind to nNOS (IC_{50} 200 μM), while the less-donating 1-phenylimidazole shows nearly 10-fold improved potency (IC_{50} 25 μM).[26] Furthermore, 2-(1-imidazolyl)pyrimidine scaffolds, such as **3**, have shown very good potency as iNOS dimerization inhibitors.[27] In addition, **3** demonstrated good cellular permeability and in vivo efficacy against iNOS in rats.[27b]

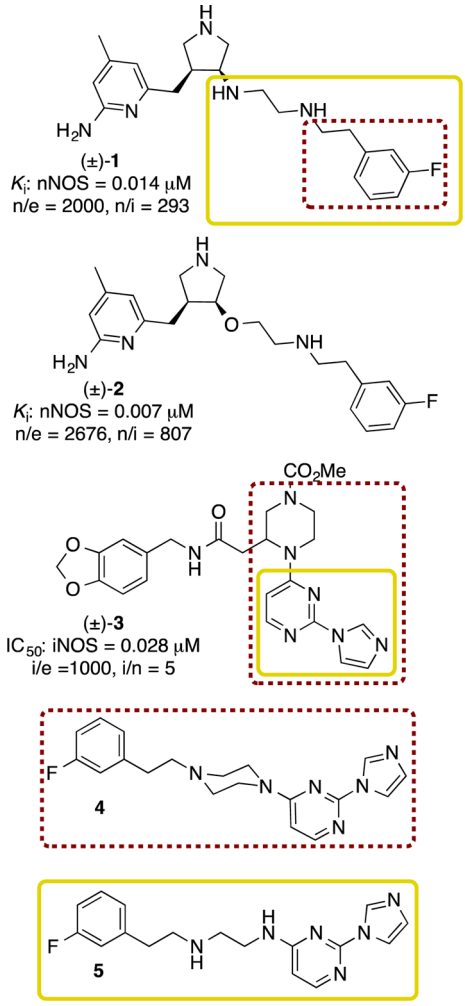

Figure 1. Representative nNOS and iNOS inhibitors and nNOS inhibitor design strategy.

Toward this end, we designed simplified compounds **4** and **5** with improved predicted physicochemical properties by hybridizing selective molecular fragments from inhibitors **1** and **3**. The key hydrophobic tail of **1** was incorporated into structures **4** and **5** based on previous precedence, where contacts between **1** and residues lining a hydrophobic pocket adjacent to the substrate access channel[28] were implicated in improving isoform selectivity.[18,29] On the basis of inhibitory assay results, docking studies, and crystallographic analysis, further modifications on **5**, such as changing the linker length between the two aromatic heads, the number of secondary amines, and utilizing various substitutions on the aromatic rings, were employed to maximize rat and human nNOS potency, improve isoform selectivity, enable cellular permeability, and minimize off-target effects. Figure 2 summarizes the

DOI: 10.1021/jm501719e
J. Med. Chem. 2015, 58, 1067–1088

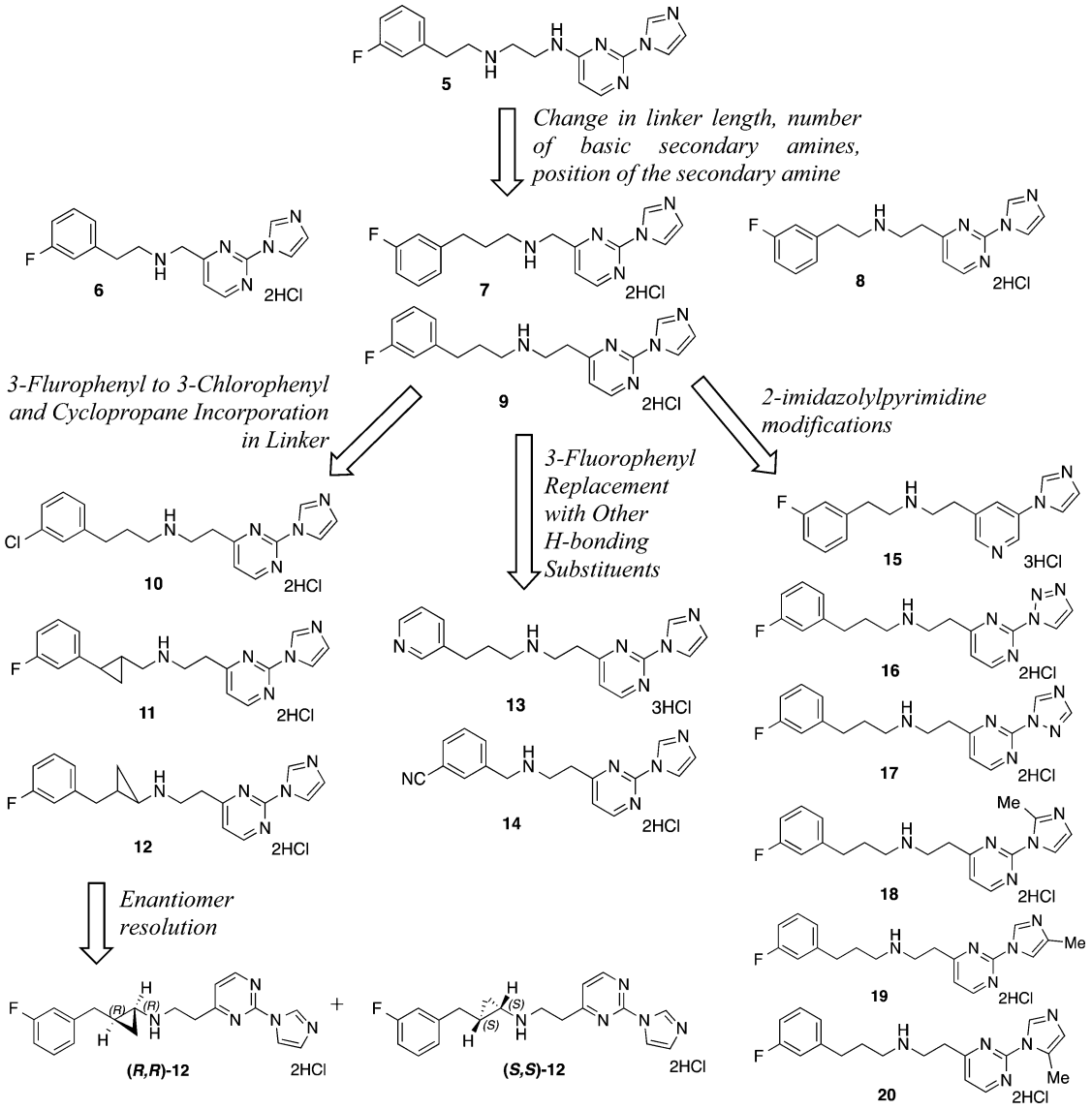

Figure 2. nNOS inhibitors synthesized in this study.

Scheme 1. Synthesis of 4 and 5[a]

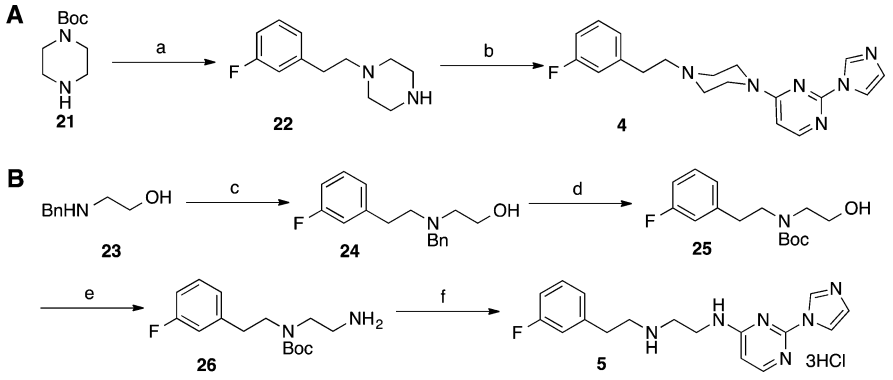

[a]Reagents and conditions: (a) (i) NaH, THF, 0 °C, 1 h, then 3-fluorophenethyl bromide, TBAI, 60 °C, 48 h, 56%, (ii) TFA, CH_2Cl_2, 0 °C → RT, 3 h, 85%; (b) 4-chloro-2-methanesulfonyl pyrimidine, K_2CO_3, MeCN, 40 °C, 19 h, then imidazole, 65 °C, 30 h, 82%; (c) 3-fluorophenyl acetaldehyde, $NaBH(OAc)_3$, RT, 14 h, 91%; (d) (i) H_2, Pd/C, MeOH, 12 h, 86%, (ii) Boc_2O, CH_2Cl_2, 3 h, 76%; (e) (i) DIAD, PPh_3, DPPA, THF, 12 h, (ii) PPh_3, THF/H_2O, 41%; (f) (i) same as (b), 60%, (ii) TFA, CH_2Cl_2, 2 h, (iii) HCl in MeOH, 10 min, 83%.

different nNOS inhibitors designed and studied in this series. Through these structure−activity optimizations, highly potent and selective inhibitors of nNOS were discovered. These compounds showed improved cellular permeability, high

DOI: 10.1021/jm501719e
J. Med. Chem. 2015, 58, 1067−1088

Scheme 2. Synthesis of 6 and 7[a]

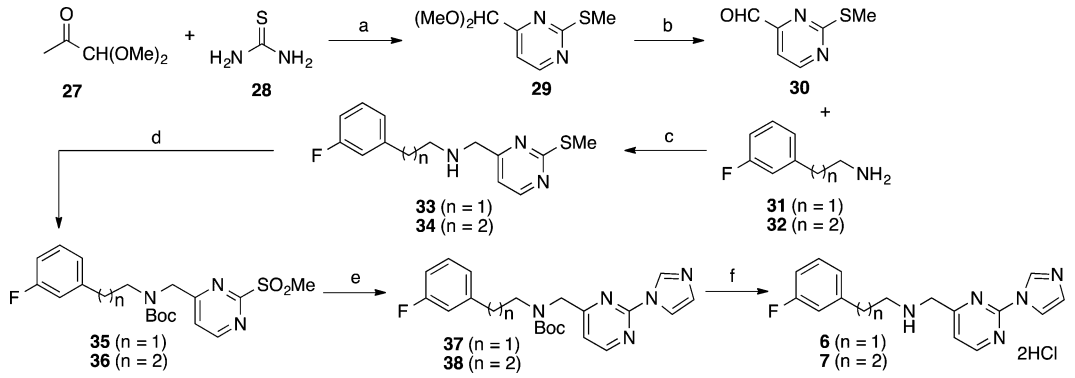

[a]Reagents and conditions: (a) (i) *N*,*N*-dimethylformamide dimethyl acetal, 110 °C, 8 h, (ii) NaOMe, MeOH, RT, 16 h, (iii) MeI, 60 °C, 12 h, 87%; (b) HCl, 85 °C, 6 h, 58%; (c) $NaBH(OAc)_3$, cat. AcOH, 3 Å sieves, CH_2Cl_2, 14 h, 85−89%; (d) (i) Boc_2O, THF, 12 h, 97−99%, (ii) mCPBA, CH_2Cl_2, 12 h, 75−89%; (e) imidazole, K_2CO_3, MeCN, 60 °C, 4 h, 84−93%; (f) (i) TFA, CH_2Cl_2, 3 h, (ii) HCl in MeOH, 10 min, 79−93%.

Scheme 3. General Scheme for Synthesis of 8−14[a]

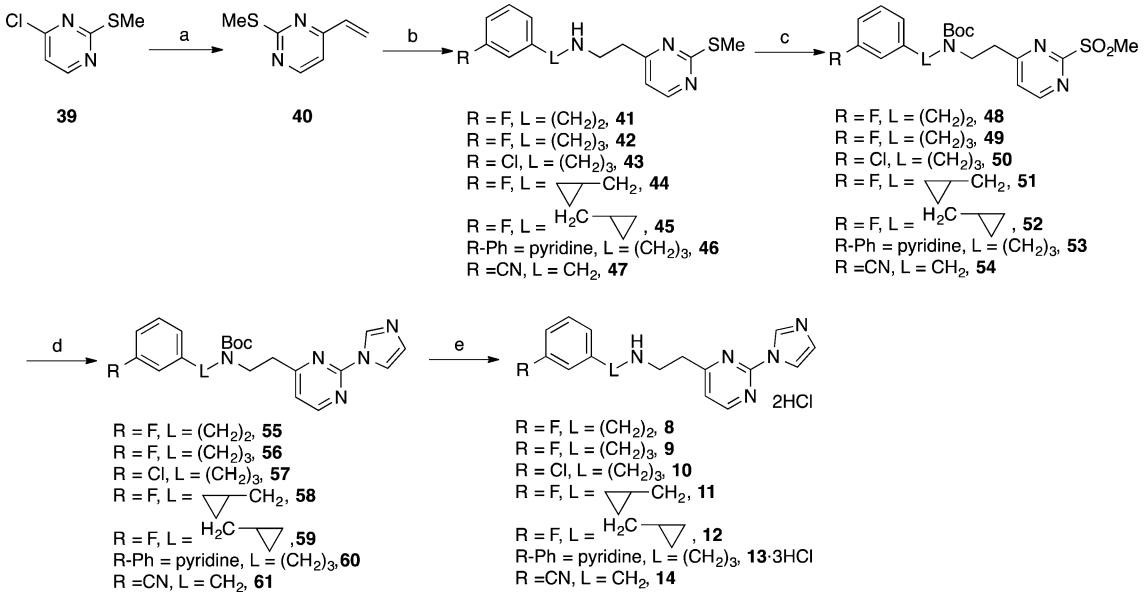

[a]Reagents and conditions: (a) tributylvinyl tin, $Pd(PPh_3)_4$, DCE, 70 °C, 48 h, 92%; (b) R-NH_2, cat. AcOH, EtOH, 8−48 h, 62−97%; (c) (i) Boc_2O, THF, 3 h, 80−95%, (ii) mCPBA, CH_2Cl_2, 3 h, 65−91% (note in case of **46**, oxone was used instead of mCPBA in a 1:1 THF/H_2O mixture for 4 h); (d) imidazole, K_2CO_3, MeCN, 65 °C, 5−10 h, 76−92%; (e) (i) TFA, CH_2Cl_2, 3 h, (ii) HCl in MeOH, 10 min, 80−99%.

selectivity against a panel of central nervous system (CNS) receptors, and attenuated CYP inhibition.

CHEMISTRY

Synthesis of the 2,4-disubstituted pyrimidine scaffolds in this study was designed to utilize common intermediates and proceed in relatively few steps. Thus, the synthesis of the 2,4-disubstituted pyrimidine cores in **4** and **5** was obtained by following a modified procedure reported by Davey et al.[27b] Alkylation of *N*-Boc piperazine (**21**) by 3-fluorophenethyl bromide gave **22**, which underwent a sequential one-pot substitution on 4-chloro-2-methanesulfonyl pyrimidine by itself and imidazole, respectively, to provide target compound **4** (Scheme 1). Similar substitutions on 4-chloro-2-methanesulfonyl pyrimidine by **26** and imidazole, respectively, gave the primary framework as a Boc-protected precursor of **5**, which was subsequently Boc-deprotected with trifluoroacetic acid and obtained as a trihydrochloride salt upon precipitation from methanolic HCl. Compound **25** was synthesized following a reported procedure,[30] from where a Mitsunobu reaction with diphenylphosphoryl azide gave the corresponding azide, which was subsequently reduced to give the primary amine **26**.

In **6** and **7**, where the secondary amine was benzylic to the pyrimidine, a reductive amination to form the C−N bond with an aromatic aldehyde was conceived as a favorable disconnection (Scheme 2). Therefore, 2-methylthio-4-pyrimidine carboxaldehyde (**30**) was first obtained by condensation between pyruvaldehyde dimethylacetal (**27**) and thiourea (**28**) and then acetal deprotection.[31] This intermediate underwent efficient reductive amination with 3-fluorophenylethylamine and 3-fluorophenylpropylamine to form secondary amines **33** and **34**, respectively. Then Boc protection of the secondary amine and oxidation of the thioether group to methanesulfonyl by mCPBA enabled the successive displacement by imidazole to get the main structural frameworks of **6** and **7**. Finally, deprotection of the Boc group under acidic conditions and

DOI: 10.1021/jm501719e
J. Med. Chem. 2015, 58, 1067−1088

Scheme 4. Synthesis of (*R,R*)-12 and (*S,S*)-12[a]

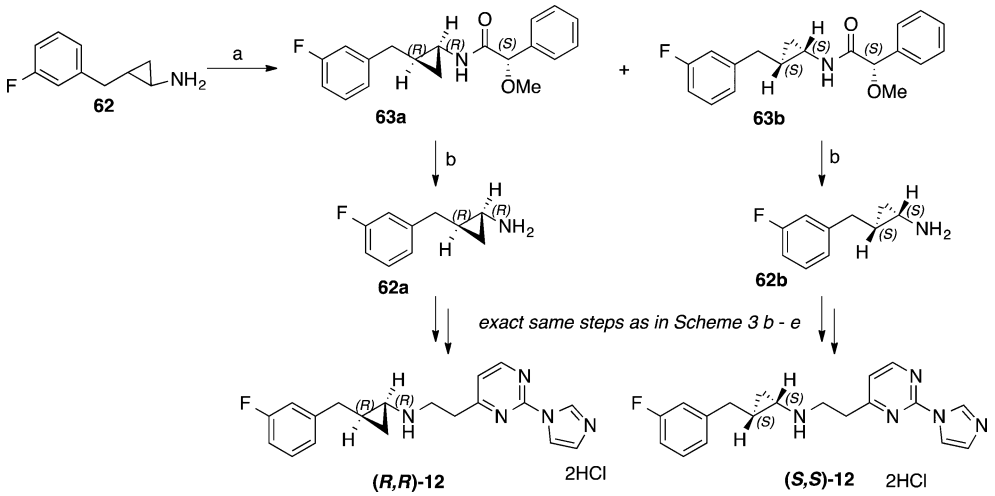

[a]Reagents and conditions: (a) (i) (*S*)-(+)-α-methoxyphenylacetic acid, DCC, CH_2Cl_2, −20 °C to RT, 12 h, (ii) chiral resolution of diastereomers on silica gel column; (b) HCl in EtOH, reflux, 12 h.

Scheme 5. Synthesis of 15[a]

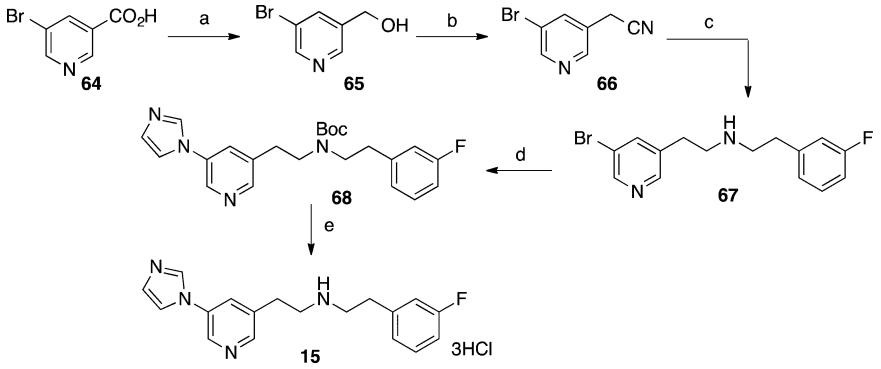

[a]Reagents and conditions: (a) (i) isobutyl chloroformate, Et_3N, THF, RT, 1 h, (ii) $NaBH_4$, H_2O, 12 h, 43%; (b) (i) $SOCl_2$, CH_2Cl_2, 2 h, (ii) KCN, DMF, RT, 12 h, 70%; (c) (i) DIBAL, CH_2Cl_2, −78 °C, 1 h, (ii) 3-fluorophenethylamine, cat. AcOH, $MgSO_4$, $NaBH(OAc)_3$, 12 h, 41%; (d) (i) Boc_2O, THF, 12 h, 92%, (ii) CuBr, 8-acetyl-5,6,7,8-tetrahydroquinoline, imidazole, Cs_2CO_3, DMSO, 100 °C, 12 h, 67%; (e) (i) TFA, CH_2Cl_2, 3 h, (ii) HCl in MeOH, 10 min, 88%.

subsequent precipitation from methanolic HCl gave **6** and **7** as dihydrochloride salts.

2,4-Disubstituted pyrimidine scaffolds possessing two methylene units between the secondary amine and the pyrimidine ring (**8**−**14**) were synthesized via a Michael addition on the electron-deficient vinyl pyrimidine ring (Scheme 3). Therefore, the 2-methylthio-4-vinyl pyrimidine (**40**) was synthesized by a Stille coupling between commercially available 4-chloro-2-methylthio pyrimidine (**39**) and tributylvinyltin in the presence of tetrakistriphenylphosphine Pd(0).[32] A Michael addition between **40** and the particular primary amines gave the corresponding homobenzylic amines (**41**−**47**). The primary amines (**31**−**32**, **S3**−**S12** (see Supporting Information), **62**) were synthesized either from commercially available bromides or carboxylic acids in 2−3 steps, as elaborated in the Supporting Information. Note that in the case of the primary amines containing a cyclopropyl group, the *cis* and *trans* isomers were completely separable by silica gel column chromatography (see Supporting Information for further details), and the *trans* isomer was carried forward for the Michael addition reaction.

Following a similar route as illustrated for the synthesis of **6** and **7**, final compounds **8**−**14** were obtained (Scheme 3). However, in the case of **46**, after Boc protection, mCPBA oxidation (regardless of conditions) always led to undesired oxidation of the pyridine ring to the *N*-oxide. Finally, oxidation of **46** in a 1:1 mixture of THF and H_2O by oxone at room temperature for 4 h gave desired sulfone **53**.[33] Similar imidazole substitution, Boc deprotection, and acidification gave final compound **13** as a pure trihydrochloride salt.

When separation of the two enantiomers of **12** became crucial, the *trans*-isomer of 2-(3-fluorophenyl)-1-cyclopropyl amine (**62**) was subjected to DCC-mediated amidation with (*S*)-(+)-α-methoxyphenylacetic acid (Scheme 4).[34] The diastereomers, **63a** and **63b**, were obtained pure by silica gel column chromatographic separation. Finally, hydrolysis of the auxiliary under refluxing ethanolic HCl gave the enantioenriched amines **62a** and **62b** in >95% enantiopurity. These amines were then independently converted to the final enantiomerically enriched isomers (*R,R*)-**12** and (*S,S*)-**12** by following the exact same route as used to synthesize **12** from **62** and 2-methylthio-4-vinylpyrimidine (**40**).

When the 2,4-disubstituted pyrimidine was replaced by a 3,5-disubstituted pyridine ring, as in **15**, synthesis was initiated from commercially available 5-bromo nicotinic acid (**64**) by

DOI: 10.1021/jm501719e
J. Med. Chem. 2015, 58, 1067−1088

Scheme 6. Synthesis of 16−20[a]

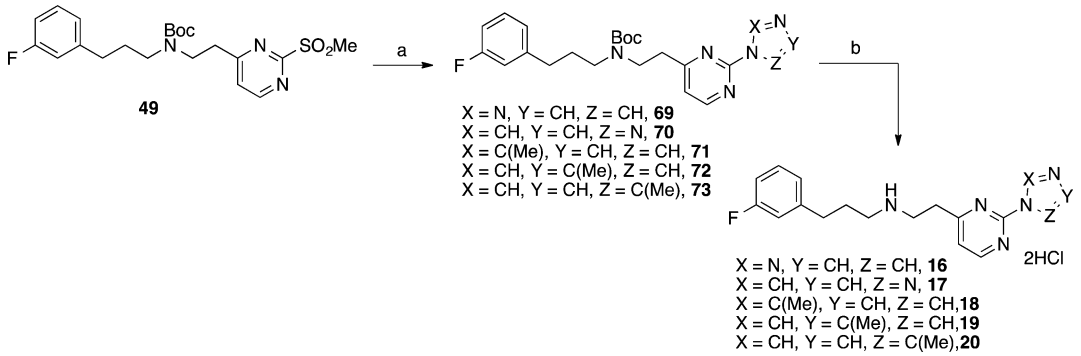

[a]Reagents and conditions: (a) imidazole/triazole, K_2CO_3, MeCN, 65 °C, 5−24 h, 82−88%; (b) (i) TFA, CH_2Cl_2, 1 h, (ii) HCl in MeOH, 10 min, 87−99%.

reduction to alcohol **65** (Scheme 5). Homologation by one methylene unit was obtained by conversion of the alcohol to a nitrile (**66**) and then to its aldehyde by DIBAL. As the intermediate aldehyde was photosensitive and unstable, it was synthesized in the dark, and the crude reaction, after work up, was immediately subjected to reductive amination with 3-fluorophenethyl amine (**31**) to provide **67** in a 41% yield (over two steps). Boc protection of the secondary amine, followed by a Cu-catalyzed amination of the 3-bromopyridine group, gave **68**,[35] which was Boc deprotected and treated with methanolic HCl to give final compound **15** as a trihydrochloride salt.

The different aromatic substitutions at the 2-position of the pyrimidine in **16−20** were synthesized from advanced intermediate **49** by substituting the sulfone with the different methyl imidazoles or triazoles (Scheme 6). Thereafter, a similar TFA-mediated Boc deprotection and salt formation gave the compounds **16−20**. However, when 4-methylimidazole was used, both 4- and 5-methyl-2-imidazolyl pyrimidines **72** and **73** were obtained, which were inseparable by chromatographic conditions. Therefore, a subsequent Boc deprotection of the mixture of **72** and **73**, followed by a chromatographic separation, provided the free bases of **19** and **20**. These were subsequently treated with methanolic HCl to obtain pure dihydrochloride salts **19** and **20**.

RESULTS AND DISCUSSION

Table 1 summarizes the binding affinity of **4−20** in the in vitro enzyme inhibitory assays against several isoforms of NOS. An oxyhemoglobin NO capture assay was used to determine the IC_{50} value of inhibitors against the purified rat and human nNOS, murine macrophage iNOS, and bovine eNOS.[36] The apparent K_i values of the inhibitors were determined from IC_{50} and substrate K_m values using the Cheng−Prusoff equation, and the corresponding isoform selectivities as ratios of their respective K_i values.

Between the two initial inhibitors designed, **4** and **5**, compound **4** only weakly inhibited nNOS ($K_i \sim 5$ μM) while **5** displayed a stronger inhibition of nNOS (K_i 0.368 μM). This nearly 10-fold difference in potency can be attributed to the key structural difference in the linker between the pyrimidine and 3-fluorophenyl ring in **4** and **5**. While a piperazine ring may be sterically favorable in a more open active site, in case of **3** binding to an iNOS monomer (and hence preventing dimerization),[27a] the same may cause unfavorable steric clashes with the peptide backbone in the nNOS dimer. Furthermore, the open and flexible linker in **5** can also engage in favorable interactions via the secondary amines, thus orienting the hydrophobic end of the molecule properly. To gain more insight into the structural basis for potencies and selectivity, we determined the crystal structure of **5** bound to nNOS and eNOS. Indeed, the crystal structure of **5** bound to nNOS (Figure 3A) shows that while the 2-imidazolyl pyrimidine head in the molecule ligates to the heme Fe,[27a] the void left between the imidazole ring and Glu592 is filled with a water molecule. The secondary amine next to the pyrimidine ring is engaged in a salt bridge with heme propionate A, while the other secondary amine makes a hydrogen bond with a water bridging in between H_4B and the heme. This also orients the rest of the linker toward the hydrophobic pocket lined by Tyr706, Met336, Leu337, and Trp306 (from the other monomer) in rat nNOS.[18] The aromatic ring of **5** engages in quite a few van

Table 1. Determination of K_i Values of Inhibitors 4−20[a]

	K_i (μM)				selectivity		
compd	rnNOS	eNOS	iNOS	hnNOS	n/e	n/i	r/hnNOS
4	4.7	NT	NT	NT			
5	0.368	40.0	6.4	NT	109	17	
6	8.7	NT	NT	NT			
7	2.7	90.0	10.5	NT	33	4	
8	0.138	4.0	1.1	0.758	30	8	5.5
9	0.019	4.95	0.77	0.193	260	41	10.1
10	0.032	8.1	0.91	0.125	253	28	3.9
11	0.056	4.0	1.9	0.359	71	34	6.4
12	0.040	14.5	2.9	0.358	363	73	8.9
13	0.054	10.9	1.8	0.125	202	33	2.3
14	0.183	10.5	3.4	0.138	57	19	0.75
15	5.5	NT	NT	NT			
16	60.0	NT	NT	NT			
17	27.0	NT	NT	NT			
18	11.5	NT	NT	NT			
19	81.0	NT	NT	NT			
20	0.060	15.4	24.0	0.303	257	400	5.0

[a]Compounds **4−20** were assayed in vitro against four purified NOS isoforms: rat nNOS (rnNOS), bovine eNOS (eNOS), murine iNOS (iNOS), and human nNOS (hnNOS) using known literature methods. K_i values are determined using the Cheng−Prusoff equation directly from IC_{50} values (see Experimental Section for details). IC_{50} values are the average of at least two replicates with nine data points; all experimental standard error values are less than 15%, and all correlation coefficients are >0.9. Selectivity values are the ratios of respective K_i values. NT = not tested.

DOI: 10.1021/jm501719e
J. Med. Chem. 2015, 58, 1067−1088

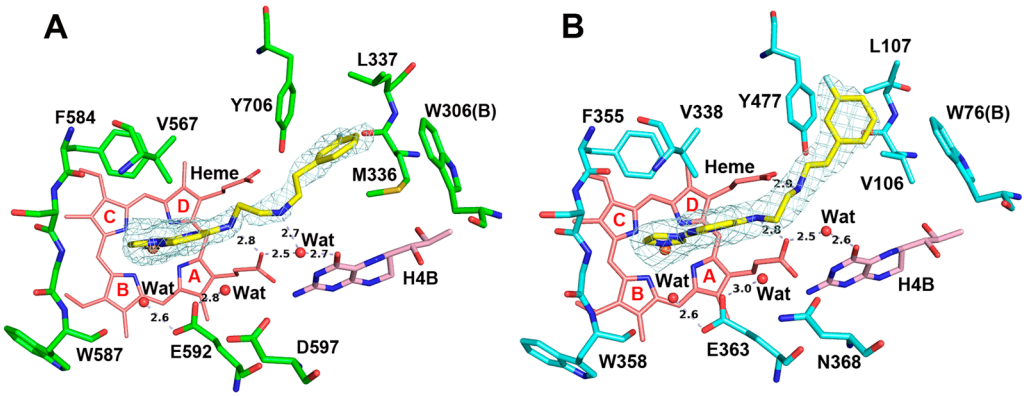

Figure 3. Active site structure of **5** bound to rat nNOS ((A) PDB 4D3B) and bovine eNOS ((B) PDB 4D33). Key hydrogen bonds are shown by dashed lines, and distances are in Å. The omit F_o-F_c map for the ligand is contoured at 2.5 σ. The heme pyrrole rings are labeled in order to identify the propionate positions. All structural figures were prepared with PyMol (www.pymol.org).

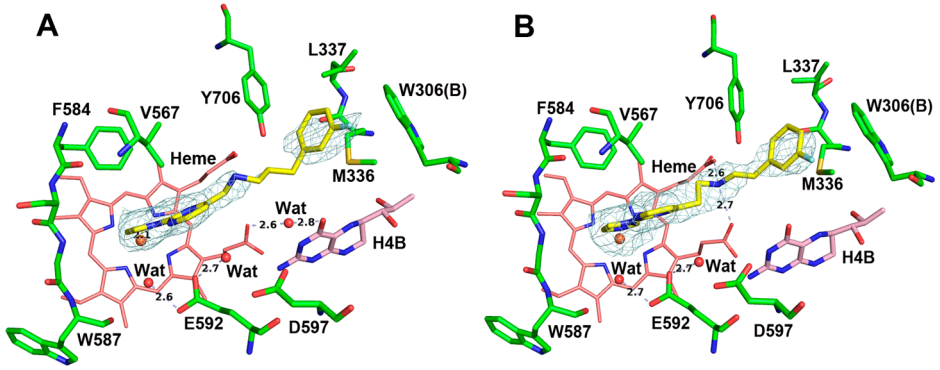

Figure 4. Active site structures of **7** ((A) PDB 4V3V) and **8** ((B) PDB 4V3W) bound to rat nNOS. Key hydrogen bonds are shown by dashed lines and distances are in Å. The omit F_o-F_c map for the ligand is contoured at 2.5 σ.

der Waals interactions with these four residues at distances from 3.5 to 4.0 Å, except for the closer distance (3.3 Å) from the fluorine atom of **5** to the carbonyl oxygen of Met336. This also represents the first structure of nNOS with a type II imidazole-based heme-bound inhibitor. The crystal structure of **5** bound to eNOS (Figure 3B) reveals two major differences compared to its binding conformation seen in nNOS. First, similar to nNOS, the tail fluorophenyl ring can still make van der Waals contacts with Tyr477, Leu107, and Trp76 (the other monomer), but the fluorine atom is no longer inserted into the pocket as in the nNOS case. Instead, the aromatic ring simply caps the pocket at its edge with the F atom pointing sideways. The reason for this binding orientation is very likely an amino acid variation, Val106 (eNOS) vs Met336 (nNOS), which is also part of this hydrophobic pocket. The more degrees of freedom of Met336 in nNOS can more readily adapt to inhibitor binding than Val106 in eNOS. As a result, the CG1 atom of Val106 in eNOS would clash with the aromatic ring of **5** if it were in its position seen in nNOS. Consequently, in eNOS the secondary amine in the linker of **5** makes a hydrogen bond with heme propionate D, rather than with a water molecule as in nNOS. The Val/Met variation is, therefore, the structural basis for the observed 100-fold selectivity for **5** (Table 1).

Because the part of inhibitor **5** positioned directly over the heme appeared optimal, we sought to improve the enzyme–inhibitor interactions beyond the active site (compounds **6**–**9**), utilizing different linker lengths between the pyrimidine and 3-fluorophenyl rings. The rationale behind the design of the shorter 4-atom-linker, as in **6**, was to avoid the twisting of methylene units on top of each other, as seen in the conformation of **5**, but still enable the aromatic end to reach the hydrophobic pocket. Also, we reasoned that moving the secondary amine away from the pyrimidine by one or two methylene units might enable it to hydrogen bond with both the heme propionates and improve the potency of the molecule. With this amine moving up along the linker, the other secondary amine in **5** becomes obsolete and thus can be removed to reduce the basicity of the inhibitors.

From evaluation of the binding affinity of these inhibitors against nNOS (Table 1), we found two crucial factors that contribute to their potency and selectivity: the position of the secondary amine and the length of the linker. Moving the secondary amine by one more methylene unit from the pyrimidine ring (**8** and **9**) dramatically decreased the K_i values relative to **6** and **7** (8.7 and 2.7 μM, respectively). The structure of **7** bound to nNOS (Figure 4A) reveals that the secondary amine can no longer make a hydrogen bond with either of the heme propionates, thus suggesting that this interaction is critical for imparting potency to these pharmacophores.[28,37] This polar interaction was regained in **8** and **9**, where the secondary amine is one carbon farther away from the pyrimidine than in **6** and **7**. The structure of **8** bound to nNOS (Figure 4B) indicates that this position of the amine enables it to engage in dual salt bridges with both the heme propionates, with the secondary amine positioned equidistant between the two. However, the five-atom linker of **8** is not long enough to bring the fluorophenyl ring into tighter van der

DOI: 10.1021/jm501719e
J. Med. Chem. 2015, 58, 1067–1088

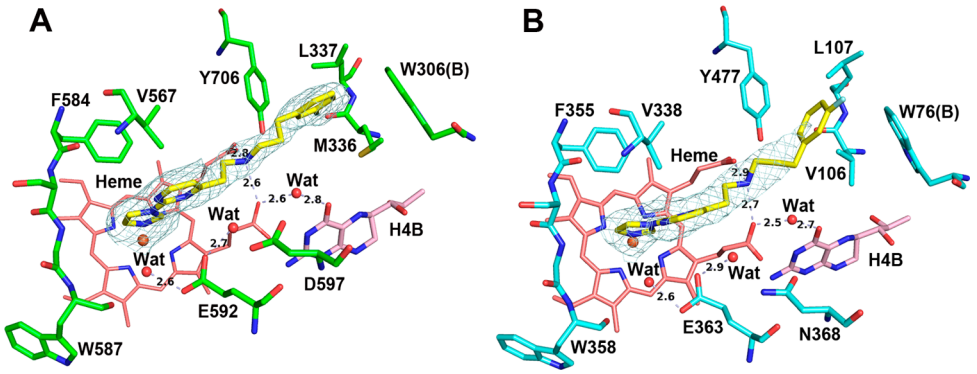

Figure 5. Active site structures of **9** bound to rat nNOS ((A) PDB 4V3X) and bovine eNOS ((B) PDB 4D35). Key hydrogen bonds are shown by dashed lines and distances are in Å. The omit F_o-F_c map for the ligand is contoured at 2.5 σ.

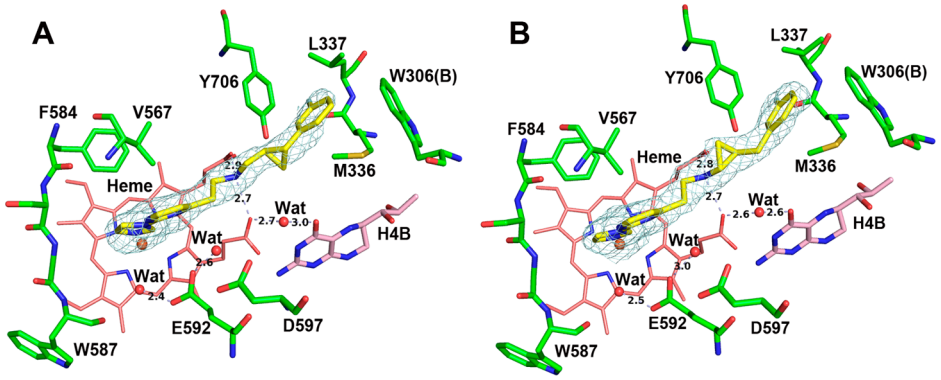

Figure 6. Active site structures of **11** ((A) PDB 4V3Z) and **12** ((B) PDB 4D2Y) bound to nNOS. There is preferential binding of one enantiomer: (*R*,*R*)-**11** and (*R*,*R*)-**12** for **11** and **12**, respectively. Key hydrogen bonds are shown by dashed lines, and distances are in Å. The omit F_o-F_c map for the ligand is contoured at 2.5 σ.

Waals contacts with the hydrophobic pocket. This, in fact was attained with the six-atom linker between the fluorophenyl and the pyrimidine to provide maximum potency. Thus, **9** is one of the most potent nNOS inhibitors in this series of 2-imidazolylpyrimidine scaffolds (K_i = 0.019 μM). Indeed, the structure of nNOS−**9** (Figure 5A) demonstrates the structural basis for this good potency. Like **8**, the secondary amine of **9** can establish dual salt bridges with both heme propionates. In addition, owing to the longer linker of **9**, the fluorine atom of the aromatic ring can be inserted into the hydrophobic pocket, as in the case of **5**. Extensive van der Waals contacts provided by the inhibitor's aromatic ring should be responsible for the 7-fold higher potency when comparing **9** with **8** (Figure 5A vs Figure 4B). Furthermore, **9** displayed 260-fold selectivity over eNOS, with an improved 41-fold selectivity over iNOS. The differences in interactions with residues lining the hydrophobic pocket also contribute to isoform selectivity. As shown in Figure 5B, even though **9** in eNOS can retain the dual salt bridges from its secondary amine in the linker, its fluorophenyl ring cannot insert into the hydrophobic pocket as it does in nNOS. This is the result of an amino acid variation (Val106 in eNOS vs Met336 in nNOS), as postulated for **5**. The lack of these van der Waals contacts reflects in the poorer potency of **9** to eNOS, which is supported by the fact that both **8** and **9** share similar potency to eNOS (see Figure S1 in the Supporting Information for structure of **8** bound to eNOS).

Encouraged by the good potency and selectivity of **9**, we sought to replace the fluorophenyl with a chlorophenyl ring at the hydrophobic end of **10**. Prior studies have shown that halogen replacements could result in enhanced inhibitory potency and selectivity from contacts between the inhibitor and residues in the hydrophobic pocket.[28,30] However, in our case, this change results in slightly diminished inhibitor potency in nNOS (32 nM for **10** vs 19 nM for **9**). The structure of nNOS−**10** (Figure S2 in Supporting Information) shows that because of the bulkiness of the chlorine atom, the aromatic ring actually retreats from the hydrophobic pocket, leading to less extensive van der Waals contacts with the protein compared to **9**. As expected, the chlorophenyl ring of **10** in the eNOS−**10** structure (Figure S3 in Supporting Information) is entirely outside of the pocket, similar to the situation in eNOS−**9** (Figure 5B), and therefore **10** still maintains good n/e selectivity (253-fold).

While **9** showed a high level of selectivity against eNOS, we looked deeper into further improving its iNOS selectivity. The three NOS isoforms have a 50−60% overall sequence identity and highly conserved, almost identical active site sequences.[17] Therefore, specificity among these NOS isoforms have relied on key differences in residues and their conformational flexibility along the substrate access channel that connects the active site to the hydrophobic pocket (vide supra) lying at the farthest end of this channel. Previous designs of nNOS inhibitors have shown that contacts between the inhibitor and residues of this pocket could be in part responsible for imparting isoform selectivity.[18,28] In murine iNOS, for example, a polar Asn115 replaces Leu337 of rat NOS in this pocket, which would strongly disfavor hydrophobic interactions. In addition, superimposition of the nNOS−**9** and iNOS crystal

DOI: 10.1021/jm501719e
J. Med. Chem. 2015, 58, 1067−1088

Table 2. Determination of K_i Values of Inhibitors (*R*,*R*)-12 and (*S*,*S*)-12[a]

	K_i (μM)				selectivity		
compd	rnNOS	eNOS	iNOS	hnNOS	n/e	n/i	r/hnNOS
(*R*,*R*)-**12**	0.018	10.32	2.14	0.137	573	119	7.6
(*S*,*S*)-**12**	0.150	40.0	3.0	0.873	267	20	5.8

[a]See Table 1 and Experimental Section for details. K_i values were determined using the Cheng–Prusoff equation directly from IC_{50} values. IC_{50} values are the average of at least two replicates with nine data points; all experimental standard error values are less than 10%, and all correlation coefficients are >0.95. Selectivity values are the ratios of respective K_i values.

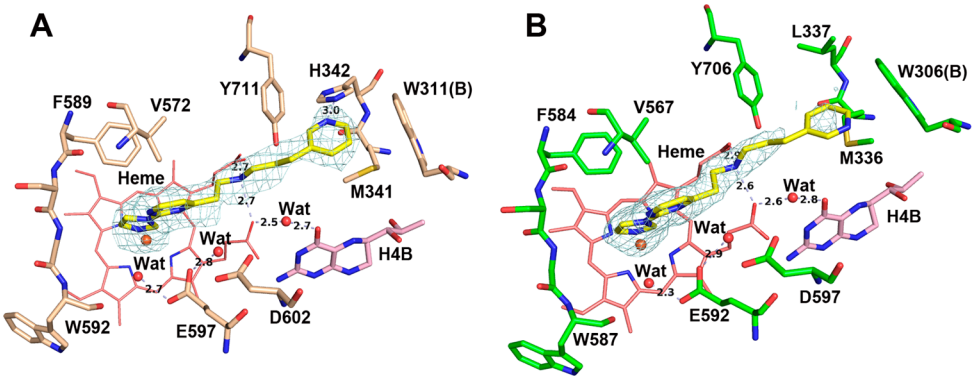

Figure 7. Active site structures of **13** bound to human nNOS ((A) PDB 4V3U) or rat nNOS ((B) PDB 4D30). Key hydrogen bonds are shown by dashed lines and distances are in Å. The omit $F_o - F_c$ map for the ligand is contoured at 2.5 σ.

structures reveals subtle differences in spatial orientations of residues along the substrate access channel. We reasoned that conformational restrictions and an increase of steric bulk in **9**, by introduction of cyclopropane rings along the methylene linker, might impose steric clashes and thereby lower binding affinity to iNOS. Furthermore, installing a cyclopropane ring as in **11** increases the metabolic stability of a more labile benzylic methylene group in **9**, while the electron-withdrawing nature of the ring can reduce the basicity of the secondary amine as in **12**, thereby increasing the probability of blood–brain barrier permeation. Although both **11** and **12** displayed a slightly lower binding affinity for nNOS, they displayed a weaker inhibitory effect on iNOS than parent compound **9**. In fact, **12** demonstrated an improved 73-fold selectivity over iNOS, more than the previous lead, and the highest n/e selectivity (363-fold) obtained so far in this series of scaffolds.

To gain more concrete evidence, we determined the crystal structures of both **11** and **12** in nNOS (parts A and B of Figure 6, respectively) and eNOS (Supporting Information, Figures S4 and S5, respectively). Because of the rigidity of the linker's cyclopropyl ring, the fluorophenyl ring of both inhibitors in nNOS retreats from the deeper position seen for **9** (Figure 5A) but is oriented similarly to **10** (Supporting Information, Figure S2). Again, less extensive van der Waals contacts for **11** and **12** relative to those by **9** are the reason for the slightly weaker potency of these two inhibitors (Table 1). Interestingly, although racemic samples of **11** and **12** were used for the crystal preparations, the electron density indicated that only one enantiomer preferably binds in each case: (*R*,*R*)-**11** in nNOS–**11** and (*R*,*R*)-**12** in nNOS–**12**. Similarly, the same enantiomer also dominates the binding of **11** or **12** to eNOS (Supporting Information, Figures S4 and S5, respectively); however, in both cases, the fluorophenyl ring caps at the edge of the hydrophobic pocket. Therefore, the less favorable enzyme–inhibitor contacts are the origin of poorer binding affinity for **11** and **12** toward eNOS. Owing to a different location of the cyclopropane in the linker, the kink caused by the cyclopropyl ring in **12** pulls the fluorophenyl ring away from the protein more severely than that observed in **11**. This explains the even poorer affinity of **12** to eNOS, which results in better n/e selectivity (Table 1).

The observation that one enantiomer of **12** dominates the binding prompted us to synthesize and test the two enantiomers of **12** separately to identify the more potent enantiomer in the pair and determine the effect of chirality on the binding of the inhibitor to the NOS active site. Table 2 summarizes the binding affinity to NOSs by the two enantiomers of **12**. While the "ring up" (*R*,*R*)-**12** shows a much tighter binding to nNOS, comparable to the affinity of **9**, this particular enantiomer also preferably binds to eNOS and iNOS. However, the very low K_i for nNOS (18 nM) compared to that for eNOS and iNOS makes (*R*,*R*)-**12** the best inhibitor in this series with 573- and 119-fold selectivities against eNOS and iNOS, respectively.

These results are also in agreement with the structural studies. The nNOS structure with (*R*,*R*)-**12** bound confirms that this enantiomer is indeed the one that dominates the binding to nNOS when racemic **12** was used for crystal preparation (Figure 6B). It is surprising that the structure of (*S*,*S*)-**12** enantiomer bound to nNOS (Figure S6 in Supporting Information) also shows a binding mode that is not that much different from that of (*R*,*R*)-**12**; both the positions of the secondary amine and the fluorine of the aromatic ring more or less overlap between the two enantiomers, even though different chiralities at the cyclopropane lead to differences in the linker conformation and phenyl ring orientation (Figure S6 in Supporting Information). Therefore, the differences in linker conformation and position of the cyclopropane ring may result in the 8-fold variation in the nNOS affinities between these two enantiomers (Table 2).

Alongside determining the potencies of these inhibitors in the three lower animal isoforms of NOS, we assayed these

DOI: 10.1021/jm501719e
J. Med. Chem. 2015, 58, 1067–1088

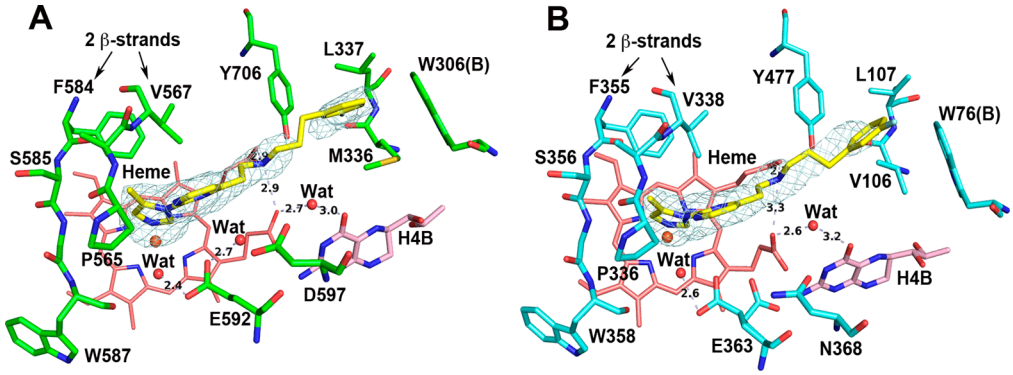

Figure 8. Active site structures of **20** bound to rat nNOS ((A) PDB 4D32) and bovine eNOS ((B) PDB 4D3A). Key hydrogen bonds are shown by dashed lines and distances are in Å. The omit $F_o - F_c$ map for ligand is contoured at 2.5 σ.

compounds with the human nNOS enzyme to see if the potency and selectivity ratios are also reflected similarly in the human isoform. Prior work on isosteric arginine mimetics developed from our lab, such as the highly potent and selective inhibitor **1**, showed a human nNOS potency of 0.070 μM, with a 5-fold selectivity difference between the human and rat isoform. This is one of the most potent human nNOS inhibitors developed in our lab to date. When compounds **8**−**12** were assayed against human nNOS, we were pleased to see that inhibitors **9**−**12** displayed good potency in human nNOS, and a similar 4−10-fold selectivity difference between the human and rat isoform of nNOS, as seen with previously reported inhibitors from our lab. The human nNOS exhibits an exact sequence identity with the rat isoform, except for the hydrophobic pocket, where a hydrophilic His342 replaces the Leu337 present in rat nNOS. Thus, the pocket in human nNOS is smaller and more hydrophilic on one side. Therefore, the modifications that we made in our chemical structures to improve nNOS potency, although generally well tolerated in human nNOS, can be modified to improve their human nNOS potency and lower the rat/human selectivity. For this target, we designed and tested compounds **13**−**14**, with smaller and polar aromatic ends that may interact effectively with His342 residue in the pocket in human nNOS. Indeed, we found that **13** is a potent inhibitor of human nNOS (0.125 μM) and rat nNOS (0.054 μM), where the selectivity between the two has dropped down to 2.3-fold (Table 1). The structure of the human nNOS−**13** complex (Figure 7A) shows, as expected, that the nitrogen of the pyridine ring indeed makes a hydrogen bond with the side chain of His342. Although the bond distances vary from 2.8 to 3.2 Å in the four independent copies of **13**, all are well ordered in structure. In contrast, the polar pyridine ring of **13** does not behave as well in the structure of rat nNOS−**13** (Figure 7B), where the ring shows the sign of disordering with weak electron density. The more hydrophobic pocket in rat nNOS prefers a phenyl ring over the pyridine ring for interactions.

Compound **10** (with a 3-chlorophenyl tail) also displayed potent human nNOS inhibition similar to **13**. With a 3-chloro substitution being bigger than a 3-fluoro, it is difficult to explain why **10** is a more potent human nNOS inhibitor than **9**. With the known behavior of **10** in rat nNOS (Figure S2 in Supporting Information), the bulkier chlorophenyl ring in human nNOS is likely pulled out a bit from the depth of the hydrophobic pocket compared to the position of a fluorophenyl ring in **9**. This movement may allow the 3-chlorophenyl ring to fit better in the pocket, which might contribute to the slightly better affinity of **10** than **9** to human nNOS. On the other hand, it is easier to explain the preference for more polar aromatic heads being tolerated better in human nNOS with **14**, where a polar 3-cyanophenyl with a shorter 4-atom linker between the arene and the pyrimidine head, demonstrated a 138 nM binding affinity for human nNOS, while a 183 nM binding affinity for rat nNOS. Thus, this is the first case of a potent human nNOS inhibitor from our lab, where the selectivity is reversed in preference toward its human isoform potency over the rat isoform. With a shorter linker, the cyanophenyl ring of **14** locates right outside the hydrophobic pocket in rat nNOS (Figure S7 in Supporting Information). The cyano group is in nonbonded contact with the Leu337 side chain. However, in human nNOS, the larger side chain of His342 is at the right distance for a hydrogen bond, as shown in Figure S8 in Supporting Information, which makes **14** a better inhibitor for human nNOS than rat nNOS. Therefore, these inhibitors clearly demonstrate that we can utilize the same pocket in the substrate access channel for both potency and selectivity determining factors in designing the NOS inhibitors.

Finally, with compounds **15**−**20**, we investigated variations in the 2-imidazolylpyrimidine part of the scaffold that may result in improving potency or minimizing off-target affinity. To this end, preliminary docking studies indicated that a 3,5-disubstituted pyridine could replace the 2,4-disubstituted pyrimidine in **8** and engage in a salt bridge formation with the Glu592 in the active site of nNOS, the same residue that forms crucial hydrogen bonds with the guanidine group of L-arginine or other arginine mimetics.[38] However, when **15** was assayed against nNOS, it showed a poor 5.5 μM inhibition against nNOS. Therefore, further variations on the imidazole ring fragment were made based on **9**, keeping the pyrimidine ring intact. We were interested from the literature examples of using of heme-nitrogenous ligands as inhibitors of aromatase enzymes for the treatment of breast cancer, and inhibitors of lanosterol demethylase enzymes as antifungal drugs.[39] Among the triazoles and methyl-substituted imidazoles incorporated as 2-pyrimidyl substituents in compounds **16**−**20**, both the 1,2,4- and 1,2,3-triazole-substituted scaffolds were poor inhibitors of nNOS, presumably because of a major depletion of the heme-Fe binding affinity by the electron-deficient triazoles. Among the substituted imidazoles, only (5-methyl)-2-imidazolylpyrimidine (**20**) retained very high potency against nNOS, and along with high selectivity against eNOS, it demonstrated a remarkably high 400-fold selectivity against iNOS as well, in sharp contrast to all the imidazole-substituted inhibitors mentioned previously. This presumably arises from the residues

DOI: 10.1021/jm501719e
J. Med. Chem. 2015, 58, 1067−1088

lining the active site over the heme-porphyrin, which makes a smaller and less flexible pocket in iNOS compared to nNOS.[28] This pocket is surrounded by Pro565, Val567, and Phe584 from two β-strands in rat nNOS (Figure 8A), but by Pro344, Val346, and Phe363 in murine iNOS. While residues facing the heme are conserved, the residue that stabilizes the second β-strand is Ser585 in nNOS and Asn364 in iNOS. Asn364 is involved in more hydrogen bonds than Ser585, which should help rigidify this part of the structure; however, the Asn364 polypeptide chain in iNOS also shrinks the active site pocket to accommodate its larger side chain compared to Ser585 in nNOS. The crystal structure of **20** bound to nNOS (Figure 8A) shows that the methyl group sticks in to this pocket just described, and the imidazole ring is bent away from the pyrimidine ring plane at a larger angle than usual because of steric hindrance between the pyrimidine ring and the methyl group. Therefore, the methyl group might create some clashes in the active site pocket of iNOS, thereby making it a very poor iNOS inhibitor. On the other hand, the 257-fold selectivity of **20** against eNOS stems from different structural features at the other end of inhibitor. Similar to parent compound **9**, the fluorophenyl ring of **20** in eNOS (Figure 8B) cannot insert into the hydrophobic pocket on the far end of the substrate access channel. Thus, lack of good van der Waals contacts in the pocket in eNOS compared to those encountered by **20** in nNOS leads to poorer affinity for eNOS.

Encouraged by the high nNOS affinity and good isoform selectivities of several compounds in this series, as one of the lead nNOS inhibitors, **9** was subjected to a Caco-2 monolayer permeability assay (Table 3). The Caco-2 cell line is a human

Table 3. Caco-2 Permeability Assay for 9[a]

	apparent permeability (P_{app}, 10^{-6} cm s^{-1})[b]			recovery	
compd	mean A→B	mean B→A	efflux ratio[c]	A→B (%)	B→A (%)
9	17.8	32.4	1.8	73	83
ranitidine[d]	0.18	1.6	8.9		
warfarin[e]	53.4	13.2	0.2		
talinolol[f]	0.11	11.0	100.0		

[a]All assays were performed over 2 h at 10 μM concentration. [b]P_{app}: apparent permeability rate coefficient. [c]Efflux ratio: P_{app} (B→A)/P_{app} (A→B). [d]Low permeability control. [e]High permeability control. [f]High efflux control.

intestinal epithelial line used to approximate the compound's permeabililty in the gastrointestinal tract as well as the blood–brain barrier.[25] Compound **9** showed good cellular permeability, thus reflecting a better potential for oral bioavailability. In addition, the efflux ratio of **9** was below 2, which indicates that it is likely not a favorable substrate for P-gp or any active transport system that might shuttle it out of the cells.

We also sought to determine the off-target effects of **9** against a panel of 50 CNS receptors, which included G-protein coupled receptors such as the serotonin, adrenergic, dopamine, and histamine receptors, as well as muscarinic and σ receptors.[40] Compound **9** showed significant inhibition (>75%) at a high 10 μM concentration in a primary binding assay only at the following targets: human serotonin 5-HT1A and 5-HT2A (83 and 88%), adrenergic α-2C (95%), σ-1 and -2 receptors (94 and 88%), and dopamine D3 receptor (87%). Therefore, a consecutive secondary binding assay on these targets were evaluated, which revealed a binding affinity (K_i) of ~0.2 μM only for α-2C and σ receptors, while the rest were 0.5 μM or higher. So, even a 0.2 μM off-target affinity holds 10-fold selectivity (relative to the nNOS K_i), which nonetheless is about 7% of the total receptors assayed. Thus, overall **9** displays a good safety profile, which is very promising for further development of this class of scaffolds.

Finally, the presence of a heme-coordinating group increases the likelihood of these compound's ability to inhibit cytochromes P450 (CYPs), the xenobiotic-metabolizing enzymes in humans. Therefore, **9** was evaluated against five major human liver microsomal P450s and, at 10 μM concentration, was found to decrease the activity of CYP2C19, CYP2D6, and CYP3A4 by more than 70%. Because CYP3A4 is the major liver and intestinal P450 that metabolizes the majority of drugs,[41] we determined IC_{50} values for **9**, (*R*,*R*)-**12**, **13**, and **20** using an in vitro CYP3A4 activity assay and 7-benzyloxy-4-trifluoromethylcoumarin as a substrate (Table 4).

Table 4. Comparison of nNOS and CYP3A4 Binding Affinity of Selected Compounds[a]

compd	nNOS K_i (μM)	CYP3A4 IC_{50} (μM)	selectivity nNOS/CYP3A4
9	0.019	2.5 ± 0.5	132
(*R*,*R*)-**12**	0.018	0.3 ± 0.02	17
13	0.054	70 ± 5	1296
20	0.060	0.9 ± 0.08	15

[a]See Table 1 and Experimental Section for details. K_i values of nNOS are determined using the Cheng–Prusoff equation directly from IC_{50} values. IC_{50} values are the average of at least two replicates with nine data points; all experimental standard error values are less than 10%, and all correlation coefficients are >0.95.

Compound **9** displayed moderate inhibitory potency for CYP3A4 (IC_{50} of 2.5 μM) and maintained >130-fold selectivity toward nNOS. When hydrophobicity in the molecules is increased through the cyclopropane ring insertion or methyl substitution of the imidazole in (*R*,*R*)-**12** and **20**, respectively, the CYP3A4 inhibitory potency is substantially increased (IC_{50} <1 μM). This is understandable given the bigger and more hydrophobic active site of CYP3A4 that preferably binds large, nonpolar molecules. The more polar and potent human nNOS inhibitor **13** acts as a weak CYP3A4 inactivator (IC_{50} of 70 μM), which suggests that modulation of hydrophobicity and bulkiness of compounds containing the heme-coordinating group can attenuate CYP inhibition, even with the presence of heme-ligating groups like imidazole.

CONCLUSIONS

We have designed and synthesized a new series of 2,4-disubstituted pyrimidine scaffolds by exploiting the much less-explored heme coordinating ability of inhibitors in the active site of NOS. This design was based on the rationale that 2-imidazolylpyrimidines might bind and inhibit nNOS with groups that are less polar and less basic than the 2-aminopyridines and therefore more bioavailable. We also speculated that by modulating other parts of the inhibitor molecule, we would be able to incorporate selectivity into the inhibitor against other NOS isozymes and heme-containing CYP enzymes. Indeed, we were able to obtain 2,4-disusbtituted pyrimidines that are highly potent inhibitors of nNOS, as shown by its low nanomolar binding affinity to both rat and

DOI: 10.1021/jm501719e
J. Med. Chem. 2015, 58, 1067–1088

human nNOS, and >200-fold and >100-fold selectivity over eNOS and iNOS, respectively. Crystal structures of the compounds bound to both rat and human nNOS indicate heme-Fe coordination by the 2-imidazolyl fragment, and the noncoordinating aryl rings are stabilized in a hydrophobic pocket at the far end of the substrate access channel. Access to this pocket is important for gaining inhibitory potency in both rat and human nNOS isoforms (via extensive van der Waals contacts and polar interactions) and isoform selectivity (owing to the sequence diversity in the pocket among NOS isoforms). Very promising compounds that came from this study were **9**, (*R*,*R*)-**12**, and **13**, which showed good Caco-2 permeability, minimal off-target binding efficacy, and good selectivity. Even with the presence of imidazole rings, CYP3A4 inhibition could be attenuated by modifications to other parts of the molecule. Therefore, these results exhibit high potential among these compounds to be orally bioavailable and brain permeable. Hence, further developments of these compounds are currently in progress.

EXPERIMENTAL SECTION

General Methods. Anhydrous solvents were purified by passage through a solvent column composed of activated alumina and a supported copper redox catalyst. All remaining solvents and reagents were purchased from commercial vendors and used without further purification. Moisture or oxygen-sensitive reactions were performed under an atmosphere of dry N_2 or argon. Analytical thin-layer chromatography was performed on Silicycle precoated silica gel 60 Å F254 plates. An Agilent 971-FP flash purification system with various SiliaSep (Silicycle, 40−63 μm, 60 Å) prepacked silica gel cartridges was used for flash column chromatography. ^{1}H NMR and ^{13}C NMR spectra were recorded at 500 and 126 MHz respectively on a Bruker Avance-III instrument. Low-resolution ESIMS was performed on a Thermo Finnigan LCQ or Bruker Amazon SL mass spectrometer consisting of an electrospray ionization (ESI) source. High-resolution mass spectral data were obtained at the Integrated Molecular Structure Education and Research Facility (Northwestern University) on an Agilent 6210A TOF mass spectrometer in positive ion mode using electrospray ionization, with an Agilent G1312A HPLC pump and an Agilent G1367B autoinjector. The purity of the compounds was evaluated on a Beckman Gold reverse phase analytical HPLC system using a Phenonemex Gemini C-18 (4.6 mm × 250 mm, 5 μm) reverse phase column with UV absorbance and evaporative light scattering detection. Purities of all final compounds that were subjected to enzymatic assays were found to be >95%. Preparative HPLC was performed at the Northwestern University Center for Molecular Innovation and Drug Discovery ChemCore lab, using an Agilent 1200 series HPLC and Agilent 6120 quadrupole mass spectrometer (API-MS mode), and a Phenomenex Gemini-NX 5 μm C18 column (150 mm × 21.2 mm). Chiral HPLC to determine enantiopurity of precursors of racemic and enantiomers of **11** was performed on an Agilent 1260 Series HPLC using a 0.46 cm × 25 cm Chiralpak AD-H column, with hexanes and 2-propanol (isocratic 10% 2-propanol in hexanes) as the mobile phases, and the flow rate of 0.5 mL/min with UV detection. 4-Chloro-2-methanesulfonyl pyrimidine,[27b] **24**, **25**, **26**,[30] **40**,[32] **65**,[42] and **66**[43] were synthesized following previously reported procedures. Syntheses of the remaining primary amines are detailed in Supporting Information.

*4-[4-(3-Fluorophenethyl)-1-piperazyl]-2-(1H-imidazol-1-yl)-pyrimidine (**4**).* To a solution of **22** (0.152 g, 0.729 mmol) in MeCN (4 mL), 4-chloro-2-methanesulfonyl pyrimidine (0.14 g, 0.729 mmol) and K_2CO_3 (0.21 g, 1.522 mmol) were added. The mixture was heated at 40 °C for 19 h and monitored by TLC for complete consumption of **22**. Then, imidazole (0.248 g, 3.645 mmol) was added and the resulting mixture heated at 65 °C for an additional 30 h. The mixture was cooled, diluted in CH_2Cl_2 (40 mL), washed with H_2O (2 × 30 mL), and the organic layer dried over anhydrous sodium sulfate. The solution was concentrated, and the resulting crude oil was purified by flash chromatography (CH_2Cl_2/MeOH) to yield **4** as clear sticky oil (0.289 g, 82%). ^{1}H NMR (500 MHz; $CDCl_3$): δ 8.51 (s, 1 H), 8.13 (d, *J* = 6.2 Hz, 1 H), 7.80 (s, 1 H), 7.26−7.21 (m, 1 H), 7.10 (s, 1 H), 6.98 (d, *J* = 7.8 Hz, 1 H), 6.94−6.86 (m, 2 H), 6.36 (d, *J* = 6.2 Hz, 1 H), 3.71 (s, 4 H), 2.82 (t, *J* = 10.5, 8.6 Hz, 2 H), 2.64 (dd, *J* = 10.1, 8.3 Hz, 2 H), 2.59 (t, *J* = 5.2 Hz, 4 H). ^{13}C NMR (126 MHz; $CDCl_3$): δ (163.74, 161.79, d, *J* = 245.9 Hz, 1 C), 162.1, 156.7, 154.1, (142.43, 142.37, d, *J* = 7.3 Hz, 1 C), 136.0, 129.9, (129.81, 129.74, d, *J* = 8.4 Hz, 1 C), (124.27, 124.25, d, *J* = 2.5 Hz, 1 C), 116.5, (115.53, 115.36, d, *J* = 21.0 Hz, 1 C), (113.08, 112.92, d, *J* = 21.0 Hz, 1 C), 100.5, 59.7, 53.4, 43.8, 33.2. HRMS (ESI): calcd for $C_{19}H_{22}FN_6$ $[M + H]^+$, 353.1884; found, 353.1887.

*N^1-[2-(1H-Imidazol-1-yl)pyrimidin-4-yl]-N^2-(3-fluorophenethyl)-ethane-1,2-diamine Trihydrochloride (**5**).* Compound **26** (0.146 g, 0.516 mmol) was diluted with MeCN (3 mL), followed by addition of 4-chloro-2-methanesulfonyl pyrimidine (0.1 g, 0.516 mmol) and K_2CO_3 (0.143 g, 1.033 mmol) and heated at 40 °C for 19 h. Imidazole (0.176 g, 2.583 mmol) was added to the resulting mixture, and heating continued at 65 °C for another 30 h. The mixture was cooled, diluted in CH_2Cl_2 (30 mL), washed with H_2O (2 × 20 mL), and the organic layer dried over anhydrous sodium sulfate. The solution was concentrated, and the resulting crude oil was purified by flash chromatography (EtOAc/MeOH) to yield the Boc-protected precursor of **5** as a clear sticky oil (0.132 g, 60%). This intermediate Boc-protected carbamate was dissolved in CH_2Cl_2 (3 mL), cooled to 0 °C, and trifluoroacetic acid was added (1.5 mL) to it. The resulting solution was stirred at room temperature for 2 h, when it was diluted with more CH_2Cl_2 (15 mL), and treated slowly with saturated K_2CO_3 (10 mL). The layers were separated, and the aqueous layer was extracted with CH_2Cl_2 (2 × 10 mL). The combined organic layers were dried with anhydrous sodium sulfate, concentrated, and chromatographed with EtOAc/MeOH to give an oily residue. Methanolic HCl (∼2 M, 2 mL) was added to the residue, stirred for 10 min, concentrated to 1 mL, and treated with excess Et_2O, when a white crystalline precipitate formed. The solid was collected by filtration and dried to obtain **5** as a white crystalline solid (0.11 g, 83%); mp = 208−210 °C. ^{1}H NMR (500 MHz; DMSO-d_6): δ 10.32 (s, 1 H), 9.49 (s, 2 H), 8.66 (t, *J* = 6.0 Hz, 1 H), 8.52 (t, *J* = 1.8 Hz, 1 H), 8.22 (d, *J* = 6.0 Hz, 1 H), 7.89 (t, *J* = 1.7 Hz, 1 H), 7.39 (td, *J* = 7.9, 6.3 Hz, 1 H), 7.19−7.07 (m, 3 H), 6.69 (d, *J* = 6.0 Hz, 1 H), 3.90−3.86 (m, 2 H), 3.23 (dq, *J* = 11.4, 6.3 Hz, 2 H), 3.18−3.14 (m, 2 H), 3.06 (dd, *J* = 9.7, 6.5 Hz, 2 H), 1.30 (dd, *J* = 15.1, 6.8 Hz, 2 H). ^{13}C NMR (126 MHz; DMSO-d_6): δ (164.16, 162.23, d, *J* = 243.9 Hz, 1 C), 164.1, 155.8, 153.1, (141.09, 141.00, d, *J* = 11.3 Hz, 1 C), 136.2, (131.52, 131.46, d, *J* = 7.6 Hz, 1 C), (125.79, 125.78, d, *J* = 1.3 Hz, 1 C), 122.1, 119.7, (116.48, 116.31, d, *J* = 21.4 Hz, 1 C), (114.69, 114.48, *J* = 26.4 Hz, 1 C), 107.7, 48.4, 46.7, 37.2, 32.0. HRMS (ESI): calcd for $C_{17}H_{20}FN_6$ $[M + H]^+$, 327.1728; found, 327.1731.

*N-[2-(1H-Imidazol-1-yl)-4-pyrimidylmethyl]-2-(3-fluorophenyl)-ethan-1-amine Dihydrochloride (**6**).* General method A for trifluoroacetic acid mediated Boc-group deprotection: Compound **37** (0.257 g, 0.647 mmol) was diluted in CH_2Cl_2 (5.5 mL) and cooled to 0 °C. Trifluoroacetic acid (2.75 mL) was added to the resulting solution and stirred at room temperature for 3 h. The reaction mixture was diluted with more CH_2Cl_2 (25 mL) and treated with saturated K_2CO_3 (15 mL). The layers were separated, and the aqueous layer was extracted again with CH_2Cl_2 (2 × 15 mL). The organics together were dried over sodium sulfate and concentrated. The resulting oily residue was purified by flash column chromatography (CH_2Cl_2/MeOH) to give the free base of **6** as a yellow oil. The oil was treated with methanolic HCl (∼2 M, 2 mL) for 10 min, when a white precipitate started forming. This suspension was concentrated to ∼0.5 mL and treated with excess Et_2O and sonicated. The white solid was filtered, washed twice with Et_2O, and dried to give a white amorphous solid of **6** as a dihydrochloride salt (0.223 g, 93%); mp = 220−222 °C. ^{1}H NMR (500 MHz, DMSO-d_6): δ 10.07 (s, 2 H), 10.02 (s, 1 H) 9.05 (d, *J* = 5.1 Hz, 1 H), 8.57 (s, 1 H), 7.78 (d, *J* = 5.0 Hz, 2 H), 7.44−7.37 (m, 1 H), 7.21−7.09 (m, 3 H), 4.61 (t, *J* = 5.2 Hz, 2 H), 4.01 (br s, 1 H), 3.39−3.28 (m, 2 H), 3.24−3.15 (m, 2 H). ^{13}C NMR (126 MHz;

DOI: 10.1021/jm501719e
J. Med. Chem. 2015, 58, 1067−1088

DMSO-d_6): δ 164.8, (164.17, 162.23, d, J = 244.4 Hz, 1 C), 161.2, 153.4, (141.05, 140.99, J = 7.6 Hz, 1 C), 136.9, (131.51, 131.44, d, J = 8.8 Hz, 1 C), (125.80, 125.78, d, J = 2.5 Hz, 1 C), 125.1, 120.7, 119.3, (116.48, 116.31, d, J = 21.4 Hz, 1 C), (114.68, 114.45, d, J = 29 Hz, 1 C), 49.7, 48.2, 31.9. HRMS (ESI): calcd for $C_{16}H_{17}FN_5$ $[M + H]^+$, 298.1463; found, 298.1462.

*N-[2-(1H-Imidazol-1-yl)-4-pyrimidylmethyl]-3-(3-fluorophenyl)-propan-1-amine Dihydrochloride (**7**).* Compound **7** was obtained as a white solid in its dihydrochloride salt form (0.37 g, 79%) from **38** (0.502 g, 1.22 mmol) following general method A; mp = 153−155 °C. ^{1}H NMR (500 MHz, DMSO-d_6): δ 9.61 (br s, 3 H), 9.01 (d, J = 4.9 Hz, 1 H), 8.40 (s, 1 H), 7.69 (d, J = 4.6 Hz, 1 H), 7.60 (s, 1 H), 7.40−7.34 (m, 1 H), 7.14−7.05 (m, 3 H), 4.57 (t, J = 5.5 Hz, 2 H), 3.69 (br s, 1 H), 3.09−3.03 (m, 2 H), 2.74 (t, J = 7.6 Hz, 2 H), 2.16−2.00 (m, 2 H). ^{13}C NMR (126 MHz; DMSO-d_6): δ 168.0, 164.9, (164.26, 162.32, d, J = 244.44, 1 C), 161.3, 153.7, (144.75, 144.69, d, J = 7.56 Hz, 1 C), 137.1, (131.38, 131.31, d, J = 8.8 Hz, 1 C), (125.52, 125.5, d, J = 2.5 Hz, 1 C), 120.3, 119.0, (116.14, 115.97, d, J = 21.42 Hz, 1 C), (114.03, 113.86, d, J = 21.42 Hz, 1 C), 49.7, 47.3, 32.5, 27.7. HRMS (ESI): calcd for $C_{17}H_{19}FN_5$ $[M + H]^+$, 312.1619; found, 312.1625.

*2-[2-(1H-Imidazol-1-yl)pyrimidin-4-yl]-N-(3-fluorophenethyl)-ethan-1-amine Dihydrochloride (**8**).* Compound **8** was obtained as a pale cream-colored amorphous solid (0.182 g, 80%) from **55** (0.244 g, 0.594 mmol) following general method A; mp = 200−201 °C. ^{1}H NMR (500 MHz, DMSO-d_6): δ 9.88 (s, 1 H), 9.39 (s, 2 H), 8.94 (d, J = 5.1 Hz, 1 H), 8.44 (s, 1 H), 7.82 (s, 1 H), 7.70 (d, J = 5.1 Hz, 1 H), 7.42 (q, J = 7.8 Hz, 1 H), 7.28−7.05 (m, 3 H), 4.08 (br s, 1 H), 3.56−3.53 (m, 2 H), 3.39 (t, J = 6.9 Hz, 2 H), 3.31−3.25 (m, 2 H), 3.13−3.03 (m, 2 H). ^{13}C NMR (126 MHz, DMSO-d_6): δ 170.1, (164.26, 162.32, d, J = 244.44 Hz, 1 C), 160.5, 153.5, (141.21, 141.15, d, J = 7.56 Hz, 1 C), 136.6, (131.63, 131.56, d, J = 8.82 Hz, 1 C), 125.9, 125.8, (122.23, 122.19, d, J = 5.0 Hz, 1 C), 119.4, (116.57, 116.40, d, J = 21.42 Hz, 1 C), (114.74, 114.57, d, J = 21.42 Hz, 1 C), 48.5, 44.9, 33.4, 32.0. HRMS (ESI): calcd for $C_{17}H_{19}FN_5$ $[M + H]^+$, 312.1619; found, 312.1622.

*N-2-[2-(1H-Imidazol-1-yl)pyrimidin-4-yl]ethyl-3-(3-fluorophenyl)-propan-1-amine Dihydrochloride (**9**).* Title compound **9** was obtained as a white amorphous solid (0.385 g, 89%) from **56** (0.462 g, 1.086 mmol) following general method A; mp = 196−198 °C. ^{1}H NMR (500 MHz, DMSO-d_6): δ 9.94 (s, 1 H), 9.39 (s, 2 H), 8.94 (d, J = 5.1 Hz, 1 H), 8.45 (s, 1 H), 7.85 (s, 1 H), 7.70 (d, J = 5.1 Hz, 1 H), 7.37 (q, J = 7.9 Hz, 1 H), 7.12 (t, J = 8.4 Hz, 2 H), 7.06 (td, J = 8.9, 2.3 Hz, 1 H), 4.25 (br s, 1 H), 3.53−3.48 (m, 2 H), 3.43−3.37 (m, 2 H), 3.0−2.94 (m, 2 H), 2.74 (t, J = 7.6 Hz, 2 H), 2.03 (p, J = 8.2 Hz, 2 H). ^{13}C NMR (126 MHz, DMSO-d_6): δ 170.2, (164.17, 162.24, d, J = 243.18 Hz, 1 C), 160.4, 153.3, (144.72, 144.66, d, J = 7.56 Hz, 1 C), 136.5, (131.29, 131.22, d, J = 8.82 Hz, 1 C), (125.44, 125.42, d, J = 2.52 Hz, 1 C), 123.9, 122.3, 119.5, (116.07, 115.91, d, J = 20.16 Hz, 1 C), (113.92, 113.75, d, J = 21.42 Hz, 1 C), 47.3, 44.7, 33.4, 32.6, 27.7. HRMS (ESI): calcd for $C_{18}H_{21}FN_5$ $[M + H]^+$, 326.1776; found, 326.1779.

*N-2-[2-(1H-Imidazol-1-yl)pyrimidin-4-yl]ethyl-3-(3-chlorophenyl)-propan-1-amine Dihydrochloride (**10**).* Compound **10** was synthesized as a white amorphous solid (0.5 g, 99%) from **57** (0.541 g, 1.224 mmol) following general method A; mp = 184−186 °C. ^{1}H NMR (500 MHz, DMSO-d_6): δ 10.03 (s, 1 H), 9.59 (s, 2 H), 8.94 (d, J = 5.1 Hz, 1 H), 8.47 (s, 1 H), 7.88 (s, 1 H), 7.71 (d, J = 5.1 Hz, 1 H), 7.39−7.32 (m, 2 H), 7.29 (d, J = 8.2 Hz, 1 H), 7.24 (d, J = 7.6 Hz, 1 H), 4.01 (s, 1 H), 3.53−3.47 (m, 2 H), 3.45−3.36 (m, 2 H), 2.99−2.93 (m, 2 H), 2.73 (t, J = 7.6 Hz, 2 H), 2.04 (p, J = 7.8 Hz, 2 H). ^{13}C NMR (126 MHz, DMSO-d_6): δ 170.2, 160.4, 153.2, 144.4, 136.3, 133.9, 131.2, 129.1, 128.0, 127.0, 123.2, 122.4, 119.6, 47.3, 44.7, 33.4, 32.5, 27.6. HRMS (ESI): calcd for $C_{18}H_{21}ClN_5$ $[M + H]^+$, 342.1480; found, 342.1483.

*2-[2-(1H-Imidazol-1-yl)pyrimidin-4-yl]-N-[2-(3-fluorophenyl)-cyclopropylmethyl]ethan-1-amine Dihydrochloride (**11**).* Compound **11** was prepared from **58** (0.25 g, 0.571 mmol) as an off-white amorphous dihydrochloride salt (0.206 g, 88%) following general method A; mp = 198−200 °C. ^{1}H NMR (500 MHz, DMSO-d_6): δ 10.00 (s, 1 H), 9.58 (s, 1 H), 9.49 (s, 1 H), 8.94 (d, J = 5.1 Hz, 1 H), 8.43 (s, 1 H), 7.88 (s, 1 H), 7.71 (d, J = 5.1 Hz, 1 H), 7.31 (q, J = 7.9 Hz, 1 H), 7.07−6.97 (m, 3 H), 4.48 (br s, 1 H), 3.59−3.50 (m, 2 H), 3.44−3.39 (m, 2 H), 3.18−3.15 (m, 1 H), 3.01−2.96 (m, 1 H), 2.21 (dt, J = 9.2, 5.2 Hz, 1 H), 1.49 (dq, J = 12.5, 7.9 Hz, 1 H), 1.22−1.09 (m, 2 H). ^{13}C NMR (126 MHz, DMSO-d_6): δ 170.2, (164.21, 162.28, d, J = 243.18 Hz, 1 C), 160.4, 153.2, (145.83, 145.77, d, J = 7.56 Hz, 1 C), 136.3, (131.0, 130.93, d, J = 8.82 Hz, 1 C), 123.4, (123.03, 123.01, d, J = 2.52 Hz, 1 C), 122.4, 119.5, (113.63, 113.46, d, J = 21.42 Hz, 1 C), (113.40, 113.24, d, J = 20.16 Hz, 1 C), 51.2, 44.2, 33.3, 22.6, 20.0, 15.4. HRMS (ESI): calcd for $C_{19}H_{21}FN_5$ $[M + H]^+$, 338.1776; found, 338.1778.

*N-2-[2-(1H-Imidazol-1-yl)pyrimidin-4-yl]ethyl-2-(3-fluorobenzyl)-cyclopropan-1-amine Dihydrochloride (**12**).* Compound **12** was synthesized as a white amorphous solid (0.256 g, 93%) from **59** (0.294 g, 0.672 mmol) following general method A; mp = 210−212 °C. ^{1}H NMR (500 MHz, DMSO-d_6): δ 9.85 (s, 1 H), 9.69 (s, 1 H), 9.60 (s, 1 H), 8.93 (d, J = 5.1 Hz, 1 H), 8.39 (s, 1 H), 7.82 (s, 1 H), 7.65 (d, J = 5.1 Hz, 1 H), 7.37 (td, J = 8.0, 6.4 Hz, 1 H), 7.22−7.14 (m, 2 H), 7.05 (td, J = 8.4, 2.3 Hz, 1 H), 4.2 (br s, 1 H), 3.55−3.42 (m, 2 H), 3.33 (t, J = 7.2 Hz, 2 H), 2.77 (m, 1 H), 2.68−2.59 (m, 2 H), 1.73−1.66 (m, 1 H), 1.23 (ddd, J = 9.7, 5.7, 4.0 Hz, 1 H), 0.84 (q, J = 6.1 Hz, 1 H). ^{13}C NMR (126 MHz, DMSO-d_6): δ 170.0, (164.11, 162.17, d, J = 244.44, 1 C), 160.4, 153.4, (144.24, 144.18, d, J = 7.56 Hz, 1 C), 136.4, (131.21, 131.14, d, J = 8.82 Hz, 1 C), 125.5, 124.2, 122.1, 119.3, (116.16, 115.99, d, J = 21.42 Hz, 1 C), (113.97, 113.80, d, J = 21.42 Hz, 1 C), 45.3, 36.7, 35.8, 33.0, 18.6, 10.7. HRMS (ESI): calcd for $C_{19}H_{21}FN_5$ $[M + H]^+$, 338.1776; found, 338.1776.

*N-2-[2-(1H-Imidazol-1-yl)pyrimidin-4-yl]ethyl-3-(pyridin-3-yl)-propan-1-amine Trihydrochloride (**13**).* Title compound **13** was obtained as a trihydrochloride salt, and as a pale-green amorphous solid (0.26 g, 91%) from **60** (0.28 g, 0.684 mmol) following general method A; mp = 212−214 °C. ^{1}H NMR (500 MHz, DMSO-d_6): δ 10.12 (s, 1 H), 9.77 (s, 2 H), 8.97 (s, 1 H), 8.95 (d, J = 5.1 Hz, 1 H), 8.85 (d, J = 5.4 Hz, 1 H), 8.61 (d, J = 7.8 Hz, 1 H), 8.50 (s, 1 H), 8.07 (dd, J = 6, 7.5 Hz, 1 H), 7.92 (s, 1 H), 7.73 (d, J = 5.1 Hz, 1 H), 3.56−3.39 (m, 4 H), 3.02−2.99 (m, 4 H), 2.15 (p, J = 7.4 Hz, 2 H). Note that the pyridinium and the imidazolium protons appear very broad on the baseline due to exchange with solvent. ^{13}C NMR (126 MHz, DMSO-d_6): δ 170.3, 160.4, 153.1, 147.0, 141.9, 141.8, 140.4, 136.3, 127.9, 122.7, 122.5, 119.7, 46.8, 44.7, 33.3, 29.5, 26.9. HRMS (ESI): calcd for $C_{17}H_{21}N_6$ $[M + H]^+$, 309.1822; found, 309.1824.

*2-[2-(1H-Imidazol-1-yl)pyrimidin-4-yl]-N-(3-cyanobenzyl)ethan-1-amine Dihydrochloride (**14**).* Compound **14** was synthesized as a white amorphous solid (0.277 g, 95%) from **61** (0.313 g, 0.774 mmol) following general method A; mp = 220−222 °C. ^{1}H NMR (500 MHz, DMSO-d_6): δ 9.93 (br s, 3 H), 8.93 (d, J = 5.1 Hz, 1 H), 8.41 (s, 1 H), 8.17 (s, 1 H), 8.02 (d, J = 7.9 Hz, 1 H), 7.92 (d, J = 7.8 Hz, 1 H), 7.85 (s, 1 H), 7.72−7.66 (m, 2 H), 4.33 (t, J = 5.3 Hz, 2 H), 3.58−3.49 (m, 2 H), 3.44 (t, J = 7.0 Hz, 2 H). Note that the imidazolium proton appears very broad on the baseline due to exchange with solvent. ^{13}C NMR (126 MHz, DMSO-d_6): δ 170.0, 160.4, 153.3, 136.4, 136.1, 134.9, 134.5, 133.5, 130.7, 123.8, 122.3, 119.4, 119.3, 112.3, 50.0, 44.5, 33.2. HRMS (ESI): calcd for $C_{17}H_{17}N_6$ $[M + H]^+$, 305.1509; found, 305.1512.

*2-[5-(1H-Imidazol-1-yl)pyridin-3-yl]-N-(3-fluorophenethyl)ethan-1-amine Trihydrochloride (**15**).* Compound **15** was obtained as a white amorphous solid (0.260 g, 88%) from **68** (0.288 g, 0.704 mmol) following general method A; mp = 230−232 °C. ^{1}H NMR (500 MHz, DMSO-d_6): δ 9.96 (s, 1 H), 9.61 (s, 2 H), 9.02 (d, J = 2.4 Hz, 1 H), 8.73 (d, J = 1.4 Hz, 1 H), 8.47 (t, J = 1.6 Hz, 1 H), 8.42 (t, J = 2.0 Hz, 1 H), 8.02 (s, 1 H), 7.42 (td, J = 7.9, 6.5 Hz, 1 H), 7.19 (dd, J = 10.0, 1.9 Hz, 1 H), 7.16 (d, J = 7.7 Hz, 1 H), 7.13 (td, J = 8.7, 2.5 Hz, 1 H), 5.57 (s, 2 H), 3.36 (dt, J = 11.9, 6.8 Hz, 2 H), 3.27−3.19 (m, 4 H), 3.15−3.03 (m, 2 H). ^{13}C NMR (126 MHz, DMSO-d_6): δ (164.19, 162.25, d, J = 244.44 Hz, 1 C), 151.3, 142.2, (141.18, 141.12, d, J = 7.56 Hz, 1 C), 136.0, 135.2, 132.6, 131.6, (131.56, 131.49, d, J = 8.82 Hz, 1 C), 125.8, 122.1, 121.9, (116.50, 116.34, d, J = 20.16 Hz, 1 C), (114.65, 114.49, d, J = 20.16 Hz, 1 C), 48.3, 47.4, 31.9, 29.1. HRMS (ESI): calcd for $C_{18}H_{20}FN_4$ $[M + H]^+$, 311.1667; found, 311.1673.

DOI: 10.1021/jm501719e
J. Med. Chem. 2015, 58, 1067−1088

*N-2-[2-(1H-1,2,3-Triazol-1-yl)pyrimidin-4-yl]ethyl-3-(3-fluorophenyl)propan-1-amine Dihydrochloride (**16**).* Title compound **16** was obtained as a pale-yellow hygroscopic solid (0.186 g, 89%) from **69** (0.224 g, 0.525 mmol) following general method A. ^{1}H NMR (500 MHz, DMSO-d_6): δ 8.94 (d, J = 5.0 Hz, 1 H), 8.69 (br s, 2 H), 8.25 (s, 2 H), 7.64 (d, J = 5.0 Hz, 1 H), 7.38 (q, J = 7.9 Hz, 1 H), 7.16−7.00 (m, 3 H), 3.62 (br s, 1 H), 3.54−3.47 (m, 2 H), 3.30−3.27 (m, 2 H), 3.05−3.02 (m, 2 H), 2.74−2.70 (m, 2 H), 1.99−1.96 (m, 2 H). ^{13}C NMR (126 MHz, DMSO-d_6): δ 169.6, (164.16, 162.22, d, J = 244.44 Hz, 1 C), 160.5, 155.7, (144.56, 144.52, d, J = 5.04 Hz, 1 C), 138.9, (131.27, 131.21, d, J = 7.56 Hz, 1 C), (125.37, 125.35, d, J = 2.52 Hz, 1 C), 121.5, (116.00, 115.83, d, J = 21.42 Hz, 1 C), (113.92, 113.75, d, J = 21.42 Hz, 1 C), 47.3, 45.5, 33.6, 32.4, 27.8. HRMS (ESI): calcd for $C_{17}H_{20}FN_6$ [M + H]$^+$, 327.1728; found, 327.1735.

*N-2-[2-(1H-1,2,4-Triazol-1-yl)pyrimidin-4-yl]ethyl-3-(3-fluorophenyl)propan-1-amine Dihydrochloride (**17**).* Compound **17** was obtained as a white amorphous solid in its dihydrochloride form (0.125 g, 99%) from **70** (0.135 g, 0.316 mmol) following general method A; mp = 177−179 °C. ^{1}H NMR (500 MHz, DMSO-d_6): δ 9.56 (s, 1 H), 9.20 (s, 2 H), 8.89 (d, J = 5.1 Hz, 1 H), 8.35 (s, 1 H), 7.60 (d, J = 5.1 Hz, 1 H), 7.37 (td, J = 8.0, 6.4 Hz, 1 H), 7.15−7.08 (m, 2 H), 7.06 (td, J = 8.8, 2.5 Hz, 1 H), 6.29 (br s, 1 H), 3.46 (p, J = 7.0 Hz, 2 H), 3.33 (t, J = 7.2 Hz, 2 H), 2.99 (dt, J = 12.3, 6.3 Hz, 2 H), 2.74 (t, J = 7.6 Hz, 2 H), 2.01 (p, J = 7.8 Hz, 2 H). ^{13}C NMR (126 MHz, DMSO-d_6): δ 169.7, (164.15, 162.22, d, J = 243.18, 1 C), 160.4, 154.6, 154.3, 145.6, (144.67, 144.61, d, J = 7.56 Hz, 1 C), (131.24, 131.18, d, J = 7.56 Hz, 1 C), (125.38, 125.36, d, J = 2.52 Hz, 1 C), 121.3, (116.02, 115.85, d, J = 21.42 Hz, 1 C), (113.88, 113.71, d, J = 21.42 Hz, 1 C0, 47.2, 45.0, 33.4, 32.5, 27.7. HRMS (ESI): calcd for $C_{17}H_{20}FN_6$ [M + H]$^+$, 327.1728; found, 327.1728.

*3-(3-Fluorophenyl)-N-2-[2-(2-methyl-1H-imidazol-1-yl)pyrimidin-4-yl]ethylpropan-1-amine Dihydrochloride (**18**).* Compound **18** was prepared from **71** (0.141 g, 0.32 mmol) following general method A to give the dihydrochloride salt, which was obtained as an off-white hygroscopic solid (0.115 g, 87%). ^{1}H NMR (500 MHz, DMSO-d_6): δ 9.33 (s, 2 H), 8.98 (d, J = 5.1 Hz, 1 H), 8.36 (d, J = 2.2 Hz, 1 H), 7.79 (d, J = 2.1 Hz, 1 H), 7.73 (d, J = 5.1 Hz, 1 H), 7.38 (td, J = 8.0, 6.5 Hz, 1 H), 7.16−7.09 (m, 2 H), 7.07 (td, J = 8.8, 2.3 Hz, 1 H), 3.51 (br s, 1 H), 3.40−3.37 (m, 4 H), 3.02 (s, 3 H), 2.99−2.94 (m, 2 H), 2.74 (t, J = 7.6 Hz, 2 H), 2.01 (p, J = 7.8 Hz, 2 H). ^{13}C NMR (126 MHz, DMSO-d_6): δ 169.9, (164.14, 162.21, d, J = 243.18, 1 C), 160.3, 154.5, 147.4, (144.65, 144.59, d, J = 7.56 Hz, 1 C), (131.25, 131.18, d, J = 8.82 Hz, 1 C), 125.4, 122.0, 121.3, 119.7, (116.01, 115.84, d, J = 21.42 Hz, 1 C), (113.89, 113.72, d, J = 21.42, 1 C), 47.2, 45.0, 33.5, 32.5, 27.6, 15.8. HRMS (ESI): calcd for $C_{19}H_{23}FN_5$ [M + H]$^+$, 340.1932; found, 340.1933.

*3-(3-Fluorophenyl)-N-2-[2-(4-methyl-1H-imidazol-1-yl)pyrimidin-4-yl]ethylpropan-1-amine Dihydrochloride (**19**).* Compounds **19** and 3-(3-fluorophenyl)-*N*-2-[2-(5-methyl-1*H*-imidazol-1-yl)pyrimidin-4-yl]ethylpropan-1-amine dihydrochloride (**20**) were obtained in an inseparable 15:1 ratio (by ^{1}H NMR) from the reaction of 15:1 mixture of compounds **72** and **73** (0.668 g, 1.52 mmol) following general method A, as a white amorphous solid of the corresponding dihydrochloride salts (0.62 g, 99% total). This mixture was separated by preparative HPLC on an Agilent 1200 series instrument using a Phenomenex Gemini-NX 5 μm C18 column (150 mm × 21.2 mm), using a gradient of 1−15% MeCN in H_2O with 0.1% formic acid, to isolate **19** and **20** separately in >95% purity. Following this, **19** and **20** were converted to their corresponding dihydrochloride salts by similar precipitation with methanolic HCl and excess Et_2O.

*For **19**.* White amorphous solid; mp =2 03−205 °C. ^{1}H NMR (500 MHz, DMSO-d_6): δ 9.53 (s, 1 H), 8.95 (s, 2 H), 8.90 (d, J = 5.1 Hz, 1 H), 8.07 (s, 1 H), 7.62 (d, J = 5.1 Hz, 1 H), 7.38 (td, J = 8.0, 6.4 Hz, 1 H), 7.15−7.09 (m, 2 H), 7.07 (td, J = 8.9, 2.2 Hz, 1 H), 3.63 (br s, 1 H), 3.50 (dt, J = 12.8, 7.1 Hz, 2 H), 3.31 (t, J = 7.2 Hz, 2 H), 3.05−2.95 (m, 2 H), 2.73 (t, J = 7.6 Hz, 2 H), 2.34 (s, 3 H), 1.99 (p, J = 7.7 Hz, 2 H). ^{13}C NMR (126 MHz, DMSO-d_6): δ 170.0, (164.14, 162.21, d, J = 243.18 Hz, 1 C), 160.4, 153.2, (144.65, 144.60, d, J = 6.3 Hz, 1 C), 135.6, 133.4, (131.25, 131.18, d, J = 8.82 Hz, 1 C0, 125.4, 122.0, (116.01, 115.85, d, J = 20.16 Hz, 1 C), 115.8, (113.88, 113.71, d, J = 21.42 Hz, 1 C), 47.3, 44.7, 33.4, 32.5, 27.6, 11.3. HRMS (ESI): calcd for $C_{19}H_{23}FN_5$ [M + H]$^+$, 340.1932; found, 340.1937.

*For **20**.* Off-white hygroscopic solid. ^{1}H NMR (500 MHz, DMSO-d_6): δ 9.74 (s, 1 H), 9.25 (s, 2 H), 8.96 (d, J = 5.1 Hz, 1 H), 7.72 (d, J = 5.1 Hz, 1 H), 7.59 (s, 1 H), 7.43−7.32 (m, 1 H), 7.11 (t, J = 7.4 Hz, 2 H), 7.09−7.03 (m, 1 H), 3.68 (br s, 1 H), 3.48−3.43 (m, 2 H), 3.37 (q, J = 6.7 Hz, 2 H), 2.97 (dt, J = 14.9, 9.5 Hz, 2 H), 2.73 (t, J = 7.6 Hz, 2 H), 2.65 (s, 3 H), 2.05−1.97 (m, 2 H). ^{13}C NMR (126 MHz, DMSO-d_6): δ 169.9, (164.14, 162.21, d, J = 243.18 Hz, 1 C), 160.3, 154.7, (144.63, 144.57, d, J = 7.56 Hz, 1 C), 137.5, (131.25, 131.18, d, J = 8.82 Hz, 1 C), 131.1, (125.37, 125.35, d, J = 2.52 Hz, 1 C), 122.1, 121.1, (116.00, 115.84, d, J = 20.16 Hz, 1 C), (113.89, 113.72, d, J = 21.42 Hz, 1 C), 47.2, 45.0, 33.5, 32.5, 27.6, 13.13. HRMS (ESI): calcd for $C_{19}H_{23}FN_5$ [M + H]$^+$, 340.1932; found, 340.1937.

*1-(3-Fluorophenethyl)piperazine (**22**).* To a suspension of NaH (0.107 g, 2.686 mmol) in THF (4 mL) cooled to 0 °C, a solution of **21** (0.5 g, 2.686 mmol) in THF (2.5 mL) was added dropwise. The reaction was stirred at room temperature for 1 h followed by the addition of 2-(3-fluorophenyl)ethyl bromide (0.66 g, 3.242 mmol) in THF (2 mL) and a pinch of tetrabutylammonium iodide (~0.05 g, 0.13 mmol). The resulting solution was heated at 60 °C for 48 h, when it was cooled to room temperature and diluted with ethyl acetate (20 mL) and water (20 mL). The layers were separated, and the aqueous layer was washed with EtOAc (2 × 10 mL). The combined organic layers were washed with brine (20 mL), dried over sodium sulfate, and concentrated. The residue was purified by flash column chromatography (hexanes/EtOAc), and the resulting oil (0.464 g, 1.504 mmol, 56%) was diluted with CH_2Cl_2 (12 mL). This solution was cooled to 0 °C and treated with trifluoroacetic acid (6 mL). The reaction was stirred for 3 h at room temperature, after which it was concentrated. The residue was diluted with EtOAc (20 mL) and treated with saturated K_2CO_3 (15 mL). The organic layer was extracted, and the aqueous layer was re-extracted with more EtOAc (2 × 10 mL). The combined organic layers were dried and concentrated to yield a colorless oil (0.266 g, 85%), clean by NMR. ^{1}H NMR (500 MHz, $CDCl_3$): δ 7.22 (q, J = 7.2 Hz, 1H), 6.96 (d, J = 7.7 Hz, 1H), 6.92−6.85 (m, 2H), 3.98 (s, 1H), 2.96 (t, J = 5.0 Hz, 4H), 2.78 (dd, J = 11.2, 8.3 Hz, 2H), 2.58 (dd, J = 11.0, 8.5 Hz, 2H), 2.53 (s, 4H). ^{13}C NMR (126 MHz, $CDCl_3$): δ (163.75, 161.80, d, J = 245.7 Hz, 1 C), (142.71, 142.65, d, J = 7.56 Hz, 1 C), (129.75, 129.69, d, J = 7.56 Hz, 1 C), (124.29, 124.27, d, J = 2.52 Hz, 1 C), (115.55, 115.38, d, J = 21.42 Hz, 1 C), (112.98, 112.81, d, J = 21.42 Hz, 1 C), 60.4, 53.5, 45.5, 33.0.

*2-(3-Fluorophenyl)-N-[(2-methylthiopyrimidin-4-yl)methyl]-ethan-1-amine (**33**).* Compound **30** (0.2 g, 1.3 mmol) was added in CH_2Cl_2 (20 mL) to a flask containing oven-dried 3 Å molecular sieves. Compound **31** (0.17 mL, 0.18 g, 1.3 mmol) was added as a solution in CH_2Cl_2 (6 mL), followed by glacial acetic acid (20 μL). The mixture was stirred for 1.5 h and cooled to 0 °C, and sodium triacetoxyborohydride (0.413 g, 1.95 mmol) was added in one portion. The mixture was stirred at room temperature for 14 h, after which it was diluted with CH_2Cl_2 (30 mL) and filtered. The filtrate was washed with saturated aqueous $NaHCO_3$ (30 mL), and the aqueous layer was extracted with CH_2Cl_2 (2 × 20 mL). The organic phase was washed with brine (40 mL), dried over anhydrous sodium sulfate, and concentrated. The resulting residue was purified by flash column chromatography, eluting with a gradient of CH_2Cl_2/MeOH to yield the intermediate **33** (0.306 g, 85%) as an off-white sticky oil. ^{1}H NMR (500 MHz, $CDCl_3$): δ 8.42 (d, J = 5.0 Hz, 1 H), 7.25 (q, J = 7.5, Hz, 1 H), 6.98 (d, J = 7.6 Hz, 1 H), 6.94−6.88 (m, 3 H), 3.83 (s, 2 H), 2.90 (t, J = 6.6 Hz, 2 H), 2.83 (t, J = 6.7 Hz, 2 H), 2.50 (s, 3 H), 2.13 (s, 1 H). ^{13}C NMR (126 MHz, $CDCl_3$): δ 172.4, 168.6, (163.84, 161.88, d, J = 246.96 Hz, 1 C), 157.1, (142.29, 142.23, d, J = 7.56 Hz, 1 C), (129.92, 129.85, d, J = 8.82 Hz, 1 C), (124.36, 124.34, d, J = 2.52 Hz, 1 C), (115.60, 115.43, d, J = 21.42 Hz, 1 C), 114.2, (113.21, 113.04, d, J = 21.42 Hz, 1 C), 53.9, 50.2, 36.1, 14.0. MS (ESI) m/z [M + H]$^+$: calcd, 278.1; found, 278.06.

*3-(3-Fluorophenyl)-N-[(2-methylthiopyrimidin-4-yl)methyl]-propan-1-amine (**34**).* Compound **34** (0.594 g, 89%) was prepared from **30** (0.352 g, 2.285 mmol) and **32** (0.35 g, 2.285 mmol) by the exact procedure used to prepare **33**. ^{1}H NMR (500 MHz, $CDCl_3$): δ

DOI: 10.1021/jm501719e
J. Med. Chem. 2015, 58, 1067−1088

8.42 (d, J = 5.0 Hz, 1 H), 7.21 (q, J = 7.5 Hz, 1 H), 6.96 (d, J = 5.0 Hz, 1 H), 6.93 (d, J = 7.6 Hz, 1 H), 6.88−6.83 (m, 2 H), 3.80 (s, 2 H), 2.68−2.63 (m, 4 H), 2.54 (s, 3 H), 2.22 (s, 1 H), 1.83 (p, J = 7.3 Hz, 2 H). ^{13}C NMR (126 MHz, $CDCl_3$): δ 172.3, 168.7, (163.77, 161.82, d, J = 245.7 Hz, 1 C), 157.1, (144.47, 144.41, d, J = 7.56 Hz, 1 C), (129.69, 129.63, d, J = 7.56 Hz, 1 C), (123.94, 123.92, d, J = 2.52 Hz, 1 C), (115.16, 115.0, d, J = 20.16 Hz, 1 C), 114.3, (112.70, 112.54, d, J = 20.16 Hz, 1 C), 54.0, 48.7, 33.1, 31.3, 14.1. MS (ESI) m/z $[M + Na]^+$: calcd, 314.11; found 314.22.

*tert-Butyl (3-Fluorophenethyl) [(2-Methylsulfonyl-4-pyrimidyl)-methyl]carbamate (**35**).* Compound **33** (0.306 g, 1.103 mmol) was dissolved in THF (10 mL), and a solution of di-*tert*-butyl dicarbonate (0.265 g, 1.213 mmol) in THF (6 mL) was added. The resulting solution was stirred overnight, and thereafter, it was diluted with EtOAc/H_2O (30 mL, 1:1). The layers were separated and the aqueous layer extracted with EtOAc (2 × 10 mL). The combined organic layers were dried, concentrated, and purified by column chromatography (hexanes/EtOAc). The resulting oil (0.412 g, 1.091 mmol, 99%) was dissolved in CH_2Cl_2 (2 mL) and added to a solution of *m*-chloroperbenzoic acid (0.69 g, 4.0 mmol) in CH_2Cl_2 (4 mL) at 0 °C. The reaction was gradually warmed to room temperature while it was stirred overnight. The resulting suspension was then filtered and the white solid washed with cold CH_2Cl_2 (∼5 mL). The collected filtrate was washed with 10% aqueous K_2CO_3 (5 mL) and the organic fraction dried, concentrated, and purified by flash column chromatography to give a sticky white solid (0.335 g, 75%). ^{1}H NMR (500 MHz, $CDCl_3$): δ (8.81 (d, J = 5.0 Hz), 8.79 (d, J = 4.9 Hz), 2:3, 1 H), (7.39 (d, J = 4.8 Hz), 7.32 (d, J = 4.0 Hz), 3:2, 1 H), 7.23 (q, J = 7.8 Hz, 1 H), 6.96−6.83 (m, 3 H), (4.53 (s), 4.46 (s), 3:2, 2 H), 3.57−3.52 (m, 2 H), 3.33 (s, 3 H), (2.89 (t, J = 6.7 Hz), 2.84 (t, J = 7 Hz), 2:3, 2 H), (1.45 (s), 1.35 (s), 3:2, 9 H). ^{13}C NMR (126 MHz, $CDCl_3$): δ (170.85, 170.17, 1 C), (165.82, 165.61, 1 C), (163.78, 161.83, d, J = 245.7 Hz, 1 C), 158.51, (155.53, 154.77, 1 C), (140.92, 140.87, d, J = 6.3 Hz, 1 C), (130.09, 130.03, d, J = 7.56 Hz, 1 C), 124.48, (121.18, 120.17, 1 C), (115.72, 115.55, d, J = 21.42 Hz, 1 C), (113.54, 113.37, d, J = 21.42 Hz, 1 C), (81.03, 80.93, 1 C), (52.99, 52.17, 1 C), (49.90, 49.83, 1 C), (39.12, 39.03, 1 C), (34.70, 34.20, 1 C), 28.20. MS (ESI) m/z $[M + Na]^+$: calcd, 432.14; found, 432.10.

*tert-Butyl (3-Fluorophenpropyl) [(2-Methylsulfonyl-4-pyrimidyl)-methyl]carbamate (**36**).* Compound **36** (0.745 g, 89%) was synthesized from **34** in two steps, following the exact same procedure as used to synthesize **35**. ^{1}H NMR (500 MHz, $CDCl_3$): δ (8.85 (d, J = 6.0 Hz), 8.83 (d, J = 4.5 Hz, 4:5, 1 H), (7.45 (d, J = 4.5 Hz), 7.40 (d, J = 4.5 Hz, 5:4, 1 H), 7.23 (q, J = 6.9 Hz, 1 H), 6.93−6.84 (m, 3 H), (4.60 (s), 4.56 (s), 5:4, 2 H), (3.37 (t, J = 7 Hz), 3.28 (t, J = 7 Hz), 4:5, 2 H), 3.33 (s, 3 H), 2.65−2.55 (m, 2 H), 1.87 (p, J = 7.4 Hz, 2 H), (1.45 (s), 1.35 (s), 5:4, 9 H). ^{13}C NMR (126 MHz, $CDCl_3$): δ (171.07, 170.43, 1 C), (165.86, 165.66, 1 C), (163.81, 161.86, d, J = 245.7 Hz, 1 C), 158.59, (155.71, 154.90, 1 C), (143.69, 143.58, d, J = 13.8 Hz, 1 C), (129.92, 129.85, d, J = 8.82 Hz, 1 C), 123.85, (121.16, 120.17, 1 C), (115.11, 114.95, d, J = 20.16 Hz, 1 C), (113.01, 112.84, d, J = 21.42 Hz, 1 C), (80.92, 80.82, 1 C), (52.30, 51.98, 1 C), (47.98, 47.81, 1 C), (39.11, 39.03, 1 C), (32.78, 32.64, 1 C), (29.66, 29.59, 1 C), 28.25. MS (ESI) m/z $[2 M + Na]^+$: calcd, 869.31; found, 869.23.

*tert-Butyl [2-(1H-Imidazol-1-yl)pyrimidin-4-yl]methyl-3-fluoro-phenethylcarbamate (**37**).* Compound **35** (0.292 g, 0.713 mmol) was dissolved in MeCN (4 mL), and imidazole (0.243 g, 3.567 mmol) and K_2CO_3 (0.197 g, 1.427 mmol) added to the solution. The resulting mixture was heated at 65 °C for 4 h, after which it was cooled and diluted with CH_2Cl_2 (20 mL). Water (20 mL) was added to the organic layer and the layers separated. The aqueous layer was washed once with CH_2Cl_2 (10 mL), and the combined organic layers were dried over anhydrous sodium sulfate, concentrated, and purified by flash column chromatography using hexanes/EtOAc. Compound **37** was obtained as a faint-yellow sticky oil (0.263 g, 93%). ^{1}H NMR (500 MHz, $CDCl_3$): δ 8.59 (s, 1 H), 8.57 (d, J = 5.2 Hz, 1 H), 7.86 (s, 1 H), 7.23 (q, J = 7.8 Hz, 1 H), 7.15 (s, 1 H), (7.07 (d, J = 4.9 Hz), 7.01 (d, J = 4.7 Hz), 3:2, 1 H), 6.99−6.83 (m, 3 H), (4.44 (s), 4.36 (s), 3:2, 2 H), (3.58 (t, J = 7.5 Hz), 3.54 (t, J = 7.2 Hz), 2:3, 2 H), (2.91 (t, J = 7.2 Hz), 2.86 (t, J = 7.1 Hz), 2:3, 2 H), (1.46 (s), 1.36 (s), 3:2, 9 H). ^{13}C NMR (126 MHz, $CDCl_3$): δ (170.13, 169.55, 1 C), (163.80, 161.85, d, J = 245.7 Hz, 1 C), 158.85, (155.58, 155.00, 1 C), 154.43, (141.15, 141.10, d, J = 6.3 Hz, 1 C), 136.13, (130.63, 130.52, d, J = 13.86 Hz, 1 C), 130.05, 124.45, (116.49, 116.09, 1 C), (115.71, 115.55, d, J = 20.91 Hz, 1 C), 115.29, (113.49, 113.32, d, J = 21.42 Hz, 1 C), 80.63, (52.81, 51.91, 1 C), 49.89, (34.83, 34.35, 1 C), 28.26. MS (ESI) m/z $[M + H]^+$: calcd, 398.21; found, 398.42.

*tert-Butyl [2-(1H-Imidazol-1-yl)pyrimidin-4-yl]methyl-3-fluoro-phenpropylcarbamate (**38**).* Compound **38** was synthesized from **36** (0.648 g, 1.53 mmol) following the same procedure as used above to synthesize **37** from **35**. Compound **38** was obtained as an off-white viscous oil after purification (0.531 g, 84%). ^{1}H NMR (500 MHz, $CDCl_3$): δ 8.61 (d, J = 4.3 Hz, 1 H), 8.58 (s, 1 H), 7.85 (s, 1 H), 7.21 (q, J = 6.5 Hz, 1 H), 7.14 (s, 1 H), (7.10 (d, J = 4.5 Hz), 7.05 (d, J = 3.9 Hz), 5:4, 1 H), 6.95−6.83 (m, 3 H), (4.50 (s), 4.44 (s), 5:4, 2 H), (3.40 (t, J = 6.9 Hz), 3.31 (t, J = 7.1 Hz), 4:5, 2 H), 2.65−2.59 (m, 2 H), 1.96−1.82 (m, 2 H), (1.46 (s), 1.35 (s), 5:4, 9 H). ^{13}C NMR (126 MHz, $CDCl_3$): δ (170.28, 169.76, 1 C), (163.81, 161.86, d, J = 245.7 Hz, 1 C), 158.84, (155.77, 155.14, 1 C), 154.42, (143.91, 143.86, d, J = 6.3 Hz, 1 C), 136.12, (130.63, 130.52, d, J = 13.86 Hz, 1 C), 129.81, 123.84, 116.47, (116.07, 115.27, 1 C), (115.10, 114.93, d, J = 21.42 Hz, 1 C), (112.98, 112.81, d, J = 21.42 Hz, 1 C), 80.50, (52.18, 51.76, 1 C), 47.84, (32.83, 32.69, 1 C), 29.66, 28.29. MS (ESI) m/z $[M + H]^+$: calcd, 412.20; found, 412.00.

*N-(3-Fluorophenethyl)-2-[2-(methylthio)pyrimidin-4-yl]ethan-1-amine (**41**).* To a solution of **40** (0.3 g, 1.971 mmol) in ethanol (12 mL), **31** (1.3 mL, 1.371 g, 9.85 mmol) and acetic acid (0.06 mL, 0.06 g, 0.985 mmol) were added. The reaction was stirred at room temperature for 8 h, after which it was diluted with CH_2Cl_2 (25 mL). The resulting solution was treated with saturated $NaHCO_3$ (20 mL), and the layers were separated. The aqueous layer was washed with CH_2Cl_2 (3 × 10 mL), and the combined organic layers were dried over anhydrous sodium sulfate and concentrated. The obtained residue was purified by flash column chromatography (CH_2Cl_2/MeOH) to obtain **41** as a clear oil (0.356 g, 62%). ^{1}H NMR (500 MHz, $CDCl_3$): δ 8.37 (d, J = 5.0 Hz, 1 H), 7.26−7.20 (m, 1 H), 6.95 (d, J = 7.6 Hz, 1 H), 6.93−6.87 (m, 2 H), 6.79 (d, J = 5.1 Hz, 1 H), 3.03 (t, J = 6.8 Hz, 2 H), 2.91 (t, J = 7.0 Hz, 2 H), 2.86 (t, J = 6.8 Hz, 2 H), 2.79 (t, J = 7.1 Hz, 2 H), 2.52 (s, 3 H), 1.61 (br s, 1 H). ^{13}C NMR (126 MHz, $CDCl_3$): δ 172.4, 168.8, (163.86, 161.91, d, J = 245.7 Hz, 1 C), 156.8, (142.30, 142.25, d, J = 6.3 Hz, 1 C), (129.92, 129.85, d, J = 8.82 Hz, 1 C), (124.29, 124.27, d, J = 2.52 Hz, 1 C), 115.8, (115.52, 115.36, d, J = 20.16 Hz, 1 C), (113.21, 113.04, d, J = 21.42 Hz, 1 C), 50.5, 47.7, 37.4, 35.9, 14.0. MS (ESI) m/z $[M + H]^+$: calcd, 292.1; found, 291.84.

Compounds **42**−**47** were synthesized from **40** and the corresponding primary amines (**32**, **62**, **S3**−**S12**; see Supporting Information), following the same procedure used to synthesize **41**.

*3-(3-Fluorophenyl)-N-2-[2-(methylthio)pyrimidin-4-yl]-ethylpropan-1-amine (**42**).* Clear sticky oil (0.812 g, 88%). ^{1}H NMR (500 MHz, $CDCl_3$): δ 8.36 (d, J = 5.0 Hz, 1 H), 7.23−7.18 (m, 1 H), 6.93 (t, J = 7.7 Hz, 1 H), 6.88−6.83 (m, 2 H), 6.81 (d, J = 5.0 Hz, 1 H), 2.98 (t, J = 6.6 Hz, 2 H), 2.85 (t, J = 6.7 Hz, 2 H), 2.75−2.68 (m, 2 H), 2.67−2.59 (m, 2 H), 2.52 (s, 3 H), 1.76 (p, J = 7.3 Hz, 2 H), 1.57 (br s, 1 H). ^{13}C NMR (126 MHz, $CDCl_3$): δ 172.3, 169.1, (163.75, 161.80, d, J = 245.7 Hz, 1 C), 156.8, (144.60, 144.54, d, J = 7.56 Hz, 1 C), (129.65, 129.58, d, J = 8.82 Hz, 1 C), (123.93, 123.91, d, J = 2.52 Hz, 1 C), 115.8, (115.13, 114.97, d, J = 20.16 Hz, 1 C), (112.62, 112.45, d, J = 21.42 Hz, 1 C), 48.9, 47.9, 37.6, 33.2, 31.2, 14.0. MS (ESI) m/z $[M + H]^+$: calcd, 306.1; found, 305.85.

*3-(3-Chlorophenyl)-N-2-[2-(methylthio)pyrimidin-4-yl]-ethylpropan-1-amine (**43**).* Pale-yellow oil (0.591 g, 75%). ^{1}H NMR (500 MHz, $CDCl_3$): δ 8.39 (d, J = 5.0 Hz, 1 H), 7.21−7.14 (m, 3 H), 7.04 (d, J = 7.2 Hz, 1 H), 6.82 (d, J = 5.0 Hz, 1 H), 3.02 (t, J = 6.6 Hz, 2 H), 2.88 (t, J = 6.6 Hz, 2 H), 2.66 (d, J = 7.5 Hz, 2 H), 2.63 (d, J = 8.0 Hz, 2 H), 2.55 (s, 3 H), 1.90 (br s, 1 H), 1.81 (p, J = 7.5 Hz, 3 H). ^{13}C NMR (126 MHz, $CDCl_3$): δ 172.4, 169.0, 156.9, 144.0, 134.0, 129.6, 128.5, 126.5, 126.0, 115.8, 48.9, 47.9, 37.5, 33.2, 31.2, 14.1. MS (ESI) m/z $[M + H]^+$: calcd, 322.1; found, 321.91.

DOI: 10.1021/jm501719e
J. Med. Chem. 2015, 58, 1067−1088

*N-[2-(3-Fluorophenyl)cyclopropyl]methyl-2-[2-(methylthio)-pyrimidin-4-yl]ethan-1-amine (**44**).* Colorless sticky oil (0.41 g, 97%). ^{1}H NMR (500 MHz, $CDCl_3$): δ 8.38 (d, J = 5.0 Hz, 1 H), 7.18 (q, J = 7.8 Hz, 1 H), 6.87−6.78 (m, 3 H), 6.76−6.68 (m, 1 H), 3.09−3.02 (m, 2 H), 2.89 (t, J = 6.7 Hz, 2 H), 2.72 (t, J = 6.0 Hz, 1 H), 2.68 (d, J = 6.5 Hz, 1 H), 2.53 (s, 3 H), 1.80 (br s, 1 H), 1.74−1.69 (m, 1 H), 1.33−1.28 (m, 1 H), 0.93−0.86 (m, 2 H). ^{13}C NMR (126 MHz, $CDCl_3$): δ 172.4, 169.0, (163.94, 161.99, d, J = 245.7 Hz, 1 C), 156.8, (145.73, 145.67, d, J = 7.56 Hz, 1 C), (129.64, 129.58, d, J = 7.56 Hz, 1 C), 121.4, 115.8, (112.48, 112.30, d, J = 22.68 Hz, 1 C), (112.33, 112.16, d, J = 21.42 Hz, 1 C), 53.8, 47.7, 37.6, 23.6, 21.9, 15.1, 14.0. MS (ESI) m/z [2 M + H]$^+$: calcd, 635.2; found, 635.08.

*2-(3-Fluorobenzyl)-N-2-[2-(methylthio)pyrimidin-4-yl]-ethylcyclopropan-1-amine (**45**).* Colorless sticky oil (0.407 g, 65%). ^{1}H NMR (500 MHz, $CDCl_3$): δ 8.37 (d, J = 5.0 Hz, 1 H), 7.27−7.20 (m, 1 H), 6.99 (d, J = 7.5 Hz, 1 H), 6.96−6.91 (m, 1 H), 6.89 (td, J = 8.6, 2.2 Hz, 1 H), 6.77 (d, J = 5.0 Hz, 1 H), 3.02−2.97 (m, 2 H), 2.80 (t, J = 6.6 Hz, 2 H), 2.59 (dd, J = 14.8, 6.8 Hz, 1 H), 2.54 (s, 3 H), 2.47 (dd, J = 14.8, 7.6 Hz, 1 H), 2.11−2.05 (m, 1 H), 1.90 (br s, 1 H), 1.07−0.99 (m, 1 H), 0.69−0.63 (m, 1 H), 0.47−0.43 (m, 1 H). ^{13}C NMR (126 MHz, $CDCl_3$): δ 172.4, 169.1, (163.82, 161.87, d, J = 245.7 Hz, 1 C), 156.8, (144.17, 144.12, d, J = 6.3 Hz, 1 C), (129.73, 129.67, d, J = 7.56 Hz, 1 C), (123.92, 123.89, d, J = 3.78 Hz, 1 C), 115.7, (115.15, 114.99, d, J = 20.16 Hz, 1 C), (112.85, 112.68, d, J = 21.42 Hz, 1 C), 47.5, 38.1, 37.4, 37.2, 21.0, 14.0, 13.7. MS (ESI) m/z [M + H]$^+$: calcd, 318.1; found, 317.9.

*N-2-[2-(Methylthio)pyrimidin-4-yl]ethyl-3-(3-pyridyl)propan-1-amine (**46**).* Yellow oil (0.443 g, 95%). ^{1}H NMR (500 MHz, $CDCl_3$): δ 8.43 (s, 1 H), 8.41 (d, J = 6.1 Hz, 1 H), 8.36 (d, J = 5.0 Hz, 1 H), 7.47 (d, J = 7.7 Hz, 1 H), 7.17 (dd, J = 7.6, 4.9 Hz, 1 H), 6.80 (d, J = 5.0 Hz, 1 H), 3.02 (t, J = 6.7 Hz, 2 H), 2.88 (t, J = 6.7 Hz, 2 H), 2.67 (t, J = 7.0 Hz, 2 H), 2.64 (t, J = 7.5 Hz, 2 H), 2.52 (s, 3 H), 2.40 (br s, 1 H), 1.81 (p, J = 7.3 Hz, 2 H). ^{13}C NMR (126 MHz, $CDCl_3$): δ 172.3, 168.8, 156.8, 149.8, 147.4, 137.0, 135.7, 123.2, 115.8, 48.7, 47.7, 37.2, 30.9, 30.5, 14.0. MS (ESI) m/z [M + H]$^+$: calcd, 289.1; found, 289.01.

*3-[2-(2-Methylthio-4-pyrimidyl)ethylamino]methyl Benzonitrile (**47**).* Cream-colored oil (0.426 g, 83%). ^{1}H NMR (500 MHz, $CDCl_3$): δ 8.39 (d, J = 5.1 Hz, 1 H), 7.63 (s, 1 H), 7.55 (d, J = 8.0 Hz, 1 H), 7.52 (d, J = 7.5 Hz, 1 H), 7.41 (t, J = 7.7 Hz, 1 H), 6.84 (d, J = 5.1 Hz, 1 H), 3.84 (s, 2 H), 3.02 (t, J = 6.6 Hz, 2 H), 2.89 (t, J = 6.6 Hz, 2 H), 2.52 (s, 3 H), 1.77 (br s, 1 H). ^{13}C NMR (126 MHz, $CDCl_3$): δ 172.2, 168.8, 156.7, 141.6, 132.3, 131.3, 130.5, 128.9, 118.7, 115.7, 112.1, 52.6, 47.1, 37.3, 13.8. MS (ESI) m/z [M + H]$^+$: calcd, 285.1; found, 284.91.

*tert-Butyl (3-Fluorophenethyl) [2-(2-Methylsulfonyl-4-pyrimidyl)-ethyl]carbamate (**48**).* To a solution of **41** (0.356 g, 1.222 mmol) in THF (10 mL), a solution of di-*tert*-butyl dicarbonate (0.293 g, 1.344 mmol) in THF (7 mL) was added. The resulting solution was stirred at room temperature for 3 h and, thereafter, it was diluted with EtOAc/H_2O (30 mL, 1:1). The layers were separated, and the aqueous layer extracted with EtOAc (2 × 10 mL). Combined organic layers were dried, concentrated, and purified by column chromatography (hexanes/EtOAc). The resulting oil (0.39 g, 0.996 mmol, 82%) was dissolved in CH_2Cl_2 (2 mL) and added to a solution of *m*-chloroperbenzoic acid (0.636 g, 3.685 mmol) in CH_2Cl_2 (3 mL) at 0 °C. The resulting solution was stirred at room temperature for 3 h. At that point, the reaction was filtered, and the white residue was washed with cold CH_2Cl_2 (∼5 mL). The collected filtrate was washed with 10% aqueous K_2CO_3 (5 mL), the organic layer was dried, concentrated, and purified by flash column chromatography (hexanes/EtOAc) to give a clear viscous oil (0.337 g, 80%). ^{1}H NMR (500 MHz, $CDCl_3$): δ 8.76 (d, J = 4.1 Hz, 1 H), (7.43 (s), 7.31 (s), 7:3, 1 H), 7.23 (q, J = 6.5 Hz, 1 H), 6.97−6.84 (m, 3 H), (3.61−3.53 (m), 3.49−3.44 (m), 7:3, 2 H), 3.37 (t, J = 7.1 Hz, 2 H), 3.34 (s, 3 H), (3.18−3.10 (m), 3.08−2.98 (m), 7:3, 2 H), ((2.86−2.80 (m), 2.78−2.72 (m), 3:7, 2 H), 1.38 (s, 9 H). ^{13}C NMR (126 MHz, $CDCl_3$): δ (170.93, 170.82, 1 C), (165.98, 165.76, 1 C), (163.79, 161.84, d, J = 245.7 Hz, 1 C), (158.01, 157.88, 1 C), (155.22, 154.87, 1 C), 141.38, (130.00, 129.94, d, J = 7.56 Hz), 124.54, 123.56, (115.75, 115.59, d, J = 20.16 Hz, 1 C), (113.37, 113.21, d, J = 20.16 Hz, 1 C), 80.05, (49.37, 49.18, 1 C), (46.80, 46.14, 1 C), 39.09, (36.91, 36.29, 1 C), (34.90, 34.19, 1 C), 28.25. MS (ESI) m/z [M + Na]$^+$: calcd, 446.15; found, 446.06.

Compounds **49**−**52** were synthesized from compounds **42**−**45** following the same procedures used to synthesize **48**.

*tert-Butyl 3-(3-Fluorophenpropyl) [2-(2-Methylsulfonyl-4-pyrimidyl)ethyl]carbamate (**49**).* Colorless oil (0.694 g, 67%). ^{1}H NMR (500 MHz, $CDCl_3$): δ 8.81−8.72 (m, 1 H), (7.47−7.43 (m), 7.37−7.32 (m), 3:2, 1 H), 7.23 (q, J = 7.4 Hz, 1 H), 6.93 (d, J = 7.5 Hz, 1 H), 6.87 (t, J = 8.0 Hz, 2 H), 3.66−3.56 (m, 2 H), 3.34 (s, 3 H), 3.24−3.08 (m, 4 H), 2.58 (t, J = 7.7 Hz, 2 H), 1.81 (p, J = 7 Hz, 2 H), 1.39 (s, 9 H). ^{13}C NMR (126 MHz, $CDCl_3$): δ (170.97, 170.87, 1 C), (165.98, 165.76, 1 C), (163.81, 161.86, d, J = 245.7 Hz, 1 C), 157.89, (155.39, 155.02, 1 C), (143.99, 143.90, d, J = 11.34 Hz, 1 C), (129.85, 129.79, d, J = 7.56 Hz, 1 C), (123.92, 123.90, d, J = 2.52 Hz, 1 C), 123.54, (115.11, 114.95, d, J = 20.16 Hz, 1 C), (112.89, 112.72, d, J = 21.42 Hz, 1 C), 79.93, (47.38, 47.04, 1 C), 46.03, 39.08, (36.94, 36.37, 1 C), 32.76, (29.85, 29.63, 1 C), 28.30. MS (ESI) m/z [2 M + Na]$^+$: calcd, 897.19; found, 897.26.

*tert-Butyl 3-(3-Chlorophenpropyl) [2-(2-Methylsulfonyl-4-pyrimidyl)ethyl]carbamate (**50**).* Colorless oil (0.613 g, 89%). ^{1}H NMR (500 MHz, $CDCl_3$): δ 8.76 (d, J = 4.5 Hz, 1 H), (7.45 (s), 7.35 (s), 3:2, 1 H), 7.20 (q, J = 7.5 Hz, 1 H), 7.18−7.13 (m, 2 H), 7.04 (d, J = 7.3 Hz, 1 H), 3.67−3.56 (m, 2 H), 3.34 (s, 3 H), 3.25−3.06 (m, 4 H), 2.56 (t, J = 7.5 Hz, 2 H), 1.81 (p, J = 7.6 Hz, 2 H), 1.39 (s, 9 H). ^{13}C NMR (126 MHz, $CDCl_3$): δ 170.96, (166.02, 165.84, 1 C), 157.91, 155.36, 143.42, 134.13, 129.69, 128.35, 126.48, 126.15, 123.50, 79.96, (47.40, 47.19, 1 C), 46.07, 39.11, (37.01, 36.46, 1 C), 32.74, 29.89, 28.34. MS (ESI) m/z [M + Na]$^+$: calcd, 476.09; found, 476.01.

*tert-Butyl [2-(3-Fluorophenyl)cyclopropyl]methyl-2-[2-(methylsulfonyl)pyrimidin-4-yl]ethyl Carbamate (**51**).* Colorless sticky oil (0.396 g, 67%). ^{1}H NMR (500 MHz, $CDCl_3$): δ 8.66 (d, J = 4.9 Hz, 1 H), (7.35 (s), 7.25 (s), 1:1, 1 H), 7.10 (q, J = 7.7 Hz, 1 H), 6.79−6.68 (m, 2 H), 6.61 (dt, J = 2, 10.3 Hz, 1 H), 3.68−3.60 (m, 2 H), 3.32−3.26 (m, 1 H), 3.21 (s, 3 H), 3.18−3.02 (m, 3 H), 1.83−1.75 (m, 1 H), 1.35 (s, 9 H), 1.20−1.16 (m, 1 H), 0.92−0.84 (m, 2 H). ^{13}C NMR (126 MHz, $CDCl_3$): δ 170.70, (165.68, 165.55, 1 C), (163.69, 161.74, d, J = 245.7 Hz, 1 C), 157.74, 155.01, 145.08, (129.56, 129.49, d, J = 8.82 Hz, 1 C), 123.33, 121.26, (112.23, 112.07, d, J = 20.16 Hz, 1 C), (112.15, 111.97, d, J = 22.68 Hz, 1 C), 79.74, (51.04, 50.41, 1 C), 45.83, 38.87, (36.67, 36.06, 1 C), (31.29, 30.58, 1 C), 28.08, (22.66, 22.35, 1 C), (14.37, 13.82, 1 C). MS (ESI) m/z [M + H]$^+$: calcd, 450.17; found, 450.07.

*tert-Butyl [2-(3-Fluorobenzyl)cyclopropyl]-2-[2-(methylsulfonyl)-pyrimidin-4-yl]ethyl Carbamate (**52**).* Colorless sticky oil (0.430 g, 83%). ^{1}H NMR (500 MHz, $CDCl_3$): δ 8.70 (d, J = 5.1 Hz, 1 H), 7.31 (d, J = 4.0 Hz, 1 H), 7.18 (q, J = 8 Hz, 1 H), 6.92 (d, J = 7.6 Hz, 1 H), 6.86 (d, J = 9.9 Hz, 1 H), 6.81 (td, J = 8.5, 2.2 Hz, 1 H), 3.52 (s, 1 H), 3.49 (t, J = 7 Hz, 1 H), 3.28 (s, 3 H), 2.99−2.92 (m, 2 H), 2.79 (dd, J = 14.5, 5.3 Hz, 1 H), 2.35 (dd, J = 8, 13.5 Hz, 1 H), 2.27−2.23 (m, 1 H), 1.34 (s, 9 H), 0.84−0.76 (m, 1 H), 0.66 (q, J = 6.1 Hz, 1 H). ^{13}C NMR (126 MHz, $CDCl_3$): δ 170.87, 165.71, (163.64, 161.69, d, J = 245.7 Hz, 1 C), 157.84, 156.00, (143.07, 143.01, d, J = 7.56 Hz, 1 C), (129.78, 129.71, d, J = 8.82 Hz, 1 C), (124.00, 123.98, d, J = 2.52 Hz, 1 C), 123.25, (115.14, 114.98, d, J = 20.16 Hz, 1 C), (112.92, 112.75, d, J = 21.42 Hz, 1 C), 79.82, 45.94, 38.96, 37.46, 36.06, 34.84, 28.20, (22.87, 22.45, 1 C), 14.84. MS (ESI) m/z [M + H]$^+$: calcd, 450.17; found, 450.20.

*tert-Butyl 2-[2-(Methylsulfonyl)pyrimidin-4-yl]ethyl-3-(3-pyridyl)-propyl Carbamate (**53**).* Compound **46** (0.443 g, 1.536 mmol) was dissolved in THF (15 mL), and a solution of di-*tert*-butyl dicarbonate (0.369 g, 1.689 mmol) in THF (6 mL) was added. The resulting solution was stirred at room temperature for 3 h, and thereafter, it was diluted with EtOAc/H_2O (40 mL, 1:1). The layers were separated, and the aqueous layer was extracted with EtOAc (2 × 15 mL). Combined organic layers were dried, concentrated, and purified by column chromatography (hexanes/EtOAc). The resulting oil (0.567 g, 1.459 mmol, 95%) was dissolved in THF (12 mL). Water (12 mL) and oxone (1.345 g, 2.188 mmol) were sequentially added, and the

DOI: 10.1021/jm501719e
J. Med. Chem. 2015, 58, 1067−1088

reaction was stirred at room temperature for 4 h. At that point, the reaction was diluted with EtOAc/H_2O (30 mL, 1:1) and the layers separated. The aqueous layer was basified to pH 10 with 6 N NaOH, saturated by addition of solid K_2CO_3, and extracted with EtOAc (3 × 15 mL). Combined organic fractions were dried over sodium sulfate, and concentrated. The resulting light-yellow oil (0.527 g, 86%) was clean by NMR and was used in the next step without further purification. ^{1}H NMR (500 MHz, $CDCl_3$): δ 8.74 (d, J = 3.9 Hz, 1 H), 8.42 (s, 2 H), 7.48 (d, J = 6.9 Hz, 1 H), (7.42 (s), 7.34 (s), 3:2, 1 H), 7.20 (dd, J = 7.3, 4.9 Hz, 1 H), 3.66−3.54 (m, 2 H), 3.31 (s, 3 H), 3.24−3.03 (m, 4 H), 2.56 (t, J = 7.8 Hz, 2 H), 1.80 (p, J = 7 Hz, 2 H), 1.36 (s, 9 H). ^{13}C NMR (126 MHz, $CDCl_3$): δ 170.87, 165.81, 157.85, 155.27, 149.53, 147.30, 136.70, 135.74, 123.47, 123.37, 79.93, (47.30, 46.94, 1 C), 46.01, 39.05, (36.87, 36.33, 1 C), 30.11, (29.84, 29.58, 1 C), 28.25. MS (ESI) m/z $[M + Na]^+$: calcd, 443.16; found, 443.03.

*tert-Butyl 3-Cyanobenzyl-2-[2-(methylsulfonyl)pyrimidin-4-yl]-ethyl Carbamate (**54**).* Compound **54** (0.396 g, 91%) was obtained as a colorless oil from **47** following the same procedure used to synthesize **48** from **41**. ^{1}H NMR (500 MHz, $CDCl_3$): δ 8.76 (d, J = 4.8 Hz, 1 H), 7.53 (d, J = 7.3 Hz, 1 H), 7.48−7.37 (m, 4 H), 4.46 (s, 2 H), 3.74−3.61 (m, 2 H), 3.33 (s, 3 H), 3.20−3.07 (m, 2 H), 1.38 (s, 9 H). ^{13}C NMR (126 MHz, $CDCl_3$): δ 170.46, 165.58, 157.79, (155.26, 154.98, 1 C), (139.96, 139.55, 1 C), (131.83, 131.28, 1 C), 130.75, 130.23, 129.26, 123.42, 118.36, 112.36, 80.49, (50.65, 49.71, 1 C), 45.59, 38.87, (36.34, 35.94, 1 C), 28.00. MS (ESI) m/z $[M + Na]^+$: calcd, 439.14; found, 438.99.

*tert-Butyl 2-[2-(1H-Imidazol-1-yl)pyrimidin-4-yl]ethyl-3-fluorophenethyl Carbamate (**55**).* Compound **48** (0.335 g, 0.791 mmol) was dissolved in MeCN (5 mL), and imidazole (0.269 g, 3.958 mmol) and K_2CO_3 (0.22 g, 1.583 mmol) were added to the solution. The resulting mixture was heated at 65 °C for 5 h, after which it was cooled and diluted with CH_2Cl_2 (20 mL). Water (20 mL) was added to the organic layer and the layers separated. The aqueous layer was washed once with CH_2Cl_2 (15 mL), and the combined organics were dried over anhydrous sodium sulfate, concentrated, and purified by flash column chromatography using hexanes/EtOAc. The desired compound (**55**) was obtained as an off-white viscous oil (0.247 g, 76%). ^{1}H NMR (500 MHz, $CDCl_3$): δ 8.61 (s, 1 H), 8.53 (d, J = 4.9 Hz, 1 H), 7.88 (s, 1 H), 7.24 (q, J = 6.0 Hz, 1 H), 7.16 (s, 1 H), (7.08 (s), 6.97 (s), 3:2, 1 H), 6.94−6.82 (m, 3 H), (3.56 (t, J = 8.5 Hz), 3.47 (s), 3:2, 2 H), 3.43−3.36 (m, 2 H), (2.99 (t, J = 8.5 Hz), 2.90 (s), 3:2, 2 H), (2.84 (s), 2.79 (t, J = 7 Hz), 2:3, 2 H), 1.38 (s, 9 H). ^{13}C NMR (126 MHz, $CDCl_3$): δ (170.39, 170.27, 1 C), (163.81, 161.85, d, J = 246.96 Hz, 1 C), (158.43, 158.33, 1 C), (155.18, 154.98, 1 C), (154.55, 154.38, 1 C), (141.54, 141.47, d, J = 8.82 Hz, 1 C), 136.09, (130.55, 130.47, 1 C), (130.00, 129.94, 1 C), (124.48, 124.46, d, J = 2.52 Hz, 1 C), 118.49, 116.48, (115.74, 115.57, d, J = 21.42 Hz, 1 C), (113.38, 113.22, d, J = 20.16 Hz, 1 C), 79.87, (49.37, 49.23, 1 C), (46.97, 46.21, 1 C), (36.84, 36.07, 1 C), (35.00, 34.29, 1 C), 28.23. MS (ESI) m/z $[M + H]^+$: calcd, 412.20; found, 412.08.

Compounds **56**−**61** were synthesized from compounds **49**−**54** following the same procedures used to synthesize **55**.

*tert-Butyl 2-[2-(1H-Imidazol-1-yl)pyrimidin-4-yl]ethyl-3-(3-fluorophenyl)propylcarbamate (**56**).* Colorless viscous oil (0.587 g, 87%). ^{1}H NMR (500 MHz, $CDCl_3$): δ 8.59 (s, 1 H), 8.52 (d, J = 4.1 Hz, 1 H), 7.86 (s, 1 H), 7.21 (q, J = 7 Hz, 1 H), 7.15 (s, 1 H), (7.07 (s), 7.00 (s), 3:2, 1 H), 6.91 (d, J = 7.5 Hz, 1 H), 6.88−6.81 (m, 2 H), 3.66−3.54 (m, 2 H), 3.24−3.14 (m, 2 H), 3.04−2.94 (m, 2 H), 2.58 (t, J = 7.7 Hz, 2 H), 1.83 (p, J = 7.6 Hz, 2 H), 1.38 (s, 9 H). ^{13}C NMR (126 MHz, $CDCl_3$): δ (170.42, 170.32, 1 C), (163.79, 161.84, d, J = 245.7 Hz, 1 C), (158.40, 158.31, 1 C), (155.36, 155.12, 1 C), (154.54, 154.39, 1 C), (144.04, 143.90, d, J = 17.6 Hz, 1 C), 136.09, 130.52, (129.81, 129.74, d, J = 8.82 Hz, 1 C), (123.84, 123.82, d, J = 2.52 Hz, 1 C), 118.43, 116.45, (115.08, 114.91, d, J = 21.42 Hz, 1 C), (112.87, 112.70, d, J = 21.42 Hz, 1 C), 79.73, (47.24, 46.97, 1 C), (46.27, 46.08, 1 C), (36.91, 36.15, 1 C), 32.76, (29.86, 29.60, 1 C), 28.27. MS (ESI) m/z $[2 M + Na]^+$: calcd, 873.43; found, 873.39.

*tert-Butyl 2-[2-(1H-Imidazol-1-yl)pyrimidin-4-yl]ethyl-3-(3-chlorophenyl)propylcarbamate (**57**).* Colorless viscous oil (0.541 g, 91%). ^{1}H NMR (500 MHz, $CDCl_3$): δ 8.63 (s, 1 H), 8.54 (d, J = 4.9 Hz, 1 H), 7.88 (s, 1 H), 7.18 (q, J = 7.5 Hz, 1 H), 7.17−7.14 (m, 3 H), (7.09 (s), 7.05 (s), 3:2, 1 H), 7.03 (d, J = 7.1 Hz, 1 H), 3.65−3.55 (m, 2 H), 3.25−3.14 (m, 2 H), 3.05−2.94 (m, 2 H), 2.57 (t, J = 7.7 Hz, 2 H), 1.83 (p, J = 7.6 Hz, 2 H), 1.39 (s, 9 H). ^{13}C NMR (126 MHz, $CDCl_3$): δ 170.49, 158.39, (155.38, 155.21, 1 C), 154.40, 143.39, 136.01, 134.14, (130.34, 130.21, 1 C), 129.65, 128.34, 126.40, 126.15, 118.55, 116.54, 79.80, (47.27, 47.06, 1 C), (46.28, 46.12, 1 C), (36.99, 36.21, 1 C), 32.77, (29.91, 29.73, 1 C), 28.32. MS (ESI) m/z $[M + H]^+$: calcd, 442.19; found, 442.06.

*tert-Butyl 2-[2-(1H-Imidazol-1-yl)pyrimidin-4-yl]ethyl[2-(3-fluorophenyl)cyclopropyl]methylcarbamate (**58**).* Pale-yellow oil (0.366 g, 95%). ^{1}H NMR (500 MHz, $CDCl_3$): δ 8.60 (s, 1 H), 8.50 (d, J = 5.0 Hz, 1 H), 7.87 (s, 1 H), 7.17 (q, J = 8 Hz, 1 H), 7.14 (s, 1 H), (7.05 (s), 6.94 (d, J = 7.7 H), 2:3, 1 H), 6.87−6.78 (m, 2 H), 6.67 (dt, J = 2.5, 10.2 Hz, 1 H), 3.75−3.63 (m, 2 H), 3.41−3.30 (m, 1 H), 3.25−3.16 (m, 1 H), 3.08−2.95 (m, 2 H), 1.92−1.78 (m, 1 H), 1.41 (s, 9 H), 1.29−1.26 (m, 1 H), 0.98−0.93 (m, 2 H). ^{13}C NMR (126 MHz, $CDCl_3$): δ 170.40, (163.93, 161.98, d, J = 245.7 Hz, 1 C), 158.34, 155.26, 154.47, 145.25, 136.05, 130.44, (129.75, 129.68, d, J = 8.82 Hz, 1 C), 121.37, 118.41, 116.46, (112.53, 112.40, d, J = 16.38 Hz, 1 C), (112.40, 112.23, d, J = 21.42 Hz, 1 C), 79.89, (51.24, 50.73, 1 C), 46.24, (36.90, 36.07, 1 C), 28.32, 22.85, 22.08, 14.65. MS (ESI) m/z $[M + H]^+$: calcd, 438.2; found, 438.03.

*tert-Butyl 2-[2-(1H-Imidazol-1-yl)pyrimidin-4-yl]ethyl[2-(3-fluorobenzyl)cyclopropyl]carbamate (**59**).* Off-white sticky oil (0.372 g, 91%). ^{1}H NMR (500 MHz, $CDCl_3$): δ 8.62 (s, 1 H), 8.52 (d, J = 5.0 Hz, 1 H), 7.88 (s, 1 H), 7.25−7.18 (m, 1 H), 7.16 (s, 1 H), 6.99 (s, 1 H), 6.96 (d, J = 7.6 Hz, 1 H), 6.91 (d, J = 9.8 Hz, 1 H), 6.87 (td, J = 8.5, 2.3 Hz, 1 H), (3.53 (t, J = 7 Hz), 3.50 (t, J = 7 Hz), 2:1, 2 H), 2.88 (t, J = 6.5 Hz, 2 H), 2.84 (dd, J = 10, 5 Hz, 1 H), 2.43 (dd, J = 14.0, 8.0 Hz, 1 H), 2.36 (dt, J = 7.2, 3.6 Hz, 1 H), 1.37 (s, 9 H), 1.23−1.20 (m, 1 H), 0.86 (dt, J = 9.3, 5.3 Hz, 1 H), 0.72 (q, J = 6.1 Hz, 1 H). ^{13}C NMR (126 MHz, $CDCl_3$): δ 170.62, (163.80, 161.85, d, J = 245.7 Hz, 1 C), 158.30, 156.21, 154.36, (143.16, 143.11, d, J = 6.3 Hz, 1 C), 136.06, 130.30, (129.86, 129.80, d, J = 7.56 Hz, 1 C), (124.08, 124.06, d, J = 2.52 Hz, 1 C), 118.39, 116.53, (115.29, 115.13, d, J = 20.16 Hz, 1 C), (113.09, 112.93, d, J = 20.16 Hz, 1 C), 79.83, 46.13, 37.67, 35.99, 34.88, 28.31, 23.02, 15.01. MS (ESI) m/z $[2 M + Na]^+$: calcd, 897.43; found, 897.32.

*tert-Butyl 2-[2-(1H-Imidazol-1-yl)pyrimidin-4-yl]ethyl-3-(3-pyridyl)propyl Carbamate (**60**).* Pale-yellow oil (0.43 g, 84%). ^{1}H NMR (500 MHz, $CDCl_3$): δ 8.57 (s, 1 H), 8.51 (d, J = 4.7 Hz, 1 H), 8.40 (s, 2 H), 7.84 (s, 1 H), 7.44 (s, 1 H), 7.17 (dd, J = 7.3, 4.9 Hz, 1 H), 7.12 (s, 1 H), (7.05 (s), 6.99 (s), 3:2, 1 H), 3.65−3.52 (m, 2 H), 3.25−3.14 (m, 2 H), 3.05−2.92 (m, 2 H), 2.56 (t, J = 7.8 Hz, 2 H), 1.82 (p, J = 7.6 Hz, 2 H), 1.36 (s, 9 H). ^{13}C NMR (126 MHz, CDCl3): δ 170.30, 158.33, 155.21, 154.43, 149.60, 147.38, 136.73, 136.03, 135.56, 130.45, 123.27, 118.40, 116.42, 79.76, (47.16, 46.97, 1 C), 46.22, (36.85, 36.09, 1 C), 30.14, (29.83, 29.58, 1 C), 28.22. MS (ESI) m/z $[M + H]^+$: calcd, 409.22; found, 409.08.

*tert-Butyl 2-[2-(1H-Imidazol-1-yl)pyrimidin-4-yl]ethyl-(3-cyanobenzyl)carbamate (**61**).* Colorless oil (0.346 g, 90%). ^{1}H NMR (500 MHz, $CDCl_3$): δ 8.57 (s, 1 H), 8.54 (d, J = 5.0 Hz, 1 H), 7.86 (s, 1 H), 7.52 (d, J = 7.3 Hz, 1 H), (7.46 (s), 7.42 (s), 1:1, 2 H), 7.40 (d, J = 7.4 Hz, 1 H), 7.15 (s, 1 H), (7.09 (s), 7.01 (s), 1:1, 1 H), 4.45 (s, 2 H), (3.71 (s), 3.64 (s), 1:1, 2 H), 3.04 (s), 3.00 (s), 1:1, 2 H), (1.45 (s), 1.38 (s), 1:1, 9 H). ^{13}C NMR (126 MHz, $CDCl_3$): δ 169.90, 158.35, (155.42, 155.02, 1 C), 154.26, 139.80, 135.85, 131.71, 131.17, 130.78, 130.57, 130.31, 129.21, 118.38, 116.31, 112.47, 80.52, (50.73, 49.94, 1 C), 46.09, (36.33, 35.69, 1 C), 28.07. MS (ESI) m/z $[2 M + Na]^+$: calcd, 831.37; found, 831.33.

*Chiral Resolution of 2-(3-Fluorobenzyl)cyclopropan-1-amine (**62**).* 2-(3-Fluorobenzyl)cyclopropan-1-amine (**62**; 0.851 g, 5.15 mmol) was diluted in CH_2Cl_2 (20 mL) and cooled to −20 °C. (*S*)-(+)-α-Methoxylphenylacetic acid (1.0 g, 6.18 mmol) was added to the resulting solution, followed by the addition of dicyclohexylcarbodiimide (1.275 g, 6.18 mmol). The reaction mixture was gradually warmed to room temperature and stirred overnight. The resulting suspension was filtered, and the white precipitate was washed with cold CH_2Cl_2 (15 mL). The combined filtrate was concentrated and

DOI: 10.1021/jm501719e
J. Med. Chem. 2015, 58, 1067−1088

chromatographed in silica gel using a gradient of hexanes/EtOAc to obtain the two diastereomers (*R,R,S*)-**63a** and (*S,S,S*)-**63b**.

*For (R,R,S)-**63a**.* Off-white amorphous solid (0.775 g, 2.472 mmol, 48%). ^{1}H NMR (500 MHz, $CDCl_3$): δ 7.42−7.29 (m, 5 H), 7.23 (q, J = 7.8 Hz, 1 H), 7.01 (d, J = 7.5 Hz, 1 H), 6.95 (d, J = 10.0 Hz, 1 H), 6.93−6.86 (m, 2 H), 4.61 (s, 1 H), 3.33 (s, 3 H), 2.91 (dd, J = 14.9, 5.8 Hz, 1 H), 2.67 (dq, J = 7.2, 3.6 Hz, 1 H), 2.39 (dd, J = 14.9, 8.0 Hz, 1 H), 1.20−1.13 (m, 1 H), 0.83 (dt, J = 9.3, 4.8 Hz, 1 H), 0.76 (q, J = 6.1 Hz, 1 H). ^{13}C NMR (126 MHz, $CDCl_3$): δ 170.8, (163.61, 161.66, d, J = 245.7 Hz, 1 C), (143.01, 142.95, d, J = 7.56 Hz, 1 C), 136.7, (129.54, 129.47, d, J = 8.82 Hz, 1 C), 128.3, 128.2, 126.8, (123.89, 123.87, d, J = 2.52 Hz, 1 C), (115.06, 114.89, d, J = 21.42 Hz, 1 C), (112.76, 112.59, d, J = 21.42 Hz, 1 C), 83.5, 56.8, 37.3, 28.4, 20.4, 13.1.

*For (S,S,S)-**63b**.* White crystalline solid (0.756 g, 2.42 mmol, 47%). ^{1}H NMR (500 MHz, $CDCl_3$): δ 7.43−7.30 (m, 5 H), 7.27 (td, J = 7.9, 6.2 Hz, 1 H), 7.07 (d, J = 7.6 Hz, 1 H), 7.03−6.99 (m, 1 H), 6.91 (td, J = 8.3, 2.5 Hz, 2 H), 4.62 (s, 1 H), 3.34 (s, 3 H), 2.87 (dd, J = 14.9, 6.3 Hz, 1 H), 2.68 (dq, J = 7.4, 3.7 Hz, 1 H), 2.48 (dd, J = 14.9, 7.6 Hz, 1 H), 1.26−1.18 (m, 1 H), 0.82−0.69 (m, 2 H). ^{13}C NMR (126 MHz, $CDCl_3$): δ 170.7, (163.59, 161.64, d, J = 245.7 Hz, 1 C), (143.04, 142.98, d, J = 7.56 Hz, 1 C), 136.7, (129.54, 129.48, d, J = 7.56 Hz, 1 C), 128.2, 128.1, 126.7, (123.89, 123.87, d, J = 2.52 Hz, 1 C), (115.05, 114.88, d, J = 21.42 Hz, 1 C), (112.75, 112.58, d, J = 21.42 Hz, 1 C), 83.5, 56.8, 37.4, 28.4, 20.5, 13.0.

*(R,R)-2-(3-Fluorobenzyl)cyclopropan-1-amine [(R,R)-**62a**].* To a solution of (*R,R,S*)-**63a** (0.775 g, 2.472 mmol) in ethanol (12 mL), 12 N HCl (12 mL) was added, and the reaction was heated to reflux for 12 h. The resulting solution was cooled to room temperature, concentrated, and treated with Et_2O/6 N HCl (30 mL, 1:1). The layers were separated, and the aqueous layer was washed with Et_2O (10 mL), basified to pH 10−12 with 6 N NaOH, and extracted with CH_2Cl_2 (4 × 15 mL). The combined CH_2Cl_2 extracts were dried over sodium sulfate and concentrated to obtain (*R,R*)-**62a** (0.347 g, 85%), which was pure by NMR and used directly in the next step without further purification.

*(S,S)-2-(3-Fluorobenzyl)cyclopropan-1-amine [(S,S)-**62b**].* (*S,S*)-**62b** was obtained from (*S,S,S*)-**63b** (0.756 g, 2.42 mmol) in 88% yield (0.352 g) following the same procedure used to synthesize (*R,R*)-**62a**.

Compounds (*R,R*)-**12** and (*S,S*)-**12** were synthesized from **62a** and **62b**, respectively, following the same procedures used to synthesize racemic **12** from 2-methylthio-4-vinylpyrimidine (**40**) and **62**. Enantiopurities of (*R,R*)-**59** (enantiomeric ratio: 97:3) and (*S,S*)-**59** (enantiomeric ratio: 96:4) were determined by chiral HPLC using a Chiralpak AD-H column using an isocratic gradient of 10% 2-propanol/hexanes at flow rate 0.5 mL/min.

*2-(5-Bromopyridin-3-yl)-N-(3-fluorophenethyl)ethan-1-amine (**67**).* Compound **66** (0.55 g, 2.78 mmol) was dissolved in CH_2Cl_2 (50 mL) and cooled to −78 °C. DIBAL in THF (25 wt % in toluene; 2.8 mL, 2.37 g, 4.17 mmol) was added dropwise, and the reaction continued at −78 °C for 1 h. At this point, sodium sulfate decahydrate was added to the reaction mixture, which was gradually warmed to room temperature over 1 h. The resulting suspension was filtered through Celite and washed with CH_2Cl_2 (20 mL), and the combined organic layers were dried and concentrated. To this crude 2-(5-bromopyridin-3-yl)acetaldehyde, $CHCl_3$ (50 mL) was added, followed by the addition of anhydrous $MgSO_4$ (~3.0 g). 3-Fluorophenethylamine (**31**; 0.36 mL, 0.387 g, 2.78 mmol) and acetic acid (60 μL) were sequentially added and stirred at room temperature for 1 h. The reaction mixture was cooled to 0 °C, and sodium triacetoxyborohydride (0.71 g, 3.336 mmol) was added in one portion. The mixture was allowed to warm to room temperature and stirred overnight. The reaction was filtered, and the filtrate was washed with saturated aqueous $NaHCO_3$ (20 mL), and the aqueous layer was extracted with $CHCl_3$ (2 × 10 mL). The organic phase was washed with brine (20 mL), dried over sodium sulfate, concentrated, and purified by flash column chromatography with CH_2Cl_2/MeOH to obtain **67** (0.37 g, 41%) as a pale-yellow oil. ^{1}H NMR (500 MHz, $CDCl_3$): δ 8.51 (d, J = 2.1 Hz, 1 H), 8.34 (d, J = 1.6 Hz, 1 H), 7.64 (t, J = 1.8 Hz, 1 H), 7.25−7.20 (m, 1 H), 6.93 (d, J = 7.5 Hz, 1 H), 6.91−6.84 (m, 2 H), 2.88 (td, J = 7.1, 4.0 Hz, 4 H), 2.76 (dt, J = 14.5, 7.1 Hz, 4 H), 1.31 (s, 1 H). ^{13}C NMR (126 MHz, $CDCl_3$): δ (163.81, 161.86, d, J = 245.7 Hz, 1 C), 148.7, 148.2, (142.27, 142.21, d, J = 7.56 Hz, 1 C), 138.6, 137.2, (129.89, 129.83, d, J = 7.56 Hz, 1 C), (124.26, 124.24, d, J = 2.52 Hz, 1 C), 120.6, (115.47, 115.31, d, J = 20.16 Hz, 1 C), (113.20, 113.04, d, J = 20.16 Hz, 1 C), 50.5, 50.2, 36.0, 33.1. MS (ESI) m/z [1:1; (M + H])$^+$]: calcd, 323.0, 325.0; found, 322.77, 324.76.

*tert-Butyl 2-[5-(1H-Imidazol-1-yl)pyridin-3-yl]ethyl-3-fluorophenethyl Carbamate (**68**).* Compound **67** (0.37 g, 1.145 mmol) was dissolved in THF (10 mL), and a solution of di-*tert*-butyl dicarbonate (0.275 g, 1.26 mmol) in THF (6 mL) was added. The resulting solution was stirred overnight, and then it was diluted with EtOAc/H_2O (30 mL, 1:1). The layers were separated and the aqueous layer extracted with EtOAc (2 × 10 mL). The combined organic layers were dried, concentrated, and purified by column chromatography (hexanes/EtOAc). The resulting oil (0.445 g, 1.051 mmol, 92%) was added to a vial along with CuBr (7.5 mg, 0.052 mmol) and Cs_2CO_3 (0.685 g, 2.102 mmol). The reaction vial was evacuated and backfilled with argon; anhydrous DMSO (previously purged for 5 min with argon), 8-acetyl-5,6,7,8-tetrahydroquinoline (17 μL, 0.018 g, 0.105 mmol), and imidazole (0.107 g, 1.576 mmol) were sequentially added, the reaction sealed, and heated at 100 °C for 12 h. It was cooled to room temperature, treated with EtOAc/H_2O (30 mL, 1:1), and the layers separated. The aqueous layer was extracted with EtOAc (2 × 10 mL), and the combined EtOAc extracts were washed with brine (20 mL), dried, and concentrated. The residue was purified by flash column chromatography using CH_2Cl_2/MeOH to obtain **68** (0.289 g, 67%) as a cream-colored oil. ^{1}H NMR (500 MHz, $CDCl_3$): δ 8.59 (s, 1 H), 8.43 (s, 1 H), 8.01 (s, 1 H), 7.59 (s, 1 H), 7.42 (s, 2 H), 7.24 (q, J = 6.5 Hz, 1 H), 7.02−6.79 (m, 3 H), 3.42−3.33 (m, 4 H), 2.96−2.69 (m, 4 H), 1.38 (s, 9 H). ^{13}C NMR (126 MHz, $CDCl_3$): δ (163.81, 161.86, d, J = 245.7 Hz, 1 C), 155.17, (154.88, 154.85, 1 C), 149.15, 141.51, (140.86, 140.71, 1 C), 135.86, 133.89, (130.02, 129.97, d, J = 6.3 Hz, 1 C), 129.13, (124.49, 124.47, d, J = 2.52 Hz, 1 C), (115.74, 115.57, d, J = 21.42 Hz, 1 C), (113.44, 113.28, d, J = 20.16 Hz, 1 C), 79.98, (49.33, 49.04, 1 C), 48.19, (34.95, 34.27, 1 C), (32.01, 31.88, 1 C), 28.27. MS (ESI) m/z [M + H]$^+$: calcd, 411.21; found, 411.33.

Compounds **69**−**73** were synthesized from **49** following the same procedure used to synthesize **56**.

*tert-Butyl 2-[2-(1H-1,2,3-Triazol-1-yl)pyrimidin-4-yl]ethyl-3-(3-fluorophenyl)propyl Carbamate (**69**).* Yellow oil (0.224 g, 82%). ^{1}H NMR (500 MHz, $CDCl_3$): δ 8.69 (s, 1 H), 7.93 (s, 1 H), 7.86 (s, 1 H), 7.68 (s, 1 H), 7.14 (q, J = 7.8 Hz, 1 H), 6.88−6.84 (m, 2 H), 6.79 (d, J = 9.0 Hz, 1 H), 3.60 (t, J = 6.8 Hz, 2 H), 3.22−3.04 (m, 4 H), 2.50 (t, J = 7.7 Hz, 2 H), 1.76 (p, J = 7 Hz, 2 H), 1.33 (s, 9 H). ^{13}C NMR (126 MHz, $CDCl_3$): δ 171.28, (163.71, 161.76, d, J = 245.7 Hz, 1 C), 158.73, (155.23, 155.08, 1 C), 143.91, 137.50, 134.86, (129.66, 129.59, d, J = 8.82 Hz, 1 C), 123.89, (123.76, 123.74, d, J = 2.52 Hz, 1 C), 119.95, (114.98, 114.82, d, J = 201.6 Hz, 1 C), (112.69, 112.52, d, J = 21.42 Hz, 1 C), 79.62, (47.31, 46.89, 1 C), 46.34, (37.23, 36.62, 1 C), 32.71, (29.78, 29.53, 1 C), 28.18. MS (ESI) m/z [M + Na]$^+$: calcd, 449.19; found, 449.05.

*tert-Butyl 2-[2-(1H-1,2,4-Triazol-1-yl)pyrimidin-4-yl]ethyl-3-(3-fluorophenyl)propyl Carbamate (**70**).* Light-yellow oil (0.135 g, 87%). ^{1}H NMR (500 MHz, $CDCl_3$): δ 9.22 (s, 1 H), 8.66 (d, J = 4.9 Hz, 1 H), 8.16 (s, 1 H), (7.22 (s), 7.13 (s), 1:1, 1 H), 7.20 (q, J = 7.2 Hz, 1 H), 6.90 (d, J = 7.5 Hz, 1 H), 6.88−6.81 (m, 2 H), 3.66−3.58 (m, 2 H), 3.23−3.15 (m, 2 H), 3.11−3.03 (m, 2 H), 2.57 (t, J = 7.7 Hz, 2 H), 1.82 (p, J = 7.7 Hz, 2 H), 1.38 (s, 9 H). ^{13}C NMR (126 MHz, $CDCl_3$): δ 171.17, (163.82, 161.87, d, J = 245.7 Hz, 1 C), 158.75, 155.37, 154.28, 153.57, 143.89, 143.73, (129.81, 129.74, d, J = 8.82 Hz, 1 C), (123.84, 123.82, d, J = 2.52 Hz, 1 C), 119.83, (115.09, 114.92, d, J = 21.42 Hz, 1 C), (112.88, 112.72, d, J = 20.16 Hz, 1 C), 79.83, (47.28, 47.06, 1 C), 46.27, (37.06, 36.45, 1 C), 32.78, (29.86, 29.65, 1 C), 28.30. MS (ESI) m/z [2 M + Na]$^+$: calcd, 875.39; found, 875.33.

*tert-Butyl 3-(3-Fluorophenyl)propyl-2-[2-(2-methyl-1H-imidazol-1-yl)pyrimidin-4-yl]ethyl Carbamate (**71**).* Colorless oil (0.141 g, 85%). ^{1}H NMR (500 MHz, $CDCl_3$): δ 8.53 (d, J = 4.5 Hz, 1 H), 7.82

DOI: 10.1021/jm501719e
J. Med. Chem. 2015, 58, 1067−1088

(s, 1 H), 7.18 (q, J = 7.1 Hz, 1 H), (7.03 (s), 6.97 (s), 1:1, 1 H), 6.92 (s, 1 H), 6.89 (d, J = 7.5 Hz, 1 H), 6.85−6.79 (m, 2 H), 3.65−3.52 (m, 2 H), 3.23−3.09 (m, 2 H), 3.01−2.89 (m, 2 H), 2.78 (s, 3 H), 2.55 (t, J = 7.7 Hz, 2 H), 1.80 (p, J = 7 Hz, 2 H), 1.37 (s, 9 H). ^{13}C NMR (126 MHz, $CDCl_3$): δ 169.92, (163.74, 161.79, d, J = 245.7 Hz, 1 C), 158.03, 155.90, 155.09, 146.41, 143.84, (129.74, 129.68, d, J = 7.56 Hz, 1 C), 127.32, (123.77, 123.75, d, J = 2.52 Hz, 1 C), 118.35, 117.63, (115.00, 114.84, d, J = 20.16 Hz, 1 C), (112.79, 112.62, d, J = 21.42 Hz, 1 C), 79.66, (47.17, 46.90, 1 C), 46.12, (36.88, 36.19, 1 C), 32.72, (29.77, 29.53, 1 C), 28.23, 18.12. MS (ESI) m/z $[M + H]^+$: calcd, 440.2; found, 440.04.

Compounds **72** and **73** were obtained as a 15:1 nonseparable mixture of isomers from reaction of **49** with 4(5)-methylimidazole, which was carried to the next step without further purification.

NOS Enzymes Inhibition Assays. All isozymes of NOS, rat and human nNOS, murine macrophage iNOS, and bovine eNOS, were recombinant enzymes, overexpressed in *Escherichia coli* and purified following previously reported procedures.[44] The enzyme inhibition was determined by measuring the production of nitric oxide from L-arginine using the hemoglobin capture assay in the presence of different concentrations of inhibitors.[36] The assay was performed at 37 °C in 100 mM HEPES buffer with 10% glycerol (pH 7.4) in the presence of 10 μM L-arginine and tetrahydrobiopterin, 100 μM NADPH, 0.83 mM $CaCl_2$, ~320 units/mL of calmodulin, and 3 μM human oxyhemoglobin. For iNOS, $CaCl_2$, and calmodulin were substituted by HEPES buffer. All assays were performed in 96-well plates using a Synergy H1 hybrid multimode microplate reader with automated dispensing of NOS enzyme and hemoglobin after 30 s (maximum delay), which initiated the assay. The initial rates of NO production were determined by monitoring the formation of methemoglobin (NO mediated conversion of oxyhemoglobin to methemoglobin) by monitoring the absorbance at 401 nm. The entire kinetic readout was performed for 5 min with measurements at every 22 s interval. Each compound was assayed at least in duplicate, and nine concentrations (100 μM to 10 nM for nNOS; 500 μM to 50 nM for iNOS and eNOS) were used to construct dose−response curves with slopes from initial readouts. IC_{50} values were calculated by nonlinear regression using GraphPad Prism (standard error values reported are from the Log IC_{50} calculations), and apparent K_i values were determined using the Cheng−Prusoff equation $[K_i = IC_{50}/(1 + [S]/K_m)]$ with the following K_m values for L-arginine: 1.3 (rat nNOS), 1.6 (human nNOS), 8.2 (murine macrophage iNOS), and 1.7 μM (bovine eNOS). The selectivity of an inhibitor was defined as the ratio of their respective K_i values.

Inhibitor Complex Crystal Preparation. The preparations of rat nNOS, bovine eNOS, and human nNOS heme domains used for crystallographic studies were carried out by the procedures described previously.[45] The heme domain samples of nNOS (at 9 mg/mL containing 20 mM histidine), bovine eNOS (10 mg/mL containing 2 mM imidazole), and human nNOS (13 mg/mL) were used for the sitting drop vapor diffusion crystallization setup under conditions reported.[45] A new orthorhombic crystal form of human nNOS was obtained when the pH was raised to 6.2 from 5.0 and the protein concentration dropped to 10 mg/mL. The well solution compositions were only slightly shifted from what were reported: 9−11% PEG3350, 40 mM citric acid, 60 mM Bis-Tris-propane, 10% glycerol, and 5 mM TCEP. From the sitting drop setup, plate-like crystals grew to full size at 4 °C in 3−4 days without seeding. Fresh crystals were first passed stepwise through cryoprotectant solutions and then soaked with 10 mM inhibitor for 4−6 h at 4 °C before being flash cooled with liquid nitrogen.

X-ray Diffraction Data Collection, Data Processing, and Structural Refinement. The cryogenic (100 K) X-ray diffraction data were collected remotely at the Stanford Synchrotron Radiation Light Source (SSRL) or Advanced Light Source (ALS) through the data collection control software Blu-Ice[46] and a crystal-mounting robot. When a Q315r CCD detector was used, 90−100° of data were typically collected with 0.5° per frame. If a Pilatus pixel array detector was used, 140−160° of fine-sliced data were collected with 0.2° per frame. Raw CCD data frames were indexed, integrated, and scaled using HKL2000[47] or MOSFLM,[48] but the pixel array data were processed with XDS[49] and scaled with Scala (Aimless).[50] For rat nNOS or bovine eNOS structures, the binding of inhibitors was detected by the initial difference Fourier maps calculated with REFMAC.[51] For human nNOS structures, molecular replacement was performed with PHASER[52] to provide the initial electron density. One homodimer in the known human nNOS structure (4D1N) was used as the search model. The new human nNOS structure closely resembles that of rat nNOS to have only one homodimer in the asymmetric unit. The inhibitor molecules were then modeled in COOT[53] and refined using REFMAC or PHENIX.[54] Water molecules were added in REFMAC or PHENIX and checked manually in COOT. The TLS[55] protocol was implemented in the final stage of refinements with each subunit as one TLS group. The omit $F_o - F_c$ density maps were calculated by removing inhibitor coordinates from the input PDB file before running one more round of TLS refinement in REFMAC or in PHENIX (simulated annealling protocol with a 2000 K initial temperature). The resulting map coefficients DELFWT and SIGDELWT were used to generate maps that are displayed in figures. The refined structures were validated with the validation service in the RCSB Protein Data Bank. The crystallographic data collection and structure refinement statistics are summarized in Table S1 of the Supporting Information, with the PDB accession codes included.

Caco-2 Permeability Assay. Caco-2 permeability assays were performed by Cyprotex (Watertown, MA) using the Caco-2 epithelial monolayers. Caco-2 cells, grown in tissue culture flasks, were trypsinized, suspended in media, and plated in 96-well plates to be grown for 3 weeks; the proper formation of monolayer was determined by fluorescent measurement of transport of an impermeable dye, Lucifer yellow. All assays were performed with compounds at a concentration of 10 μM for 2 h. For apical to basolateral (A→B) permeability, compounds were added on the apical side (A) and permeation determined on the basolateral side (B), where the receiving buffer was removed for analysis by LC/MS/MS using an Agilent 6410 mass spectrometer (ESI, MRM mode) coupled with an Agilent 1200 HPLC. The buffers used were 100 μM Lucifer yellow in transport buffer (1.98 g/L glucose in 10 mM HEPES, 1× Hank's Balanced Salt Solution, pH 6.5) (apical side) and transport buffer, pH 7.4 (basolateral side). The apparent permeability (P_{app}) is expressed using the following equation: $P_{app} = (dQ/dt)/C_0A$, where dQ/dt is the rate of permeation, C_0 is initial concentration, and A is the monolayer area. For bidirectional permeability, the efflux ratio was defined as $P_{app}(B\rightarrow A)/P_{app}(A\rightarrow B)$; high efflux ratio (>3) indicates that a compound is a potential substrate for P-gp or other active transport systems.

CNS Receptors Screening Assay. Screening of compound **9** for off-target receptor activity was performed at the NIMH Psychoactive Drug Screening Program at UNC Chapel Hill. In the primary radioligand binding assays, the compound was tested at a single concentration (10 μM) in quadruplicate in 96-well plates. For receptors with which a compound displayed more than 50% inhibition at 10 μM concentration, the compound was subjected to secondary radioligand binding assays to determine equilibrium binding affinity at specific targets. In the secondary binding assays, compound **9** was tested at 11 concentrations (10−0.1 μM) and in triplicate. Both primary and secondary radioligand binding assays were carried out in a final volume of 125 μL per well in the appropriate binding buffer, and the radioligand concentration was at a concentration close to the K_d. In a typical assay, 25 μL of radioligand was added to each well of a 96-well plate, followed by addition of 25 μL binding buffer with or without compound. The reaction started upon addition of 75 μL of fresh membrane protein (typically 25−50 μg per well), and the reaction was incubated in the dark at room temperature for 90 min. The reaction was stopped by vacuum filtration onto cold 0.3% polyethylenimine (PEI)-soaked 96-well filter mats using a 96-well Filtermate harvester, followed by three washes with cold wash buffers. Scintillation cocktail was then melted onto the microwave-dried filters on a hot plate, and radioactivity was counted in a Microbeta counter. For primary binding assay analysis, nonspecific binding in the presence

DOI: 10.1021/jm501719e
J. Med. Chem. 2015, 58, 1067−1088

of 10 μM of an appropriate reference compound was set as 100% inhibition; total binding in the absence of test compound or reference compound was set as 0% inhibition. The radioactivity in the presence of test compound was calculated with the equation: % inhibition = (sample cpm − nonspecific cpm)/(total cpm − nonspecific cpm) × 100, where the radioactivity was measured in counts per minute (cpm/well). For secondary binding results, counts (cpm/well) were pooled and fitted to a three-parameter logistic function for competition binding in Prism to determine IC_{50} values: Y = bottom + (top − bottom)/1 + $10^{X-LogIC_{50}}$, where Y is the total binding in the presence of a corresponding concentration of compound (X, in this case, concentration of **9**), and top and bottom are the total and nonspecific binding in the absence and presence of 10 μM reference compound. K_i is determined from the corresponding IC_{50} value using the Cheng−Prusoff equation.

CYP Inhibition Assay. The CYP inhibition assay of **9** was performed against the five major liver microsomal CYP enzymes: CYP1A2, CY2C9, CYP2C19, CYP2D6, and CYP3A4 (by Sai Life Sciences). In the assay, a 25 μL aliquot of microsomes diluted in Kphos buffer (0.4 mg/mL) was added to individual wells of the reaction plate. Fluvoxamine, sulfaphenazole, quinidine, ticlopidine, and ketoconazole (positive control inhibitors for CYP1A2, CYP2C9, CYP2D6, CYP2C19, and CYP3A4, respectively), diluted in buffer (25 μL), were added separately to the respective wells. Compound **9**, diluted in DMSO to a concentration of 10 μM, was directly spiked into microsomal mix (2×), and 50 μL was aliquoted into individual wells. An aliquot of 25 μL of phenacetin, diclofenac, bufuralol, *S*-mephenytoin, and midazolam (4×) for CYP1A2, CYP2C9, CYP2D6, CYP2C19, and CYP3A4, respectively, was added separately to wells and incubated for 5 min at 37 °C. The reactions were initiated using 25 μL of NADPH (4×) and further incubated for 5 min for CYP3A4 (Midazolam), 10 min for CYP1A2, CYP2C9, and CYP2D6, and 20 min for CYP2C19. All reactions were terminated using 100 μL of ice-cold acetonitrile containing internal standard (imipramine and glipizide at 1 μM). The plates were centrifuged at 4000 rpm for 15 min, 100 μL aliquots were subjected to LC-M/MS on a Shimadzu API 4000 system (MRM mode), and the metabolites were detected. The respective peak area ratios (PA) of metabolites and internal standard was used to determine % inhibition, where % activity = (PA ratios in the presence of compound/PA ratios in DMSO control) × 100, and % inhibition = 100 − % activity.

CYP3A4 Inhibition Assay. The inhibitory potency of **9**, (*R*,*R*)-**12**, **13**, and **20** on the 7-benzyloxy-4-(trifluoromethyl)coumarin (BFC) debenzylase activity of human CYP3A4 was evaluated fluorimetrically in a reconstituted system with cytochrome P450 reductase (CPR). The reaction was carried out at room temperature in 100 mM phosphate buffer, pH 7.4, containing catalase and superoxide dismutase (2 U/mL each). A mixture of 1 μM CYP3A4 and 1 μM CPR was preincubated for 1 h at room temperature and diluted by 20-fold before measurements. BFC (50 μM) and various concentrations of inhibitors were added 2 min prior to initiation of the reaction with 100 μM NADPH. Formation of 7-hydroxy-4-trifluoromethylcoumarin (λ_{ex} = 430 nm; λ_{em} = 500 nm) was followed in a Hitachi F100 fluorimeter. IC_{50} values were derived from the [% activity] vs [inhibitor] plots.

■ ASSOCIATED CONTENT

Supporting Information

Synthesis of the primary amines in Scheme 3, additional X-ray crystal structures of inhibitors bound to NOSs, and X-ray crystallographic data collection and refinement statistics. This material is available free of charge via the Internet at http://pubs.acs.org.

Accession Codes

4D3B, 4V3V, 4V3W, 4V3X, 4D33, 4D35, 4V3Z, 4D2Y, 4V3U, 4D30, 4D32, 4D3A, 4D34, 4V3Y, 4V36, 4D37, 4D38, 4D2Z, 4D31, 4UCH, and 4D39.

■ AUTHOR INFORMATION

Corresponding Authors

*Phone: 949-824-7020. Fax: (949) 824-3280. E-mail: poulos@uci.edu.

*Phone: 847-491-5653. Fax (847) 491-7713. E-mail: Agman@chem.northwestern.edu.

Notes

The authors declare no competing financial interest.

■ ACKNOWLEDGMENTS

We are grateful for financial support from the National Institutes of Health (GM049725 to R.B.S. and GM057353 to T.L.P.). We thank Dr. Bettie Sue Masters, whose nitric oxide synthase research is supported by the Robert A. Welch Foundation Distinguished Chair in Chemistry (AQ-0012) and with whom L.J.R. is affiliated. P. Martásek is supported by grant P24/LF1/3 from Charles University, the Czech Republic. P. Mukherjee (in R.B.S. lab) thanks Dr. Arsen Gaisin of the Center for Molecular Innovation and Drug Discovery (Northwestern University) for assistance with preparative HPLC and Saman Shafaie for assistance with HRMS experiments. We also thank the beamline staff at SSRL and ALS for their assistance during the remote X-ray diffraction data collections.

■ ABBREVIATIONS USED

NO, nitric oxide; nNOS, neuronal nitric oxide synthase; iNOS, inducible nitric oxide synthase; eNOS, endothelial nitric oxide synthase; L-Arg, L-arginine; FAD, flavin adenine dinucleotide; FMN, flavin mononucleotide; NADPH, reduced nicotinamide adenine dinucleotide phosphate; H_4B, (6*R*)-5,6,7,8-tetrahydrobiopterin; CNS, central nervous system; CYP, cytochrome P450; P_{app}, apparent permeability; HEPES, 4-(2-hydroxyethyl)-1-piperazineethanesulfonic acid

■ REFERENCES

(1) Ignarro, L. J. Nitric oxide as a unique signaling molecule in the vascular system: a historical overview. *J. Physiol. Pharmacol.* **2002**, *53*, 503−514.

(2) Knowles, R. G.; Moncada, S. Nitric oxide synthases in mammals. *Biochem. J.* **1994**, *298*, 249−258.

(3) Schlossman, J.; Hofmann, F. cGMP-dependent protein kinases in drug discovery. *Drug Discovery Today* **2005**, *10*, 627−634.

(4) Malinski, T.; Bailey, F.; Zhang, Z. G.; Chopp, M. Nitric oxide measured by a porphyrinic microsensor in rat brain after transient middle cerebral artery occlusion. *J. Cereb. Blood Flow Metab.* **1993**, *13*, 355−358.

(5) Ischiropoulos, H.; Zhu, L.; Chen, J.; Tsai, M.; Martin, J. C.; Smith, C. D.; Beckman, J. S. Peroxynitrite-mediated tyrosine nitration catalyzed by superoxide dismutase. *Arch. Biochem. Biophys.* **1992**, *298*, 431−437.

(6) Stamler, J. S.; Lamas, S.; Fang, F. C. Nitrosylation: the prototypic redox-based signaling mechanism. *Cell* **2001**, *106*, 675−683.

(7) (a) Blough, N. V.; Zafiriou, O. C. Reaction of superoxide with nitric oxide to form peroxonitrite in alkaline aqueous solution. *Inorg. Chem.* **1985**, *24*, 3502−3504. (b) Lipton, S. A.; Choi, Y.-B.; Pan, Z.-H.; Lei, S.; Chen, H.-S. V.; Sucher, N.; Loscalzo, J.; Singel, D. J.; Stamler, J. S. A redox-based mechanism for the neuroprotective and neurodestructive effects of nitric oxide and related nitroso-compounds. *Nature* **1993**, *364*, 626−632. (c) Beckman, J. S.; Beckman, T. W.; Chen, J.; Marshall, P. A.; Freeman, B. A. Apparent hydroxyl radical production by peroxynitrite: implications for endothelial injury from nitric oxide and superoxide. *Proc. Natl. Acad. Sci. U. S. A.* **1990**, *87*, 1620−1624.

DOI: 10.1021/jm501719e
J. Med. Chem. 2015, 58, 1067−1088

(8) (a) Dorheim, M. A.; Tracey, W. R.; Pollock, J. S.; Grammas, P. Nitric oxide synthase activity is elevated in brain microvessels in Alzheimer's disease. *Biochem. Biophys. Res. Commun.* **1994**, *205*, 659−665. (b) Giasson, B. I.; Duda, J. E.; Murray, I. V.; Chen, Q.; Souza, J. M.; Hurtig, H. I.; Ischiropoulos, H.; Trojanowski, J. Q.; Lee, V. M. Oxidative damage linked to neurodegeneration by selective alpha-synuclein nitration in synucleinopathy lesions. *Science* **2000**, *290*, 985−989. (c) Drechsel, D. A.; Estévez, A. G.; Barbeito, L.; Beckman, J. S. Nitric oxide-mediated oxidative damage and the progressive demise of motor neurons in ALS. *Neurotoxic. Res.* **2012**, *22*, 251−264.

(9) (a) Li, H.; Forstermann, U. Nitric oxide in the pathogenesis of vascular disease. *J. Pathol.* **2000**, *190*, 244−254. (b) Ramachandran, R.; Ploug, K. B.; Hay-Schmidt, A.; Olesen, J.; Jansen-Olesen, I.; Gupta, S. Nitric oxide synthase (NOS) in the trigeminal vascular system and other brain structures related to pain in rats. *Neurosci. Lett.* **2010**, *484*, 192−196.

(10) (a) Huang, Z.; Huang, P. L.; Panahian, N.; Dalkara, T.; Fishman, M. C.; Moskowitz, M. A. Effects of cerebral ischemia in mice deficient in neuronal nitric oxide synthase. *Science* **1994**, *265*, 1883−1885. (b) Hantraye, P.; Brouillet, E.; Ferrante, R.; Palfi, S.; Dolan, R.; Matthews, R. T.; Beal, M. F. Inhibition of neuronal nitric oxide synthase prevents MPTP-induced parkinsonism in baboons. *Nature Med.* **1996**, *2*, 1017−1021. (c) Yokoyama, H.; Yano, R.; Aoki, E.; Kato, H.; Araki, T. Comparative pharmacological study of free radical scavenger, nitric oxide synthase inhibitor, nitric oxide synthase activator and cyclooxygenase inhibitor against MPTP neurotoxicity in mice. *Metab. Brain Dis.* **2008**, *23*, 335−349. (d) Ikeda, K.; Iwasaki, Y.; Kinoshita, M. Neuronal nitric oxide synthase inhibitor, 7-nitroindazole, delays motor dysfunction and spinal motoneuron degeneration in the wobbler mouse. *J. Neurol. Sci.* **1998**, *160*, 9−15.

(11) Mukherjee, P.; Cinelli, M. A.; Kang, S.; Silverman, R. B. Development of nitric oxide synthase inhibitors for neurodegeneration and neuropathic pain. *Chem. Soc. Rev.* **2014**, *43*, 6814−6838.

(12) (a) Alderton, W. K.; Cooper, C. E.; Knowles, R. G. Nitric oxide synthases: structure, function and inhibition. *Biochem. J.* **2001**, *357*, 593−615. (b) Li, H.; Raman, C. S.; Glaser, C. B.; Blasko, E.; Young, T. A.; Parkinson, J. F.; Whitlow, M.; Poulos, T. L. Crystal structures of zinc-free and -bound heme domain of human inducible nitric-oxide synthase. Implications for dimer stability and comparison with endothelial nitric-oxide synthase. *J. Biol. Chem.* **1999**, *274*, 21276−21284.

(13) Bredt, D. S.; Hwang, P. M.; Glatt, C. E.; Lowenstein, C.; Reed, R. R.; Snyder, S. H. Cloned and expressed nitric oxide synthase structurally resembles cytochrome P-450 reductase. *Nature* **1991**, *351*, 714−718.

(14) (a) Abu-Soud, H. M.; Stuehr, D. J. Nitric oxide synthases reveal a role for calmodulin in controlling electron transfer. *Proc. Natl. Acad. Sci. U. S. A.* **1993**, *90*, 10769−10772. (b) Smith, B. C.; Underbakke, E. S.; Kulp, D. W.; Schief, W. R.; Marletta, M. A. Nitric oxide synthase domain interfaces regulate electron transfer and calmodulin activation. *Proc. Natl. Acad. Sci. U. S. A.* **2013**, *108*, E3577−E3586.

(15) (a) Groves, J. T.; Wang, C. C.-Y. Nitric oxide synthase: models and mechanisms. *Curr. Opin. Chem. Biol.* **2000**, *4*, 687−695. (b) Zhu, Y.; Silverman, R. B. Revisiting heme mechanisms. A perspective on the mechanisms of nitric oxide synthase (NOS), heme oxygenase (HO), and cytochrome P450s (CYP450s). *Biochemistry* **2008**, *47*, 2231−2243. (c) Daff, S. NO synthase: structures and mechanisms. *Nitric Oxide* **2010**, *23*, 1−11.

(16) (a) Maddaford, S.; Annedi, S. C.; Ramnauth, J.; Rakhit, S. Advancements in the development of nitric oxide synthase inhibitors. *Annu. Rep. Med. Chem.* **2009**, *44*, 27−50. (b) Huang, H.; Silverman, R. B. Recent advances toward improving the bioavailability of neuronal nitric oxide synthase inhibitors. *Curr. Top. Med. Chem.* **2013**, *13*, 803−812.

(17) Fischmann, T. O.; Hruza, A.; Niu, X. D.; Fossetta, J. D.; Lunn, C. A.; Dolphin, E.; Prongay, A. J.; Reichert, P.; Lundell, D. J.; Narula, S. K.; Weber, P. C. Structural characterization of nitric oxide synthase isoforms reveals striking active-site conservation. *Nature Struct. Biol.* **1999**, *6*, 233−242.

(18) (a) Ji, H.; Stanton, B. Z.; Igarashi, J.; Li, H.; Martásek, P.; Roman, L. J.; Poulos, T. L.; Silverman, R. B. Minimal pharmacophoric elements and fragment hopping, an approach directed at molecular diversity and isozyme selectivity. Design of selective neuronal nitric oxide synthase inhibitors. *J. Am. Chem. Soc.* **2008**, *130*, 3900−3914. (b) Ji, H.; Delker, S. L.; Li, H.; Martásek, P.; Roman, L. J.; Poulos, T. L.; Silverman, R. B. Exploration of the active site of neuronal nitric oxide synthase by the design and synthesis of pyrrolidinomethyl 2-aminopyridine derivatives. *J. Med. Chem.* **2010**, *53*, 7804−7824.

(19) Ji, H.; Tan, S.; Igarashi, J.; Li, H.; Derrick, M.; Martásek, P.; Roman, L. J.; Vasquez-Vivar, J.; Poulos, T. L.; Silverman, R. B. Selective neuronal nitric oxide synthase inhibitors and the prevention of cerebral palsy. *Ann. Neurol.* **2009**, *65*, 209−217.

(20) (a) Veber, D. F.; Johnson, S. R.; Cheng, H.-Y.; Smith, B. R.; Ward, H. W.; Kopple, K. D. Molecular properties that influence the oral bioavailability of drug candidates. *J. Med. Chem.* **2002**, *35*, 2615−2623. (b) Seelig, A. The role of size and charge for blood−brain barrier permeation of drugs and fatty acids. *J. Mol. Neurosci.* **2007**, *33*, 32−41.

(21) Li, H.; Xue, F.; Kraus, J. M., II; Ji, H.; Jansen Labby, K.; Mataka, J.; Delker, S. L.; Martásek, P.; Roman, L. J.; Poulos, T. L.; Silverman, R. B. Cyclopropyl- and methyl-containing inhibitors of neuronal nitric oxide synthase. *Bioorg. Med. Chem.* **2013**, *21*, 1333−1343.

(22) Xue, F.; Fang, J.; Lewis, W. W.; Martásek, P.; Roman, L. J.; Silverman, R. B. Potent and selective neuronal nitric oxide synthase inhibitors with improved cellular permeability. *Bioorg. Med. Chem. Lett.* **2010**, *15*, 554−557.

(23) Labby, K. J.; Xue, F.; Kraus, J. M.; Ji, H.; Mataka, J.; Li, H.; Martásek, P.; Roman, L. J.; Poulos, T. L.; Silverman, R. B. Intramolecular hydrogen bonding: a potential strategy for more bioavailable inhibitors of neuronal nitric oxide synthase. *Bioorg. Med. Chem.* **2012**, *20*, 2435−2443.

(24) Huang, H.; Li, H.; Martásek, P.; Roman, L. J.; Poulos, T. L.; Silverman, R. B. Structure-guided design of selective inhibitors of neuronal nitric oxide synthase. *J. Med. Chem.* **2013**, *56*, 3024−3032.

(25) (a) Lohmann, C.; Huwel, S.; Galla, H. J. Predicting blood−brain barrier permeability of drugs: evaluation of different in vitro assays. *J. Drug Targeting* **2002**, *10*, 263−276. (b) Stewart, B. H.; Chan, O. H.; Lu, R. H.; Reyner, E. L.; Shmid, H. L.; Hamilton, H. W.; Steinbaugh, B. A.; Taylor, M. D. Comparison of intestinal permeabilities determined in multiple in vitro and in situ models: relationship to absorption in humans. *Pharm. Res.* **1995**, *12*, 693−699. (c) Yee, S. In vitro permeability across Caco-2 cells (colonic) can predict in vivo (small intestinal) absorption in man—fact or myth? *Pharm. Res.* **1997**, *14*, 763−766.

(26) Wolff, D. J.; Datto, G. A.; Samatovicz, R. A.; Tempsick, R. A. Calmodulin-dependent nitric-oxide synthase. Mechanism of inhibition by imidazole and phenylimidazoles. *J. Biol. Chem.* **1993**, *268*, 9425−9429.

(27) (a) McMillan, K.; Adler, M.; Auld, D. S.; Baldwin, J. J.; Blasko, E.; Browne, L. J.; Chelsky, D.; Davey, D.; Dolle, R. E.; Eagen, K. A.; Erickson, S.; Feldman, R. I.; Glaser, C. B.; Mallari, C.; Morrissey, M. M.; Ohlmeyer, M. H. J.; Pan, G.; Parkinson, J. F.; Phillips, G. B.; Polokoff, M. A.; Sigal, N. H.; Vergona, R.; Whitlow, M.; Young, T. A.; Devlin, J. J. Allosteric inhibitors of inducible nitric oxide synthase dimerization discovered via combinatorial chemistry. *Proc. Natl. Acad. Sci. U. S. A.* **2000**, *97*, 1506−1511. (b) Davey, D. D.; Adler, M.; Arnaiz, D.; Eagen, K.; Erickson, S.; Guilford, W.; Kenrick, M.; Morrissey, M. M.; Ohlmeyer, M.; Pan, G.; Paradkar, V. M.; Parkinson, J.; Polokoff, M.; Saionz, K.; Santos, C.; Subramanyam, B.; Vergona, R.; Wei, R. G.; Whitlow, M.; Ye, B.; Zhao, Z. S.; Devlin, J. J.; Phillips, G. Design, synthesis, and activity of 2-imidazol-1-ylpyrimidine derived inducible nitric oxide synthase dimerization inhibitors. *J. Med. Chem.* **2007**, *50*, 1146−1157. (c) Gahman, T. C.; Herbert, M. R.; Lang, H.; Thayer, A.; Symons, K. T.; Nguyen, P. M.; Massari, M. E.; Dozier, S.; Zhang, Y.; Sablad, M.; Rao, T. S.; Noble, S. A.; Shiau, A. K.; Hassig, C. A. Identification and SAR of selective inducible nitric oxide synthase (iNOS) dimerization inhibitors. *Bioorg. Med. Chem. Lett.* **2011**, *21*, 6888−6894. (d) Wei, R. G.; Adler, M.; Davey, D.; Ho, E.; Mohan, R.; Polokoff, M.; Tseng, J.-L.; Whitlow, M.; Xu, W.; Yuana, S.; Phillips, G.

DOI: 10.1021/jm501719e
J. Med. Chem. 2015, 58, 1067−1088

1-(1,3-Benzodioxol-5-ylmethyl)-3-[4-(1*H*-imidazol-1-yl)phenoxy]-piperidine analogs as potent and selective inhibitors of nitric oxide formation. *Bioorg. Med. Chem. Lett.* **2007**, *17*, 2499−2504.
(28) Fedorov, R.; Vasan, R.; Ghosh, D. K.; Schlichting, I. Structures of nitric oxide synthase isoforms complexed with the inhibitor AR-R17477 suggest a rational basis for specificity and inhibitor design. *Proc. Natl. Acad. Sci. U. S. A.* **2004**, *101*, 5892−5897.
(29) Xue, F.; Li, H.; Fang, J.; Roman, L. J.; Martásek, P.; Poulos, T. L.; Silverman, R. B. Peripheral but crucial: a hydrophobic pocket (Tyr706, Leu337, and Met336) for potent and selective inhibition of neuronal nitric oxide synthase. *Bioorg. Med. Chem. Lett.* **2010**, *20*, 6258−6261.
(30) Ji, H.; Li, H.; Martásek, P.; Roman, L. J.; Poulos, T. L.; Silverman, R. B. Discovery of highly potent and selective inhibitors of neuronal nitric oxide synthase by fragment hopping. *J. Med. Chem.* **2009**, *52*, 779−797.
(31) Baldino, C. M.; Caserta, J. L.; Dumas, S. A.; Lee, C.-S.; Flanders, Y. L. Aminopyrimidine kinase inhibitors. U.S. Patent 2012/0270892Al, 2012.
(32) Benneche, T. Pyrimidinylpalladium(II) complexes in the synthesis of alkenyl pyrimidines. *Acta Chem. Scand.* **1990**, *44*, 927−931.
(33) Cui, J. J.; Deal, J. G.; Gu, D.; Guo, C.; Johnson, M. C.; Kania, R. S.; Kephart, S. E.; Linton, M. A.; McApline, I. J.; Pairish, M. A.; Palmer, C. L. Pyrazole compounds and their use as raf inhibitors. U.S. Patent WO 2009016460 A2, 2009.
(34) Other resolving chiral reagents, such as (*S*)-camphanic chloride, and (*S*)-(+)-*O*-acetylphenylacetic acid were unable to resolve the two diastereomers by chromatography or recrystallization techniques.
(35) Chen, H.; Wang, D.; Wang, X.; Huang, W.; Cai, Q.; Ding, K. Mild conditions for copper-catalyzed *N*-arylation of imidazoles. *Synthesis* **2010**, 1505−1511.
(36) (a) Hevel, J. M.; Marletta, M. A. Nitric-oxide synthase assays. *Methods Enzymol.* **1994**, *233*, 250−258. (b) Kang, S.; Tang, W.; Li, H.; Chreifi, G.; Martásek, P.; Roman, L. J.; Poulos, T. L.; Silverman, R. B. Nitric oxide synthase inhibitors that interact with both heme propionate and tetrahydrobiopterin show high isoform selectivity. *J. Med. Chem.* **2014**, *57*, 4382−4396.
(37) Huang, H.; Li, H.; Yang, S.; Chreifi, G.; Martásek, P.; Roman, L. J.; Meyskens, F. L.; Poulos, T. L.; Silverman, R. B. Potent and selective double-headed thiophene-2-carboximidamide inhibitors of neuronal nitric oxide synthase for the treatment of melanoma. *J. Med. Chem.* **2014**, *57*, 686−700.
(38) Raman, C. S.; Li, H.; Martásek, P.; Kral, V.; Masters, B. S. S.; Poulos, T. L. Crystal structure of constitutive endothelial nitric oxide synthase: a paradigm for pterin function involving a novel metal center. *Cell* **1998**, *95*, 939−950.
(39) (a) Cole, P. A.; Robinson, C. H. Mechanism and inhibition of cytochrome P-450 aromatase. *J. Med. Chem.* **1990**, *33*, 2933−2942. (b) Koltin, Y.; Hitchcock, C. A. The search for new triazole antifungal agents. *Curr. Opin. Chem. Biol.* **1997**, *1*, 176−182.
(40) Percent inhibition and K_i data were generously provided by the National Institute of Mental Health's Psychoactive Drug Screening Program, contract no. HHSN-271-2013-00017-C (NIMH PDSP). The NIMH PDSP is Directed by Bryan L. Roth MD, Ph.D. at the University of North Carolina at Chapel Hill and Project Officer Jamie Driscol at NIMH, Bethesda MD, USA.
(41) de Wildt, S. N.; Kearns, G. L.; Leeder, J. S.; van den Anker, J. N. Cytochrome P450 3A: ontogeny and drug disposition. *Clin. Pharmacokinet.* **1999**, *37*, 485−505.
(42) Lin, Y.-S.; Park, J.; De Schutter, J. W.; Huang, X. F.; Berghuis, A. M.; Sebag, M.; Tsantrizos, Y. S. Design and synthesis of active site inhibitors of the human farnesyl pyrophosphate synthase: apoptosis and inhibition of ERK phosphorylation in multiple myeloma cells. *J. Med. Chem.* **2012**, *55*, 3201−3215.
(43) Johnson, J.; Lloyd, J.; Finlay, H.; Jiang, J.; Neels, J.; Dhondi, N. K.; Gunaga, P.; Banerjee, A.; Adisechan, A. Quinazolines as potassium ion channel inhibitors. U.S. Patent WO2011/028741 A1, 2011.
(44) (a) Roman, L. J.; Sheta, E. A.; Martásek, P.; Gross, S. S.; Liu, Q.; Masters, B. S. S. High-level expression of functional rat neuronal nitric oxide synthase in *Escherichia coli*. *Proc. Natl. Acad. Sci. U. S. A.* **1995**, *92*, 8428−8432. (b) Hevel, J. M.; White, K. A.; Marletta, M. A purification of the inducible murine macrophage nitric oxide synthase: identification as a flavoprotein. *J. Biol. Chem.* **1991**, *266*, 22789−22791. (c) Gerber, N. C.; Ortiz de Montellano, P. R. Neuronal nitric oxide synthase: expression in *Escherichia coli*, irreversible inhibition by phenyldiazene, and active site topology. *J. Biol. Chem.* **1995**, *270*, 17791−17796.
(45) (a) Li, H.; Jamal, J.; Delker, S.; Plaza, C.; Ji, H.; Jing, Q.; Huang, H.; Kang, S.; Silverman, R. B.; Poulos, T. L. The mobility of a conserved tyrosine residue controls isoform-dependent enzyme−inhibitor interaction in nitric oxide synthases. *Biochemistry* **2014**, *53*, 5272−5279. (b) Li, H.; Jamal, J.; Plaza, C.; Pineda, S. H.; Chreifi, G.; Jing, Q.; Cinelli, M. A.; Silverman, R. B.; Poulos, T. L. Structures of human constitutive nitric oxide synthases. *Acta Crystallogr., Sect. D: Biol. Crystallogr.* **2014**, *D70*, 2667−2674.
(46) McPhillips, T. M.; McPhillips, S. E.; Chiu, H. J.; Cohen, A. E.; Deacon, A. M.; Ellis, P. J.; Garman, E.; Gonzalez, A.; Sauter, N. K.; Phizackerley, R. P.; Soltis, S. M.; Kuhn, P. Blu-Ice and the Distributed Control System: Software for Data Acquisition and Instrument Control at Macromolecular Crystallography Beamlines. *J. Synchrotron Radiat.* **2002**, *9*, 401−406.
(47) Otwinowski, Z.; Minor, W. Processing of X-ray diffraction data collected in oscillation mode. *Methods Enzymol.* **1997**, *276*, 307−326.
(48) Leslie, A. G. W.; Powell, H. R.; Read. R. J.; Sussman, J. L. Processing diffraction data with MOSFLM. In *Evolving Methods in Macromolecular Crystallography*; Read. R. J., Sussman, J. L., Eds.; Springer: New York, 2007; Vol *245*, pp 41−51.
(49) Kabsch, W. XDS. *Acta Crystallogr., Sect. D: Biol. Crystallogr.* **2010**, *D66*, 125−132.
(50) Evans, P. R. Scaling and assessment of data quality. *Acta Crystallogr., Sect D: Biol. Crystallogr.* **2006**, *D62*, 72−82.
(51) Murshudov, G. N.; Vagin, A. A.; Dodson, E. J. Refinement of macromolecular structures by the maximum-likelihood method. *Acta Crystallogr., Sect. D: Biol. Crystallogr.* **1997**, *D53*, 240−255.
(52) McCoy, A. J.; Grosse-Kunstleve, R. W.; Adams, P. D.; Winn, M. D.; Storoni, L. C.; Read, R. J. Phaser crystallographic software. *J. Appl. Crystallogr.* **2007**, *40*, 658−674.
(53) Emsley, P.; Cowtan, K. Coot: model-building tools for molecular graphics. *Acta Crystallogr., Sect. D: Biol. Crystallogr.* **2004**, *D60*, 2126−2132.
(54) Adams, P. D.; Afonine, P. V.; Bunkóczi, G.; Chen, V. B.; Davis, I. W.; Echols, N.; Headd, J. J.; Hung, L.-W.; Kapral, G. J.; Grosse-Kunstleve, R. W.; McCoy, A. J.; Moriarty, N. W.; Oeffner, R.; Read, R. J.; Richardson, D. C.; Richardson, J. S.; Terwilliger, T. C.; Zwart, P. H. PHENIX: a comprehensive Python-based system for macromolecular structure solution. *Acta Crystallogr., Sect. D: Biol. Crystallogr.* **2010**, *D66*, 213−221.
(55) Winn, M. D.; Isupov, M. N.; Murshudov, G. N. Use of TLS parameters to model anisotropic displacements in macromolecular refinement. *Acta Crystallogr., Sect. D: Biol. Crystallogr.* **2001**, *D57*, 122−133.

DOI: 10.1021/jm501719e
J. Med. Chem. 2015, 58, 1067−1088